Theoretical and Computational Aspects of Phase Transitions in Elastic Ferroelectric Materials

Antonios I. Arvanitakis

Department of Materials Science and Engineering

University of Ioannina

A thesis submitted for the degree of

PhilosophiæDoctor (PhD)

Ioannina, 2010

1. Supervisor: *Vassilios K. Kalpakides, Professor, Department of Materials Science and Engineering, University of Ioannina*

2. Advisor: *Evangelos P. Hadjigeorgiou, Assistant Professor, Department of Materials Science and Engineering, University of Ioannina*

3. Advisor: *Cristian Dascalu, Professeur, Laboratoire Sols, Solides, Structures UJF Grenoble*

4. Reviewer: *Charalambopoulos Antonios, Professor, Department of Materials Science and Engineering, University of Ioannina*

5. Reviewer: *Georgios E. Stavroulakis, Professor, Institute of Computational Mechanics and Optimization, Technical University of Crete*

6. Reviewer: *Nicolas C. Charalambakis, Professor and Chairman of the Institute of Mechanics of Materials Department of Civil Engineering, Aristotle University of Thessaloniki*

7. Reviewer: *Georgiadis Haralampos, Professor, Mechanics Division, National Technical University of Athens*

Day of the defense: 12 January 2011

Signature from head of PhD committee:

Abstract

The last fifty years a great interest from both academics and industries is shown towards materials that are capable of undergoing phase transformations. Phase transitions are an important characteristic of crystalline materials based on the fact that they can alter their crystal symmetry at various ranges of temperature. Ferroelectric materials have become important materials in a wide variety of electronics due to their pronounced dielectric and piezoelectric properties. The material macroscopic properties are related to the microscopic domain structure of the materials. To understand and predict the relation between the macroscopic properties and the domain structure, continuum models are employed in this work.

More specifically, this thesis is organized as follows:

In the first chapter, an introduction to the physics of ferroelectrics is presented. Explanations are given on the nature of ferroelectricity from the crystallographic point of view, but since we are interested in the modelization of these materials we present a brief introduction of the famous Landau model, which serves as a conceptual bridge between microscopic models and observed macroscopic phenomena. Moreover, we provide useful information on the behavior of these materials at very low scales.

In the second chapter, we focus on the so called phase field models that use polarization as the first order parameter of the evolutionary process inside bulk ferroelectrics. The proposed phase field model is based on a theory that accumulates gradients of the Maxwelian electric field and also introduces spontaneous quadrupoles. The aim of this chapter is to reveal the role of both spontaneous and linear quadrupole polarization in the domain structure of ferroelectrics. It is proved that spontaneous quadrupoles are

responsible for the thickness of domain walls and linear quadrupoles have a serious impact on low dimensional ferroelectrics, such as thin films.

The third chapter introduces the level set method and we use this method to describe the kinetics of a phase boundary. Level set methods have been introduced by Osher and Sethian and soon have become a very powerful tool for tracking a moving interface within a body. The method is based on an implicit representation of the interface by considering a smooth scalar function, which changes sign across the interface. Thus the zero level set of the implicit function coincides with the interface. The introduction of a level set function results in regularization of the sharp interface model in solids. In level set methods the interfaces transform into thin transition layers where all discontinuous quantities take inhomogeneous but continuous expressions. In this way, we can make a connection to configurational mechanics proving that the forces moving the interfaces are inhomogeneity forces. Computational results provide the microstructure of ferroelectrics and they are in agreement with the results of the phase field model presented in the second chapter.

In the fourth chapter, we use the previous models to study special topics in ferroelectrics. To be more precise we study the influence of point charge and dipolar defects in the motion of domain walls so as to extract useful information of damaged ferroelectrics. Moreover, we present a combined level set–phase field model to study the behavior of bi-crystals, which can be easily expanded to polycrystals.

To my dear brother Alexandros

Acknowledgements

This work would not have been completed without the support and guidance of several people over the course of completing my Ph.D.

First, I would like to sincerely thank my supervisor Professor Vassilios Kalpakides for his immense help in shaping this work. Professor Kalpakides was always near for any kind of problem that has arisen during the preparation of this thesis. He is the kind of teacher that inspires trust and close to him i have learned that research requires patience and dedication.

I would also like to thank Pr. Evangelos Hadjigeorgiou for his guidance and valuable discussions through the preparation of my thesis. I also thank Professor Cristian Dascalu, who accepted to be an advisor and even though he was far away, he kept watching my progress with great interest. I sincerely thank my many colleagues in our mechanics of materials research group for their support and encouragement during my course of study. Most importantly, I would like to thank my family and all my good friends. I could not have achieved this goal without their love and support. I especially thank my brother Alexandros and my sister Peny for their encouragement and love.

Finally, I would like to thank the Department of Materials Science and Engineering for its warm hospitality and the *State Scholarships Foundation (I. K.Y.) of Greece* for providing a scholarship which supported financially this research.

Contents

List of Figures

List of Tables

Chapter 1

Introduction

"You may say anything you like but we are all made up of ferroelectrics."
B.T. Matthias

1.1 What are ferroelectrics?

Investigation of phase transformations represents a currently active research area for mechanics of materials. In models of macroscopic behavior, phase transformations are modeled by weak solutions of the partial differential equations of the corresponding continuum theories; i.e. those solutions in which quantities such as stress and strain suffer discontinuities across certain surfaces. Materials on the two sides of such a surface exhibit distinct physical properties and are identified as distinct phases. These surfaces represent interfaces between different material phases, and motions of these surfaces model phase transformations. Studies carried out within the framework of the purely mechanical theory are appropriate for the modeling of load-induced phase transformations taking place at a given temperature. Incorporation of thermodynamics into the corresponding mechanical theory opened the way to the modeling of thermomechanical phase transformations. A material exhibits different physical properties in distinct phases, and the interfaces between the distinct phases are therefore surfaces of abrupt change in material properties. The abrupt change in mechanical, electromagnetic and optical properties results in an interface which reflects optical and acoustic

waves. On the other hand, phase transformations in solids sometimes take place at speeds comparable to wave speeds in the material, so that inertial effects become important.

Many materials are capable of undergoing phase transformations under the combined influence of thermo-mechanical loading and applied electromagnetic fields, such as ferroelectric crystals. From the crystallography point of view, any one crystal can be classified in one of 32 point groups according to the symmetry elements which it possesses. Out of these 32 classes, 10 are characterized by the fact that they have a polar axis, i.e. an axis which shows properties at one end different from those at the other. Crystals in these classes are called polar. One feature of polar crystals is that they are polarized even in the absence of applied electric fields, and this feature is referred to as spontaneous polarization. A ferroelectric crystal undergoes a structural transformation at a critical temperature which, in the absence of applied electric fields, is often referred to as the Curie point. Above this temperature, it has a non-polar structure, called paraelectric, and below this temperature, it has a polar structure, called ferroelectric. This structural transformation is the so-called paraelectric – ferroelectric phase transformation, and it can be characterized by the spontaneous polarization of the crystal. The spontaneous polarization diminishes as temperature increases and disappears at the transformation temperature. This is a typical feature for almost every ferroelectric crystal (Rochelle salt is an exception). Application of mechanical stresses may change the transformation temperature as well as other ferroelectric properties, such as the spontaneous polarization and the hysteresis loop in the electric field-polarization response. The polar axis of a ferroelectric crystal is often referred to as the ferroelectric axis along which the crystal is polarized. Since a polar axis corresponds to two opposite directions, a ferroelectric crystal exhibits two distinct ferroelectric phases whose crystal lattices are identical but are oriented differently with respect to the lattice of the paraelectric phase. The spontaneous polarization vectors in these two ferroelectric phases are equal in magnitude but opposite in direction. Two ferroelectric phases which share the same polar axis are sometimes referred to as the electric twins, and a transformation between them is called polarization reversal. Differing from ferromagnetic materials a ferroelectric single crystal may be polarized spontaneously only in certain directions with respect to its lattice. A macroscopic region in which the direction of the spontaneous polarization differs from that in adjacent regions is referred

to as a ferroelectric domain. An interface separating two domains is called a domain wall. A single crystal may contain domain walls, even though it can not have grain boundaries, by definition. Domains are related in a manner which is quite analogous to the relationship of crystallographic twins which are commonly observed in some binary metallic systems, such as those of martensites. Experimental observation indicates that polarization reversal often takes place in the form of domain wall motions. Both ferroelectric–paraelectric transformation and polarization reversal may be induced by application of thermomechanical loading, electric field or their combined influence.

1.2 Crystallography of ferroelectricity: The perovskite oxide family

In ferroelectric crystals, the spontaneous polarization is produced by the atomic arrangement of ions in the crystal structure, depending on their positions, as in conventional ferroelectrics, or on charge ordering of multiple valences, as in electronic ferroelectrics. A nonzero spontaneous polarization can be present only in a crystal with a polar space group, as mentioned before. However, for ferroelectricity it must also be possible to switch between different variants with an applied electric field, which implies that many polar crystals are not considered ferroelectric. One condition that ensures the presence of discrete states of different polarization and enhances the possibility of switching between them with an accessible electric field is that the crystal structure can be obtained as a symmetry-breaking distortion of a higher-symmetry reference state. This involves a polar displacement of the atoms in the unit cell, which may be coupled to non–polar atomic displacement patterns and to the corresponding strain; the latter coupling can be quite strong in some ferroelectric oxides, producing piezoelectric behavior and epitaxial strain phase diagrams. In most ferroelectrics, there is a phase transition from the ferroelectric state, with multiple symmetry-related variants, to a non–polar paraelectric phase, with a single variant, with increasing temperature. In most of these cases the high–symmetry reference structure is the same as the crystallographic structure observed in the paraelectric phase. Measured ferroelectric transition temperatures range from very low (-200^0C) to very high (*over* 1000^0C); for the latter systems there is the possibility that the material melts before the transition

temperature is reached. The symmetry-breaking relation between the high-symmetry paraelectric structure and the ferroelectric structure is consistent with a second-order transition, and can be described with a Landau theory where polarization is the primary order parameter. This analysis naturally leads to the prediction that the dielectric susceptibility diverges at the transition. Most of the information about crystal structure

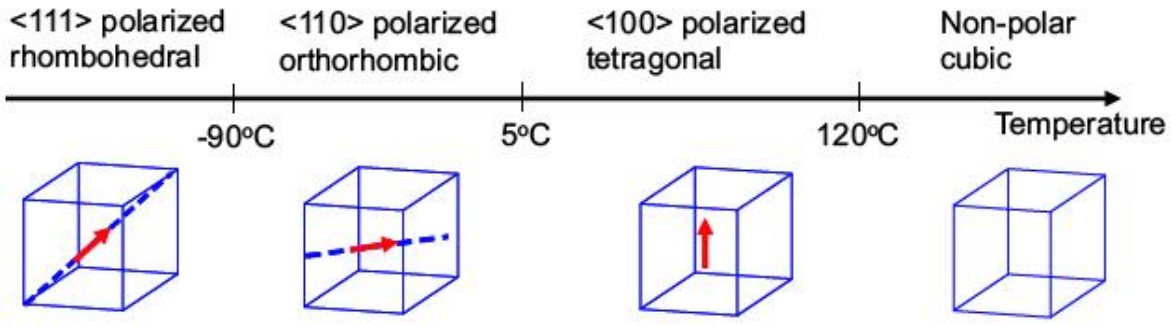

Figure 1.1: The different structures of $BaTiO_3$ at various temperatures

of ferroelectrics has been experimentally obtained from X–ray and neutron–diffraction structural determinations. These yield the average crystallographic structure. Studies of diffuse scattering and local probes, such as pair-density correlation function analysis and extended X-ray absorption fine-structure spectroscopy reveal that local distortions and fluctuations are also very important features of the crystal structure.

While ferroelectricity was discovered in hydrogen-bonded materials, Rochelle salt and K-D-P, the discovery in 1949 of ferroelectricity in the much simpler, nonhydrogen-containing, perovskite oxide $BaTiO_3$ dramatically changed the physical understanding of this phenomenon. Barium Titanate is the first of the very large and extensively studied perovskite oxide family, which includes not only perovskite compounds, but also ordered and disordered solid solutions. The relative simplicity of the perovskite structure led to a deeper understanding of the origin of ferroelectricity and quantitative phenomenological and first-principles modeling.

The perovskite oxide family own the composition ABO_3, where A and B each represent a cation element or mixture of two or more such elements or vacancies. The physical properties of the entire family are extremely diverse: depending on the composition and cationic ordering, they can be metallic or insulating and exhibit many

different types of structural and magnetic order. The perovskite oxides that are ferroelectrics in bulk crystalline form are a subfamily; other related compounds might have a tendency to a ferroelectric instability that is, however, not manifest in the bulk crystal due to the dominance of other, non–ferroelectric, competing types of order. The first

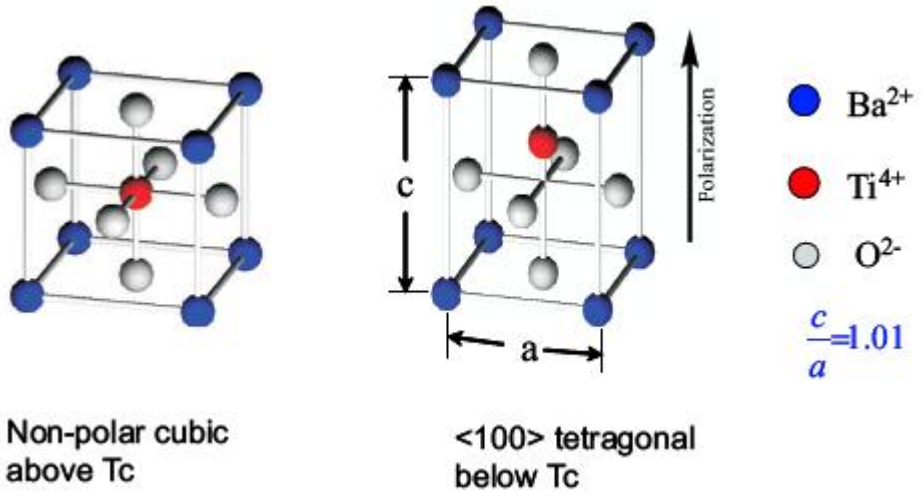

Figure 1.2: Cubic to tetragonal phase transformation of the unit cell

perovskite oxide compound identified as being ferroelectric was $BaTiO_3$. The formal valences are +2 for Ba and +4 for Ti, exactly balancing the negative total valence of the oxygens. At high temperature, it has a paraelectric cubic perovskite structure. At 120^0C, it transforms from a cubic phase to a ferroelectric tetragonal phase. This phase remains stable until 5^0C, where there is a second transformation to a ferroelectric phase of orthorhombic symmetry . The last transition occurs at -90^0C. The low-temperature ferroelectric phase is rhombohedral. Each transition is accompanied by small atomic displacements, dominated by displacement of the Ti ion relative to the oxygen octahedron network, and a macroscopic strain. In the successive ferroelectric phases, the polar axis is aligned respectively along the $< 100 >$, $< 110 >$ and $< 111 >$ directions corresponding to the direction of the atomic displacements with respect to their position in the cubic reference structure, as shown in Figure 1.1. In Figure 1.2 the cubic to tetragonal phase transition is depicted, where one can notice the ionic displacements.

1.3 Macroscopic view

1.3.1 Landau Theory

Based on symmetry considerations, Landau theory (25) can provide a reliable description of a systems equilibrium behavior near a phase transition. Landau theory can serve as a conceptual bridge between microscopic models and observed macroscopic phenomena. In this section we give a brief presentation of the application of Landau theory to bulk ferrolectrics with spatially uniform polarization.

For bulk ferroelectrics the thermodynamic state in equilibrium can be completely specified by the values of specific variables .These include the temperature T, the polarization P, the electric field E, the strain e, and the stress σ. Usually electric fields and elastic stresses are applied externally, so we can regard the polarization and the strain as internal or dependent variables. A fundamental postulate of thermodynamics applied to a ferroelectric is that its free energy F can be generally expressed as a function of ten variables (three components of polarization, six components of the stress tensor, and finally one of temperature). The most important thermodynamic principle that we will employ is that the values of the dependent variables in thermal equilibrium are obtained at the free-energy minimum when the free energy is optimized. We make the key approximation that in the vicinity of a phase transition we can expand the free energy in powers of the dependent variables with coefficients that can be fitted to experiment. In order to be more specific, we take a simple example where we expand the free energy in terms of a single component of the polarization; for simplicity we ignore the strain field, an assumption that might be appropriate for a uniaxial ferroelectric. We shall choose the origin of energy for the free unpolarized, unstrained crystal to be zero, and hence we write

$$F = \frac{1}{2}aP^2 + \frac{1}{4}bP^4 + \frac{1}{3}cP^6 - E\,P, \tag{1.1}$$

where a,b and c are material parameters. The equilibrium configuration is determined by finding the minima of the free energy

$$\frac{\partial F}{\partial P} = 0 \Rightarrow E = aP + bP^3 + cP^5 \tag{1.2}$$

where one can notice the non-linearity between the two fields.

Thus we can determine the linear dielectric susceptibility above the transition by differentiating this equation with respect to P and setting polarization to zero $P = 0$ to obtain

$$\chi = \frac{P}{E} = \frac{1}{a}. \tag{1.3}$$

In the Landau-Devonshire theory it is assumed that around the Curie point $a = a_0(T - T_0)$ and the other coefficients in the free-energy expansion are independent of temperature. Substituting in Eq. (1.2) we find an expression for the dielectric stiffness

$$k = \frac{1}{\chi} = a_0(T - T_0) \tag{1.4}$$

which captures the Curie-Weiss behavior observed in most ferroelectrics for $T > T_0$. If we include the linear temperature dependence of a, we have the general expression for the free energy

$$F = \frac{1}{2}a_0(T - T_0)P^2 + \frac{1}{4}bP^4 + \frac{1}{3}cP^6 - E\,P, \tag{1.5}$$

where a_0 and c are both positive in all ferroelectrics. The sign of the parameter b is proved to be essential in characterizing the type of transition in ferroelectrics.

1.3.2 Second-Order Transition

If $b > 0$ and $c = 0$ (not necessary), then a second-order transition occurs at $T = T_0$, and the free energy will evolve continuously as a function of decreasing temperature from the plot with $P = 0$ in Figure 1.3a to the second, that has minima at finite polarizations $P = P_0$. The spontaneous polarization can be estimated by setting $E = 0$ in Eq. (1.2); since all the coefficients are positive, we will only retain the two lowest-order terms. The value of P_0 is

$$P_0 = \sqrt{\frac{a_0(T - T_0)}{b}} \tag{1.6}$$

where it is deduced that the spontaneous polarization increases with decreasing temperature from the point $T = T_0$. We note that if we determine the dielectric stiffness below the transition ($T < T_0$) then we find

$$k = 2a_0(T_0 - T), \tag{1.7}$$

which is to be compared with Eq. (1.4), its value just above T_0; these two expressions suggest that k vanishes at $T = T_0$ and that consequently the dielectric susceptibility diverges (see Figure 1.3b).

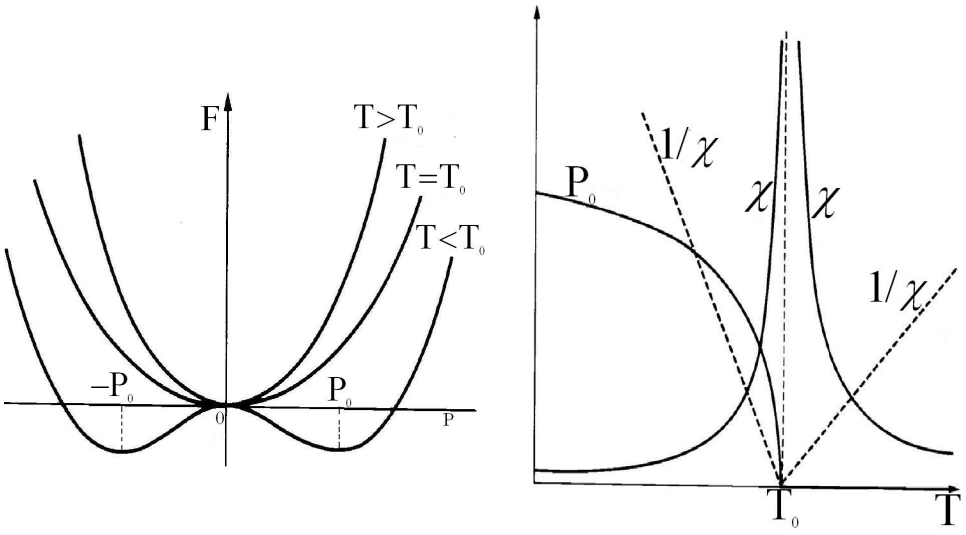

Figure 1.3: Second-order phase transition (a) free energy for various ranges of temperature, (b) spontaneous polarization and dielectric susceptibility as functions of temperature.

1.3.3 First-Order Transition

Now, considering the case of $b < 0$, while c remains positive it is clear that even if $T > T_0$ (such that the quadratic coefficient is positive) the free energy may have a subsidiary minimum at nonzero polarization. As the temperature reduces, this minimum will drop in energy below that of the unpolarized state, and so will be the thermodynamically favored configuration. The temperature at which this happens is, by definition, the Curie temperature T_c, which, however, now exceeds T_0. At any temperature between T_c and T_0 the unpolarized phase exists as a local minimum of the free energy. The most important feature of this phase transition is that the order parameter jumps discontinuously to zero at T_c. This type of phase spontaneous polarization, the

dielectric stiffness and the linear susceptibility are shown in Figure 1.4. We note that

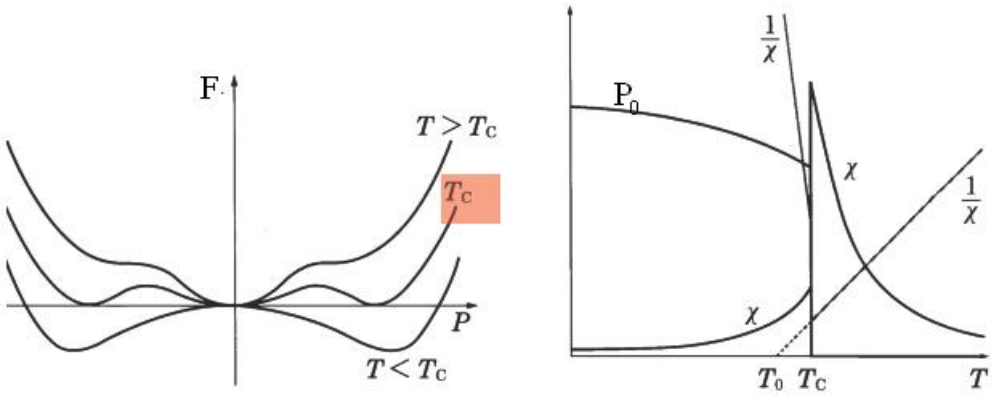

(a) (b)

Figure 1.4: First-order phase transition (a) free energy for various ranges of temperature, (b) spontaneous polarization and dielectric susceptibility as functions of temperature.

at $T = T_c$ the three minima are energetically degenerate. As a result, the systems behavior at $T = T_c$ will depend on whether it is approaching T_c from lower or higher temperatures. More specifically, the system will be in one of the two finite polarization ($P \neq 0$) minima if it is heated from an initial low temperature, whereas it will be in a paraelectric state ($P = 0$) if the initial temperature is high. Indeed, the phenomenon of thermal hysteresis, where the transition temperature depends on whether the sample is heated or cooled, is prevalent in a number of first-order ferroelectrics including barium titanate. We emphasize that it is only for $T_0 < T_c$ that the ferroelectric minima are thermodynamically favorable. In a ferroelectric below T_0 there are (at least) two minima of the free energy, corresponding to spontaneous polarizations of different spatial orientations. The barrier between these minima means that a small electric field will not immediately switch the polarization.

As before, the spontaneous polarization can be estimated by setting $E = 0$ in Eq. (1.2), thus for $T \geq T_c$

$$P_0 = \frac{-b \pm \sqrt{b^2 - 4ac(T - T_0)}}{2c} \tag{1.8}$$

and for $T \leq T_c$ its value becomes

$$P_0 = \frac{-b + \sqrt{b^2 - 4ac(T - T_0)}}{2c}. \tag{1.9}$$

1.3.4 Electrostriction

So far we restricted ourselves in rigid ferroelectrics, i.e. strain effects were assumed negligible. In real ferroelectrics, phase transitions from the paraelectric to the ferroelectric state are accompanied by the existence of a remanent strain. Consider a cubic crystal (e.g., $BaTiO_3$) that undergoes a ferroelectric phase transition to a state where the polarization can point along one of the six orthogonal cubic directions. Now it is clear that there is a special axis and so it would no longer be expected that the crystal as a whole will remain cubic one expects a distortion into a tetragonal crystal, which can be described by a tetragonal strain e_0. In the framework of a phenomenological theory spontaneous strain for a uniaxial ferroelectric will take the form

$$e_0 = \gamma P^2, \tag{1.10}$$

where γ is the so called electrostrictive coefficient.

Thus we can easily extend the Landau theory to elastic ferroelectrics by writing the free energy as

$$F = \frac{1}{2}C(e - e_0)^2 + \frac{1}{2}aP^2 + \frac{1}{4}bP^4 + \frac{1}{3}cP^6 - E\,P - e\,\sigma, \tag{1.11}$$

where C is the elastic coefficient. Using the above free energy, which now consists of elastic and electric terms we can now determine the properties in equilibrium by minimizing with respect to both P and e. For more details one is referred to (59; 72).

1.4 Domains in ferroelectric single crystals

It seems useful to describe the formation of domains in a single ferroelectric crystal belonging to the perovskite oxide family, such as Barium Titanate. The spontaneous polarization in a ferroelectric crystal is usually not uniformly aligned throughout the material along the same direction. The six directions (including positive and negative orientations) along the three of the cubic cell (see Figure 1.2) in $BaTiO_3$ are equivalent,

and spontaneous polarization may arise with equal probability along any of them when the crystal is cooled through the ferroelectric phase-transition temperature. Directions along which the polarization will develop depend on the electrical and mechanical boundary conditions imposed on the sample. The regions of the crystal with uniformly oriented spontaneous polarization are called ferroelectric domains. The region between two domains is called a domain wall. The walls that separate domains with oppositely oriented polarization are called 180° walls and those that separate regions with mutually perpendicular polarization are called 90° walls. In the domain-wall region, the polarization changes from one domain to another continuously but steeply. The ferroelectric domain walls are therefore much narrower than the domain walls in ferromagnetic materials. Experimental observations show that the width of the domain walls in ferroelectric materials is of the order of $1 - 10\,\mathrm{nm}$, that is, as little as 2–3 crystal unit cells. The width of the domains increases with increasing temperature, as the phase transition is approached.

The ferroelectric domains form to minimize the electrostatic energy of the depolarizing fields and the elastic energy associated with the mechanical constraints to which the ferroelectric material is subjected as it is cooled through the paraelectric–ferroelectric phase transition . Onset of spontaneous polarization at the transition temperature leads to the formation of surface charges. This surface charge produces an electric field, called the depolarizing field, which is oriented oppositely to the polarization. The depolarizing field will form whenever there is a nonhomogeneous distribution of the spontaneous polarization, for example, due to a change in the direction of the polarization at grain boundaries. The depolarizing field may be very strong rendering the single-domain state of the ferroelectric energetically unfavorable. The electrostatic energy associated with the depolarizing field may be minimized if: (1) the ferroelectric splits into domains with oppositely oriented polarization, or (2) the depolarizing charge is compensated by electrical conduction through the crystal or by charges from the surrounding material. The depolarizing field often cannot be completely compensated, and as grown ferroelectric crystals often exhibit reduced or even zero pyroelectric and piezoelectric effects due to the presence of ferroelectric domains. Splitting of a ferroelectric crystal into domains may also occur due to the influence of mechanical stresses. The domain walls in $BaTiO_3$ may separate regions in which polarization orientation is antiparallel (180° domain walls) or perpendicular (90° domain walls) to each other.

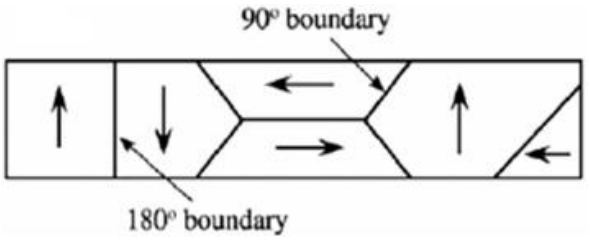

Figure 1.5: Domain structure in a single crystal of Barium Titanate

Both 90° and 180° walls may reduce the effects of depolarizing electric fields but only formation of 90° walls may minimize the elastic energy. A combination of electrical and elastic boundary conditions to which a crystal is subjected as it is cooled through the ferroelectric phase-transition temperature usually leads to a complex domain structure with many 90° and 180° domain walls, as shown schematically in Figure 1.5. Since domain walls themselves carry energy, the resulting domain-wall configuration will be such that the sum of the domain-wall energy, crystal surface energy, and elastic and electric fields energy is minimal.

The domain walls that differ in orientation from the spontaneous polarization vector are called ferroelectric domain walls and those that differ in orientation from the spontaneous strain tensor are called ferroelastic domain walls. In $BaTiO_3$, the 180° walls are purely ferroelectric because they differ only in orientation of the polarization vector. The 90° domain walls are both ferroelectric and ferroelastic, as their differ in orientation of both the polarization vector and the spontaneous strain tensor.

The types of domain walls that can occur in a ferroelectric crystal depend on the symmetry of both non-ferroelectric and ferroelectric phases of the crystal. In the rhombohedral phase of the $BaTiO_3$, for example, the direction of the polarization develops along the body diagonals (direction $< 111 >$) of the paraelectric cubic unit cell. This gives eight possible directions of the spontaneous polarization with 180°, 71° and 109° domain walls.

From a continuum point of view, domain walls can be considered as sharp interfaces. Obviously, one can describe the motion of the domain walls by a standard implementation of the sharp interface theory in electro-elastic solids. The treatment of the domain walls in ferroelectrics as sharp interfaces will be the subject of the third chapter.

1.5 Low dimensional ferroelectrics

Advances in computer and technological science are closely related to the properties of the materials at very low scales. Ferroelectric epitaxial islands and thin films receive considerable attention from academics and industries over the world, due to their usage as non-volatile computer memories (FE-RAM), sensors and transducers. The behavior of low dimensional ferroelectrics substantially deviate from the bulk behavior. For instance, in a $PbTiO_3$ particle the domain structure vanishes when its diameter is less than 20nm and ferroelectricity may disappear when the diameter is below 4nm. Thus, it is important to explore and produce theoretical models that give a satisfactory explanation on the size effect of ferroelectric properties. Therefore, different theoretical approaches, including phenomenological Landau theories, and atomic-level first-principles calculations have been used in order to study thin films, nanorods and nanodisks.

From a continuum point of view, the behavior of nanoscale ferroelectrics may be accomplished by utilizing the powerful Landau–Ginzburg theory supplied with the appropriate information. In ferroelectrics, size effects turn out to be a more loosely defined problem than in ferromagnets (59). In reality this is not the case: ferroelectricity is instead limited by the relevant electrical and mechanical boundary conditions, and in fact more frequently by the practical issues involved in producing high-quality samples on the extreme nanoscale. Within the Ginzburg-Landau type phenomenological theory, Kretschmer and Binder (44) introduced a framework for considering size effects through two lengths, the correlation length and the extrapolation length. This framework was then expanded and applied to a number of situations by Tilley and Zeks (67). The idea of an intrinsic size effect is largely driven by the concept of a correlation volume, this being related to the required number of aligned dipoles for ferroelectricity to occur. In fact, the strong longrange interactions along the polar axis and the weaker interactions perpendicular to this axis lead to an anisotropic correlation volume. Reducing the sample size below the critical length parallel to the polar axis modifies the balance between the short–range forces, which favor a centro-symmetric para-electric phase, and the long-range interactions. Thus, an instability of the ferroelectric phase might be expected for films below a certain thickness. Extremely pertinent to this discussion, however, is the question of what the size of this correlation length should be. In fact

this depends greatly on how close to the phase transition the system is, as it is given by $\xi = \sqrt{(\kappa/|\alpha|)}$, where $\alpha = \alpha_0(T - T_0)$ and κ is a material constant. While it is only a few lattice parameters far from the transition temperature, it should diverge close to the phase transition. Kretschmer and Binder (44) used a phenomenological approach to describe polarization variations at the film surface. To do so, a surface term was added to the Ginzburg-Landau-Devonshire expansion of the total free energy, leading to the introduction of the so-called extrapolation length δ, such that $dP/dz = P_0/\delta$ (for a uniaxial material). A positive extrapolation length δ indicates a decrease of the polarization near the surface, while a negative extrapolation length indicates an increase. By introducing this term, a polarization gradient is introduced into the film. This concept has then been used in many works to calculate polarization profiles. The weakness of the phenomenological approach resides in the fact that an extrapolation length has to be introduced. Theoretical works based on Ginzburg-Landau-Devonshire theory predicted that ferroelectricity is suppressed in small particles and thin films at relatively large sizes compared to what has been recently observed experimentally.

In this work, we study the behavior of thin films within the context of a new phase field model accumulating electric field gradient effects (see Subsection 2.5.5). Perhaps this attempt may shed light to special aspects of thin films and provide new insights as well as detailed simulations.

Chapter 2

Continuum phase field approaches

"The miracle of the appropriateness of the language of mathematics for the formulation of the laws of physics is a wonderful gift which we neither understand nor deserve."

E.P. Wigner

There are two basic formulations concerning the electrical constitutive behavior of dielectric materials. Normally, it is the electric polarization density that used as an independent constitutive variable in the stored energy function (68). Alternatively, the electric field itself – or equivalently, the electric potential gradient – can be used for the same purpose (66). Thus one may distinguish two main approaches in the development of elastic dielectric theories: the polarization and the electric field based models. The mathematical description of the linear elastic dielectric materials, e.g. piezoelectrics, consists of two partial differential equations: the mechanical equilibrium and the Gauss equation. Consequently, one has to determine two unknown fields: the displacement and the polarization vector (or the electric potential). In that case, polarization and electric field vectors are thermodynamically conjugate to each other thus, it is a matter of taste which should be considered as dependent or as an independent constitutive variable.

A well–established theory for the equilibrium and the evolution of the microstructure is the key–factor for the understanding of the macroscopic behavior of ferro-

electrics. It is apparent that a new constitutive variable accounting for the microstructure is needed. Hence, the complete mathematical description of elastic ferroelectrics needs an additional equation. Toupin (68) has already introduced such an additional equation, the so–called intramolecular balance equation, for the description of general non–linear elastic dielectrics (see also 31; 32; 50). In classical Landau theory on rigid ferroelectrics (25) presented in the previous section, the order parameter, i.e., the polarization vector, has been used as (the sole) constitutive variable. The standard theories on elastic ferroelectrics use also the polarization vector as basic constitutive variable (18; 19; 22; 63; 65; 74; 81**?** , etc.). Nevertheless, all of them use also the electric field as constitutive variable. Thus, polarization and electric field have their own position in the energy functional and, certainly, in the final partial differential equations.

It is well–documented that higher gradient theories, in general, account for non–local and size effect phenomena (53; 64). Thus, it seems they are appropriate to model aspects related to the microstructure of a material. For instance, the polarization gradient tensor has been proposed as an additional constitutive variable in a general elastic dielectric theory to account for surface effects (54). In elastic ferroelectric theories based on polarization vector, the addition of the polarization gradient in the list of the constitutive variables plays an important role in connection with the geometry of the domain walls (17; 19; 65).

As concerns the electric field based models, the insertion of the electric field gradient into the list of the constitutive variables has been proposed for rigid dielectrics by Kafadar (35). In elastic dielectrics, the electric field gradient (or equivalently, the second gradient of the electric potential) has already been used in the formulation of non–linear theories (20; 28; 31; 32; 39; 40; 76) as well as in many interesting applications (75; 77). However, to our best knowledge, there are no applications of the electric field gradient theories in ferroelectrics. The insertion of the electric field gradient results in a new constitutive equation and gives an alternative form to the overall mathematical description of ferroelectrics. For instance, while the energetically conjugate of the electric field is the (dipole) polarization vector, the energetically conjugate of the electric field gradient is the quadrupole polarization tensor. In that case, a model with quadrupole polarization is arisen, instead of the polarization gradient tensor of the standard theories.

In this work, in addition to the electric field, the electric field gradient is added as a constitutive variable in the stored energy function. Thus besides the dipole polarization vector (the conjugate variable of electric field), the quadrupole polarization tensor (conjugate to the electric field gradient) is introduced. However, these quantities represent the reversible electrical behavior of the material. The irreversible behavior is inserted into the picture through the phase separation energy, a function of the total spontaneous polarization. The spontaneous polarization is also a new constitutive variable consisting of two distinct parts: the spontaneous dipole polarization and the spontaneous quadrupole polarization. Summing up, the objective of this work is an alternative theory for elastic ferroelectrics by the use of the electric field gradient and the total spontaneous polarization as independent constitutive variables in addition to those ones of electric field and strain tensor.

2.1 The polarization gradient theory of ferroelectrics

The polarization gradient theory has proved to be successful in modeling the microscopic and macroscopic behavior of elastic ferroelectrics. Several researchers over the years have proposed different continuum models that are under the umbrella of the polarization gradient theory. These models use the total polarization vector as the first order parameter and the mechanical strain as the second order parameter of the evolutionary process. We think it is appropriate to outline these phase field models so as to give a complete picture of the current modeling techniques in ferroelectrics.

2.1.1 Model I

The temporal evolution of the domain structure is governed by the TDGL (Time Dependent Ginzburg Landau) equations as follows (18; 63; 70)

$$\frac{\partial P_i(\mathbf{r},t)}{\partial t} = -L\,\frac{\delta F}{\delta P_i(\mathbf{r},t)},\ i=1,2,3 \tag{2.1}$$

where t and L denote time and the kinetic coefficient, respectively, and $\mathbf{r}$ represents the spatial vector. The quantity F represents the total free energy of the system given by

$$F = \int_\Omega (f_L + f_G + f_{dip} + f_{elec} + f_{elas})d\Omega \tag{2.2}$$

where $f_L, f_G, f_{dip}, f_{elec}, f_{elas}$ are the bulk-free energy, the gradient energy, the long–range interaction of dipole-dipole, the electric energy because of the external electric field, and the elastic strain energy, respectively.

The bulk-free energy density is responsible for the different orientations of the polarization within the material and takes the form

$$\begin{aligned} f_L(P_i) &= \alpha_1(P_1^2+P_2^2+P_3^2)+\alpha_{11}(P_1^4+P_2^4+P_3^4) \\ &+ \alpha_{12}(P_1^2P_2^2+P_2^2P_3^2+P_1^2P_3^2)+\alpha_{111}(P_1^6+P_2^6+P_3^6) \\ &+ \alpha_{112}[P_1^4(P_2^2+P_3^2)+P_2^4(P_1^2+P_3^2)+P_3^4(P_1^2+P_2^2)] \\ &+ \alpha_{123}(P_1^2P_2^2P_3^2), \end{aligned} \tag{2.3}$$

where $a_{11}, a_{12}, a_{111}, a_{112}, a_{123}$ are the material coefficients. It is noted that $\alpha_1 = (T - T_0)/2\epsilon_0 C_0$ where T and T_0 are the temperature and Curie temperature, respectively, and ϵ_0 and C_0 are the dielectric constant and Curie constant, respectively.

The contribution of domain wall energy is given by the gradient of the polarization field. For a cubic system, the domain wall energy density in the lowest order is considered as follows

$$\begin{aligned} f_G(P_{i,j}) &= G_{11}(P_{1,1}^2+P_{2,2}^2+P_{3,3}^2)+G_{12}(P_{1,1}P_{2,2}+P_{3,3}P_{2,2}+P_{1,1}P_{3,3}) \\ &+ G_{44}[(P_{1,2}+P_{2,1})^2+(P_{2,3}+P_{3,2})^2+(P_{1,3}+P_{3,1})^2] \\ &+ G_{44}^{'}[(P_{1,2}-P_{2,1})^2+(P_{2,3}-P_{3,2})^2+(P_{1,3}-P_{3,1})^2], \end{aligned} \tag{2.4}$$

where G_{ij} are the gradient coefficients.

The long-range interaction of dipole-dipole is very important in the formation of the "head-to-tail" structure. Its expression is given by

$$\begin{aligned} f_{dip} &= \frac{1}{8\pi\epsilon}\int d^3r_i d^3r_j \left(\frac{P(r_i)\cdot P(r_j)}{|r_i-r_j|^3}-\frac{3(P(r_i)\cdot(r_i-r_j))(P(r_j)\cdot(r_i-r_j))}{|r_i-r_j|^5}\right) \\ &= \frac{1}{2\pi\epsilon}\int \frac{d^3\xi}{(2\pi)^3}|\mathbf{P}(\xi)\cdot\mathbf{n}|, \end{aligned} \tag{2.5}$$

where

$$\mathbf{P}(\xi) = \int \frac{d^3\mathbf{r}}{(2\pi)^3}\mathbf{P}(\mathbf{r})e^{-i\xi\cdot\mathbf{r}} \tag{2.6}$$

is the Fourier transformation of the polarization field and $n_i = \xi_i/\xi$, $(i = 1, 2, 3)$ is the unit vector in the reciprocal Fourier space.

The electrical energy density is given by the relation

$$f_{elec} = -E_i^{ext} P_i \tag{2.7}$$

where E_i^{ext} represents the external electric field. Finally, the elastic strain e_{ij} and elastic strain energy f_{elas} are involved in the course of polarization switching as follows

$$f_{elas} = \frac{1}{2} c_{ijkl} e_{ij} e_{kl} \tag{2.8}$$

where c_{ijkl} is the elastic stiffness tensor; the elastic strain $e_{ij} = \varepsilon_{ij} - \varepsilon_{ij}^{\circ}$ in which ε_{ij} is the total strain and the spontaneous strain ε_{ij} can be taken as eigenstrains and associated with the spontaneous polarizations as follows

$$\varepsilon_{ij}^{\circ} = \gamma_{ijkl} P_k P_l \tag{2.9}$$

where γ_{ijkl} are the electrostrictive coefficients.

2.1.2 Model II

Consider an elastic ferroelectric body occupying a domain Ω with boundary $\partial\Omega$. The total energy functional I of the body may be written as

$$I[u_i, \phi, P_i] = \int_{\Omega} \left[f_G(P_{i,j}) + W(e_{ij}, P_i) \right] d\Omega + \frac{\varepsilon_0}{2} \int_{\mathbb{R}^3} \phi_{,i}^2 d\Omega, \tag{2.10}$$

where f_G is the domain wall energy as it is given by Eq. (2.4) and $W = f_L + f_{elas}$ is the Landau-Devonshire energy density due to elastic strain and polarization. The last term is the electrostatic energy associated with electric field $E_i = -\phi_{,i}$ caused (in all of space) by the polarization.

The governing equations of polarization evolution are obtained as the **gradient flow** associated with the total potential energy. According to Zhang and Bhattacharya (81) these equations are

$$\mu \dot{P}_i = \left(\frac{\partial f_G}{\partial P_{i,j}} \right)_{,j} - \frac{\partial W}{\partial P_i} - \phi_{,i} \tag{2.11}$$

$$P_{i,i} - \varepsilon_0 \phi_{,ii} = 0, \tag{2.12}$$

$$\sigma_{ji,j} = 0, \tag{2.13}$$

where μ^{-1} is the mobility of the process. Equation (2.11) governs the evolution of the polarization within the body, with boundary conditions concerning either a prescribed value for the polarization ($\mathbf{P} = \bar{\mathbf{P}}$) or for the polarization flux ($\nabla \mathbf{P}\mathbf{n} = \boldsymbol{\pi}^*$).Equations (2.12) and (2.13) are the Gauss law and mechanical equilibrium, respectively.

The treatment of electrostatics here is different from that in the Model I. Here, the electrostatic field is computed explicitly instead of being included implicitly using dipole-dipole interactions in the energy. Consequently, one is not restricted to periodic domains and fast Fourier transforms. Instead it is possible to apply realistic boundary conditions and perform easier computations.

2.2 An electric field gradient theory for ferroelectrics

Theories concerning elastic dielectrics with quadrupole polarization have been proposed in the last decades. These theories make use of the fundamental principles of continuum electrodynamics. A well known macroscopic continuum model is that of Tiersten's (66), which provides a satisfactory interpretation of the the electric properties of an elastic dielectric. Kalpakidis and Massalas (39) presented an extension of Tiersten's model accounting for quadrupole effects. According to this theory, one can define the dipole and quadrupole polarization as

$$p_i(x_k, t) = \rho^e \xi_i, \tag{2.14}$$

$$q_{ij}(x_k, t) = \frac{1}{2}\rho^e \xi_i \xi_j = \frac{1}{2} p_i \xi_j, \tag{2.15}$$

where ξ_i is the displacement vector of the electronic continuum with respect to the lattice and ρ^e the electronic charge density (see (66) for the details).

Equation (2.15) is an indication of a possible link between the quadrupole and dipole polarization. Taking this as motivation, one can assume that

$$q_{ij} = f_{ij}(p_k p_l). \tag{2.16}$$

It is clearly stated that this is a heuristic relation that facilitates the set up of the proposed theory. Trimarco (69) proposed an analogous relation between the quadrupole polarization and the dipole polarization gradient.

In the case where the quadrupole polarization is accounted for, the total polarization π_i has the form (28; 32; 69)

$$\pi_i = p_i - q_{ij,j}. \tag{2.17}$$

2.2.1 The energy functional

Consider an elastic ferroelectric body occupying a domain Ω with boundary $\partial\Omega$. The total energy functional I of the body can be written as

$$\begin{aligned} I[u_i, \phi, \pi_i^s] = \int_\Omega \left[W\left(e_{ij}, \phi_{,i}, \phi_{,ij}\right) + \Psi(\pi_i^s) - \tfrac{1}{2}\varepsilon_0 \phi_{,i}\phi_{,i} + \pi_i^s \phi_{,i}\right] dv \\ - \int_{\partial\Omega} \left(t_i u_i + \bar{\sigma}\phi + \bar{\pi}_i \phi_{,i}\right) ds, \end{aligned} \tag{2.18}$$

where e_{ij} is the infinitesimal strain, u_i the displacement field, ϕ the electric potential, π_i^s the total spontaneous polarization and ε_0 the vacuum permittivity. Also, W is the energy of deformation and electric field and Ψ denotes the spontaneous polarization energy or the phase separation energy. The last integral contains the external loading terms with t_i, $\bar{\sigma}$ and $\bar{\pi}_i$ denoting the traction, the surface charge density and the surface dipole polarization density.

The first integral in Eq. (2.18) is the energy stored within the body and the space occupied by the body. One may assume that this energy density consists of three parts: the energy of the matter, the field energy and the interaction field–matter energy (40). Here, the matter energy consists of the first two terms in Eq. (2.18), i.e.:

$$\Sigma(e_{ij}, \phi_{,i}, \phi_{,ij}, \pi_i^s) = W(e_{ij}, \phi_{,i}, \phi_{,ij}) + \Psi(\pi_i^s).$$

The field energy is represented by the third term which is the standard electrostatic field energy. The fourth term of the first integral, i.e., $\pi_i^s \phi_{,i}$ concerns the interaction energy between matter and field.

2.2.2 The extremum principle

The arguments of functional in Eq. (2.18) are the displacement field, the electric potential and the spontaneous polarization vector. It is assumed that among all admissible functions, the real ones (the solution) provide an extremum to the the energy function.

Consequently, if $(\mathbf{u}, \phi, \boldsymbol{\pi}^s)$ represents a solution of a physical problem, the variation of I with respect to its arguments should vanish, that means

$$\delta I(\mathbf{u}, \phi, \boldsymbol{\pi}^s; \delta\mathbf{u}, \delta\phi, \delta\boldsymbol{\pi}^s) = 0, \tag{2.19}$$

for any arbitrary variation $\delta\mathbf{u}$, $\delta\phi$, and $\delta\boldsymbol{\pi}^s$. Thus the variation of the energy with each one of the fields u_i, ϕ and π_i^s should vanish.

2.2.2.1 Variation of displacement

We start examining the variation of I with respect to the displacement u_i:

$$\delta I(u_i, \phi, \pi_i^s; \delta u_i) = 0,$$

or, equivalently

$$\begin{aligned}
&\int_\Omega \frac{\partial W}{\partial e_{ij}} \delta e_{ij} dv - \int_{\partial\Omega} t_i \delta u_i ds \\
&= \int_\Omega \frac{\partial W}{\partial e_{ij}} \delta u_{i,j} dv - \int_{\partial\Omega} t_i \delta u_i ds \\
&= \int_{\partial\Omega} \left(\frac{\partial W}{\partial e_{ij}} n_j - t_i \right) \delta u_i ds - \int_\Omega \left(\frac{\partial W}{\partial e_{ij}} \right)_{,j} \delta u_i dv = 0,
\end{aligned} \tag{2.20}$$

2.2.2.2 Variation of electric potential

The variation of the total potential energy functional with respect to the electrostatic field should vanish

$$\delta I(u_i, \phi, \pi_i^s; \delta\phi) = 0,$$

or

$$\begin{aligned}
&\int_\Omega \left[\left(\frac{\partial W}{\partial \phi_{,i}} \right) \delta(\phi_{,i}) + \left(\frac{\partial W}{\partial \phi_{,ij}} \right) \delta(\phi_{,ij}) - \varepsilon_0 \phi_{,i} \delta(\phi_{,i}) + \pi_i^s \delta(\phi_{,i}) \right] dv \\
&- \int_{\partial\Omega} \left[\bar{\sigma} \delta\phi + \bar{\pi}_i \delta(\phi_{,i}) \right] ds = 0.
\end{aligned}$$

After some integrations by parts, one obtains

$$\begin{aligned}
&\int_\Omega \left[-\left(\frac{\partial W}{\partial \phi_{,i}}\right)_{,i} + \left(\frac{\partial W}{\partial \phi_{,ij}}\right)_{,ij} + \varepsilon_0 \phi_{,ii} - \pi^s_{i,i} \right] \delta\phi dv \\
&+ \int_{\partial\Omega} \left[\left(\frac{\partial W}{\partial \phi_{,i}} - \left(\frac{\partial W}{\partial \phi_{,ij}}\right)_{,j} - \varepsilon_0 \phi_{,i} + \pi^s_i \right) n_i - \bar{\sigma} \right] \delta\phi ds \\
&- \int_{\partial\Omega} \Pi_i \delta(\phi_{,i}) ds = 0.
\end{aligned} \tag{2.21}$$

where

$$\Pi_i = \frac{\partial W}{\partial \phi_{,ij}} n_j + \bar{\pi}_i. \tag{2.22}$$

The last integral in Eq. (2.21) needs further elaboration. Using the analysis presented in (40), one can prove

$$\int_{\partial\Omega} \Pi_i \delta(\phi_{,i}) ds = -\int_\gamma [\![\Pi^\alpha b_\alpha]\!] \, \delta\phi dl - \int_{\partial\Omega} \Pi^\alpha_{;\alpha} \delta\phi ds + \int_{\partial\Omega} \Pi_n n_i (\delta\phi)_{,i} ds, \tag{2.23}$$

where γ is a possible singular curve on $\partial\Omega$ (i.e. an edge of a parallelepid) and b_α is the bi-normal vector of γ, Π^α and Π_n the surface and normal component, respectively.

Finally, inserting Eq. (2.23) into Eq. (2.21), one obtains

$$\begin{aligned}
&\int_\Omega \left[-\left(\frac{\partial W}{\partial \phi_{,i}}\right)_{,i} + \left(\frac{\partial W}{\partial \phi_{,ij}}\right)_{,ij} + \varepsilon_0 \phi_{,ii} - \pi^s_{i,i} \right] \delta\phi dv \\
&+ \int_{\partial\Omega} \left[\left(\frac{\partial W}{\partial \phi_{,i}} - \left(\frac{\partial W}{\partial \phi_{,ij}}\right)_{,j} - \varepsilon_0 \phi_{,i} + \pi^s_i \right) n_i - \bar{\sigma} + \Pi^\alpha_{;\alpha} \right] \delta\phi ds \\
&+ \int_{\partial\Omega} \Pi_n n_i (\delta\phi)_{,i} ds + \int_\gamma [\![\Pi^\alpha b_\alpha]\!] \, \delta\phi dl = 0.
\end{aligned} \tag{2.24}$$

2.2.2.3 Variation of spontaneous polarization

The variation of I with respect to π^s_i provides

$$\delta I(u_i, \phi, \pi^s_i; \delta\pi^s_i) = \int_\Omega \left(\frac{\partial \Sigma}{\partial \pi^s_i} \delta\pi^s_i + \phi_{,i} \delta\pi^s_i \right) dv. \tag{2.25}$$

2.2.3 Field equations, boundary conditions and constitutive relations

Focusing on the volume integrals of the variational Eqs. (2.20), (2.24) and (2.25) and taking into account that the variations δu_i, $\delta\phi$ and $\delta\pi_i^s$ are arbitrary, one can extract the following field equations:

$$\left(\frac{\partial W}{\partial e_{ij}}\right)_{,j} = 0, \tag{2.26}$$

$$\left(\frac{\partial W}{\partial \phi_{,i}}\right)_{,i} - \left(\frac{\partial W}{\partial \phi_{,ij}}\right)_{,ij} - \varepsilon_0\phi_{,ii} + \pi^s_{i,i} = 0, \tag{2.27}$$

$$-\frac{\partial \Sigma}{\partial \pi_i^s} - \phi_{,i} = 0, \tag{2.28}$$

for all $\mathbf{x}$ in Ω.

On the other hand, since there are no data for the displacement field on the boundary $\partial\Omega$, the variation of the displacement is arbitrary on $\partial\Omega$, thus the surface integral of Eq. (2.20) vanishes only if

$$\frac{\partial W}{\partial e_{ij}} n_j = t_i. \tag{2.29}$$

Besides, there is no boundary data for the electric potential ϕ, thus the variation $\delta\phi$ will be arbitrary on $\partial\Omega$ as well. However, one should be cautious because there are two surface integrals in Eq. (2.24). However, it is useful to recall that $\delta\phi$ is initially defined on $\Omega \subset \mathbb{R}^3$. Hence, being constrained on $\partial\Omega$ (i.e., a two dimensional set of zero measure in $\mathbb{R}^3$) one can easily conclude that the variation $\delta\phi$ is independent of its gradient $\delta\phi_{,i}$ on the boundary surface $\partial\Omega$. Hence, the following boundary (jump) conditions are obtained from the surface and line integrals of Eq. (2.24)

$$\left[\frac{\partial W}{\partial \phi_{,i}} - \left(\frac{\partial W}{\partial \phi_{,ij}}\right)_{,j} - \varepsilon_0\phi_{,i} + \pi_i^s\right] n_i = \bar{\sigma} - \Pi^\alpha_{;\alpha}, \quad \text{on} \quad \partial\Omega, \tag{2.30}$$

$$\begin{aligned} &\Pi_n = \Pi \cdot \mathbf{n} = 0, \quad \text{on} \quad \partial\Omega, \\ &[\![\Pi^\alpha b_\alpha]\!] = 0, \quad \text{on} \quad \gamma. \end{aligned} \tag{2.31}$$

The next step is to introduce the Cauchy stress tensor, the electric dipole polarization and the electric reversible quadrupole polarization density through the following relations

$$\sigma_{ij} = \frac{\partial W}{\partial e_{ij}}, \quad p_i^r = \frac{\partial W}{\partial \phi_{,i}}, \quad q_{ij}^r = \frac{\partial W}{\partial \phi_{,ij}} \tag{2.32}$$

Inserting the above constitutive relations into Eqs. (2.26)–(2.27), one obtains

$$\sigma_{ij,j} = 0 \tag{2.33}$$

and

$$D_{i,i} = 0, \tag{2.34}$$

for all $\mathbf{x} \in \Omega$, where D_i and P_i stand for the electric displacement and the total polarization field defined as

$$D_i = \varepsilon_0 E_i + \pi_i \tag{2.35}$$

and

$$\pi_i = \pi_i^s + p_i^r - q_{ij,j}^r \tag{2.36}$$

respectively. According to Eq. (2.17) the total spontaneous polarization vector can be written

$$\pi_i^s = p_i^s - q_{ij,j}^s, \tag{2.37}$$

where p_i^s and q_{ij}^s denote spontaneous dipole and quadrupole densities , respectively. Inserting Eq. (2.37) into Eq. (2.36) one obtains

$$\pi_i = \overbrace{p_i^s - q_{ij,j}^s}^{\substack{irreversible \\ part}} + \overbrace{p_i^r - q_{ij,j}^r}^{\substack{reversible \\ part}}. \tag{2.38}$$

Notice that the total polarization vector is separated in two parts.

After the above considerations, the boundary conditions (2.29), (2.30) and (2.31) take the form

$$\sigma_{ij} n_j = t_i, \quad \text{on} \quad \partial\Omega \tag{2.39}$$

$$D_i n_i = \bar{\sigma} - \Pi_{;\alpha}^{\alpha}, \quad \text{on} \quad \partial\Omega \tag{2.40}$$

and

$$q_{ij}^r n_i n_j = -\bar{\pi}_n, \quad \text{on} \quad \partial\Omega, \qquad [\![\Pi^{\alpha} b_{\alpha}]\!] = 0, \quad \text{on} \quad \gamma, \tag{2.41}$$

where

$$\bar{\pi}_n = \bar{\pi}_i n_i$$

represents the normal component of the applied surface dipole polarization density.

> **Remark 2.1:** *It is worth noting that both Eqs.*(2.40) *and* $(2.41)_1$ *concern boundary conditions on* $\partial\Omega$*. The second one contains solely the quadrupole tensor* q^r_{ij}*. Notice that the unknown tensor field* q^r_{ij} *on the boundary is constrained by the externally applied field* $\bar{\pi}_i$*, as the polarization field is constrained by an applied surface charge in the standard theory. The applied field* $\bar{\pi}_i$ *contributes manifoldly in the boundary conditions as it is present, in addition in the last term of Eq.* (2.40) *and* $(2.41)_2$ *as well. It is noted that the surface dipole polarization density* $\bar{\pi}_i$ *might be a distribution of dipolar defects on the boundary. Kalpakides et al. (36) used the additional boundary conditions to study the influence of dipole defects in the microstructure of ferroelectrics. The present analysis seems to be close to that one developed in (75; 77). The two analyses are in accordance under the assumption that the applied polarization* $\bar{\pi}_i$ *is constrained to be normal to the surface* $\partial\Omega$*. On the other hand, assuming that the quadrupole polarization (irreversible and reversible part) vanishes one obtains a theory very close to the standard Landau model for elastic ferroelectrics.*

Finally, the proposed variational principle for elastic ferroelectrics provides the field equations (2.28), (2.33) and (2.34) accompanied by the boundary conditions (2.39)–(2.41). The unknown functions are the displacement field, the electric potential and the direction of the spontaneous polarization vector; its magnitude is considered as a material parameter that is given. In the case of Dirichlet boundary conditions where the displacement and the electric potential are given on a part of the boundary, say $\partial\Omega_D$, then Eqs. (2.39), (2.40) hold only for the complementary of the boundary, $\partial\Omega_N$, where

$$\partial\Omega_D \cup \partial\Omega_N = \partial\Omega \quad \text{and} \quad \partial\Omega_D \cap \partial\Omega_N = \emptyset. \tag{2.42}$$

Due to the presence of the (undetermined) functions W and Ψ, the above equations and boundary conditions are quite general. To use the above results in a specific boundary value problem a special choice of the constitutive functions W and Ψ is necessary.

2.3 Constitutive assumptions

In this section a specific form for the constitutive functions W and Ψ is proposed in order a particular boundary value problem to be formulated.

2.3.1 The stored energy function

We start with the stored energy of deformation and electric field. This part of energy is responsible for the linear (reversible) behavior of the material, thus one can assume a quadratic form for W. Consequently, the stored energy of deformation and electric field can be written

$$\begin{aligned} W(e_{ij},\phi_{,i},\phi_{,ij}) &= \frac{1}{2}c_{ijkl}\left(e_{ij}-e^{\circ}_{ij}\right)\left(e_{kl}-e^{\circ}_{kl}\right)+d_{ijk}\phi_{,i}\left(e_{jk}-e^{\circ}_{jk}\right) \\ &- \frac{1}{2}\varepsilon_0\varepsilon_{ij}\phi_{,i}\phi_{,j}-\frac{1}{2}\varepsilon_0 a_{ijkl}\phi_{,ij}\phi_{,kl}-\varepsilon_0\beta_{ijk}\phi_{,i}\phi_{,jk}, \\ & \qquad\qquad i,j=1,2, \end{aligned} \tag{2.43}$$

where c_{ijkl} is the elastic coefficient tensor, ε_{ij} is the dielectric susceptibility tensor and d_{ijk} is the piezoelectric coefficient tensor that depends on the spontaneous polarization orientation. The coefficient tensors β_{ijk} and a_{ijkl} are new material parameters that related with the insertion of the second gradient of the electric potential into the set of the independent constitutive variables. The tensor e°_{ij} denotes the spontaneous strain. The existence of spontaneous strain is exclusively due to the presence of spontaneous polarization thus, it is reasonable to assume that there exists a function relating these two quantities, i.e.,

$$e^{\circ}_{ij}=e^{\circ}_{ij}(p^{s}_{k}). \tag{2.44}$$

Inserting Eq. (2.43) into constitutive relations (2.32), one further determines the latter as

$$\sigma_{ij}=c_{ijkl}(e_{kl}-e^{\circ}_{kl})+d_{kij}\phi_{,k}, \tag{2.45}$$

$$p^{r}_{i}=d_{ijk}(e_{jk}-e^{\circ}_{jk})-\varepsilon_0\varepsilon_{ij}\phi_{,j}-\varepsilon_0\beta_{ijk}\phi_{,jk}, \tag{2.46}$$

$$q^{r}_{ij}=-\varepsilon_0\beta_{kij}\phi_{,k}-\varepsilon_0\alpha_{ijkl}\phi_{,kl}. \tag{2.47}$$

Due to the symmetry of the quadrupole tensor q_{ij}, one easily concludes that the material tensor α_{ijkl} is symmetric with respect to its first two indices. Obviously, the last two indices can be interchanged, as well.

Using Eqs. (2.45)–(2.47), one may compute the total polarization and the electric displacement with the aid of Eqs. (2.35) and (2.38) as follows

$$\begin{aligned}\pi_i &= p_i^s - q_{ij,j}^s + d_{ijk}(e_{jk} - e_{jk}^\circ) - \varepsilon_0\varepsilon_{ij}\phi_{,j} + \varepsilon_0\left(\beta_{kij} - \beta_{ijk}\right)\phi_{,jk} + \varepsilon_0\alpha_{ijkl}\phi_{,jkl},\\ D_i &= p_i^s - q_{ij,j}^s - \varepsilon_0\epsilon_{ij}\phi_{,j} + d_{ijk}(e_{jk} - e_{jk}^\circ) + \varepsilon_0\left(\beta_{kij} - \beta_{ijk}\right)\phi_{,jk}\\ &\qquad + \varepsilon_0\alpha_{ijkl}\phi_{,jkl},\end{aligned} \tag{2.48}$$

where $\epsilon_{ij} = \varepsilon_{ij} + \delta_{ij}$.

2.3.2 The phase separation energy

In the Landau theory one considers an energy in the form of a high order polynomial in terms of the (dipole) polarization vector. Here, we assume a phase separation energy depended on the total spontaneous polarization so as to introduce the quadrupole polarization tensor as well. Thus we adopt an energy function of the form

$$\Psi(\pi_i^s) = \alpha_{ij}\pi_i^s\pi_j^s + \bar{\alpha}_{ijkl}\pi_i^s\pi_j^s\pi_k^s\pi_l^s, \tag{2.49}$$

where higher order terms can be used if necessary. Consequently its derivative with respect to π_i^s is written

$$\frac{\partial\Psi}{\partial\pi_i^s} = \alpha_{ij}\pi_j^s + \bar{\alpha}_{ijkl}\pi_j^s\pi_k^s\pi_l^s,$$

or, with the aid of Eq. (2.37)

$$\frac{\partial\Psi}{\partial\pi_i^s} = \alpha_{ij}p_j^s - \alpha_{ij}q_{jk,k}^s + \bar{\alpha}_{ijkl}(p_j^s - q_{jm,m}^s)(p_k^s - q_{kn,n}^s)(p_l^s - q_{lr,r}^s).$$

Simplifying our analysis we keep only the linear terms in quadrupole tensor, thus one can write

$$\frac{\partial\Psi}{\partial\pi_i^s} \simeq -\alpha_{ij}q_{jk,k}^s + \alpha_{ij}p_j^s + \bar{\alpha}_{ijkl}p_j^sp_k^sp_l^s = -\alpha_{ij}q_{jk,k}^s + \frac{\partial\Psi}{\partial p_i^s},$$

Also taking account Eq. (2.28), the intramolecular balance can be finally written with respect to the spontaneous polarization vector as

$$\alpha_{ij}q_{jk,k}^s - \frac{\partial\Sigma}{\partial p_i^s} - \phi_{,i} = 0. \tag{2.50}$$

Summing up, with the use of Eqs. (2.48) and (2.50) the field equations take the form:

$$\begin{cases} \alpha_{ij} q^s_{jk,k} - \dfrac{\partial \Sigma}{\partial p^s_i} - \phi_{,i} = 0, \\ p^s_{i,i} - q^s_{ij,ji} - \varepsilon_0 \epsilon_{ij} \phi_{,ij} + d_{ikl} \left(e_{kl} - e^{\circ}_{kl} \right)_{,i} + \varepsilon_0 a_{ijkl} \phi_{,ijkl} = 0, \\ c_{ijkl} \left(e_{kl} - e^{\circ}_{kl} \right)_{,j} + d_{kij} \phi_{,kj} = 0. \end{cases} \tag{2.51}$$

It is worth noting that the material constant β_{ijk} does not appear into the above field equations due to the symmetry of $\phi_{,ij}$. Hereafter, the interaction between $\phi_{,i}$ and $\phi_{,ij}$ is ignored, thus the β_{ijk} tensor is taken to be zero.

2.3.3 Material symmetry considerations

To proceed further to build a simple model and study the influence of quadrupoles in ferroelectrics, we make several simplifications. First, we consider that the body is isotropic as concerns its elastic properties. Thus, the elastic constants are only two and the tensor c_{ijkl} is reduced to

$$\begin{pmatrix} c_{11} & c_{12} & c_{12} & 0 & 0 & 0 \\ c_{12} & c_{11} & c_{12} & 0 & 0 & 0 \\ c_{12} & c_{12} & c_{11} & 0 & 0 & 0 \\ 0 & 0 & 0 & c_{66} & 0 & 0 \\ 0 & 0 & 0 & 0 & c_{66} & 0 \\ 0 & 0 & 0 & 0 & 0 & c_{66} \end{pmatrix}, \tag{2.52}$$

where $c_{66} = (c_{11} - c_{12})/2$. Furthermore, the material tensor α_{ijkl} and the dielectric tensor ϵ_{ij} are considered to be isotropic, i.e.

$$\begin{pmatrix} \alpha_{11} & \alpha_{12} & \alpha_{12} & 0 & 0 & 0 \\ \alpha_{12} & \alpha_{11} & \alpha_{12} & 0 & 0 & 0 \\ \alpha_{12} & \alpha_{12} & \alpha_{11} & 0 & 0 & 0 \\ 0 & 0 & 0 & \alpha_{66} & 0 & 0 \\ 0 & 0 & 0 & 0 & \alpha_{66} & 0 \\ 0 & 0 & 0 & 0 & 0 & \alpha_{66} \end{pmatrix} \tag{2.53}$$

and

$$\varepsilon_{ij} = \varepsilon \delta_{ij} \Rightarrow \epsilon_{ij} = \epsilon \delta_{ij} = (\varepsilon + 1) \delta_{ij}, \quad i, j = 1, 2, 3. \tag{2.54}$$

where $\alpha_{66} = (\alpha_{11} - \alpha_{12})/2$.

As far as the piezoelectric tensor concerns, it should be transversally isotropic about the spontaneous polarization axis. More precisely one can choose the piezoelectric tensor as (42; 60)

$$\begin{aligned} d_{kij}\left(p_i^s\right) = \frac{||p_i^s||}{p_0} \big\{ & d_{||} e_i e_j e_k + d_{\perp} \left(\delta_{ij} - e_i e_j\right) e_k \\ & + d_{=\frac{1}{2}} \left[\left(\delta_{ki} - e_k e_i\right) e_j + \left(\delta_{kj} - e_k e_j\right) e_i\right] \big\} , \end{aligned} \tag{2.55}$$

where the constants $d_{||}$, $d_{\perp}$, $d_{=}$ correspond to the classical parameters d_{33}, d_{31}, and d_{15}, respectively, in the case of a fully poled state oriented in the x_3-direction. In the specific example we examine here we are not interested in piezoelectric effects, thus the piezoelectric tensor is taken to be zero.

2.3.4 The 2-D case

To reduce even more the number of material constants, we confine ourselves in 2-D problems so conditions for plane strain and plane electric field are adopted. For the problem under study, that means $u_i = u_i(x_1, x_2)$, $i = 1, 2$ and $\phi = \phi(x_1, x_2)$. In that case, Eqs. (2.52) and (2.53) take the simple form:

$$\begin{pmatrix} c_{11} & c_{12} & 0 \\ c_{12} & c_{11} & 0 \\ 0 & 0 & c_{66} \end{pmatrix} \quad \text{and} \quad \begin{pmatrix} \alpha_{11} & \alpha_{12} & 0 \\ \alpha_{12} & \alpha_{11} & 0 \\ 0 & 0 & \alpha_{66} \end{pmatrix} , \tag{2.56}$$

where $\alpha_{66} = (\alpha_{11} - \alpha_{12})/2$.

Taking into account the above considerations and inserting the reduced material tensors into Eqs. (2.45–2.48), the following relations for polarization, quadrupole polarization and total polarization are obtained:

$$\begin{aligned} p_1^r &= -\varepsilon_0 \varepsilon \phi_{,1} \\ p_2^r &= -\varepsilon_0 \varepsilon \phi_{,2} \\ q_{11}^r &= -\varepsilon_0 \left(\alpha_{11}\phi_{,11} + \alpha_{12}\phi_{,22}\right) \\ q_{22}^r &= -\varepsilon_0 \left(\alpha_{12}\phi_{,11} + \alpha_{11}\phi_{,22}\right) \\ q_{12}^r &= -2\varepsilon_0 \alpha_{66} \phi_{,12} \\ \pi_1 &= p_1^s - q_{11,1}^s - q_{12,2}^s - \varepsilon_0 \left(\varepsilon\phi_{,1} - \alpha_{11}\phi_{,111} - \alpha_{12}\phi_{,221} - 2\alpha_{66}\phi_{,122}\right) \\ \pi_2 &= p_2^s - q_{21,1}^s - q_{22,2}^s - \varepsilon_0 \left(\varepsilon\phi_{,2} - 2\alpha_{66}\phi_{,121} - \alpha_{12}\phi_{,112} - \alpha_{11}\phi_{,222}\right) . \end{aligned} \tag{2.57}$$

Also, the components of the electric displacement field and the stress tensor become

$$\begin{aligned} D_1 &= p_1^s - q_{11,1}^s - q_{12,2}^s - \varepsilon_0 \left(\epsilon\phi_{,1} - \alpha_{11}\phi_{,111} - \alpha_{12}\phi_{,221} - 2\alpha_{66}\phi_{,122}\right) \\ D_2 &= p_2^s - q_{21,1}^s - q_{22,2}^s - \varepsilon_0 \left(\epsilon\phi_{,2} - 2\alpha_{66}\phi_{,121} - \alpha_{12}\phi_{,112} - \alpha_{11}\phi_{,222}\right) . \end{aligned} \tag{2.58}$$

and

$$\begin{aligned}\sigma_{11} &= c_{11}(e_{11} - e^{\circ}_{11}) + c_{12}(e_{22} - e^{\circ}_{22}),\\ \sigma_{12} &= 2c_{12}(e_{12} - e^{\circ}_{12}),\\ \sigma_{22} &= c_{11}(e_{22} - e^{\circ}_{22}) + c_{12}(e_{11} - e^{\circ}_{11}),\\ \sigma_{33} &= c_{11}(e_{11} - e^{\circ}_{11}) + c_{11}(e_{22} - e^{\circ}_{22}).\end{aligned} \tag{2.59}$$

Certainly, the component σ_{33} of the stress tensor can be written in terms of σ_{11} and σ_{22}.

We turn now to the phase separation energy Ψ, the role of which is crucial for the interpretation of the material's microstructure. The spontaneous polarization can take only specific orientations depended on the material symmetry. For instance, Barium titanate possesses six such different orientations (16) corresponding to the different crystallographic variants of the material in room temperature. For the two–dimensional case examined here, it is assumed that Ψ is a fourth order polynomial of spontaneous polarization p_i. Such a choice secures adequate smoothing for Ψ and multiple minima corresponding to the four crystallographic directions of the crystal for the 2–d case. Hence, one can write

$$\Psi(p_i) = \frac{a_1}{2}\left(p_1^2 + p_2^2\right) + \frac{a_2}{4}\left(p_1^4 + p_2^4\right) + \frac{a_3}{2}p_1^2 p_2^2, \tag{2.60}$$

where the coefficients $a_1,\ a_2$ and a_3 are material parameters and also we drop the notation of spontaneous polarization replacing p_i^s with p_i, because there is no danger of confusion since the reversible parts of polarization and quadrupole are given as derivatives of the electric potential. In Figure 2.1 the spontaneous polarization energy versus the components of the spontaneous polarization is illustrated for the normalized values of the material parameters used in the numerical simulations of Section 2.5. One can easily see that the spontaneous polarization energy attains four minima corresponding to the crystallographic axes of the material. According to the above selection for the polarization energy, the spontaneous polarization will tend to take the values $(\pm p_0, 0)$ and $(0, \pm p_0)$ which are energetically more favorable.

Last, we have to make an assumption on the form of Eq. (2.44). Motivated by the work of Chen (18), we assume that the spontaneous strain is a quadratic function of spontaneous polarization, thus for the plane strain conditions Eq. (2.44) is of the form

$$\begin{aligned}e^{\circ}_{11} &= \gamma_{11}p_1^2 + \gamma_{12}p_2^2,\\ e^{\circ}_{22} &= \gamma_{11}p_2^2 + \gamma_{12}p_1^2,\\ e^{\circ}_{12} &= \gamma_{44}p_1 p_2,\end{aligned} \tag{2.61}$$

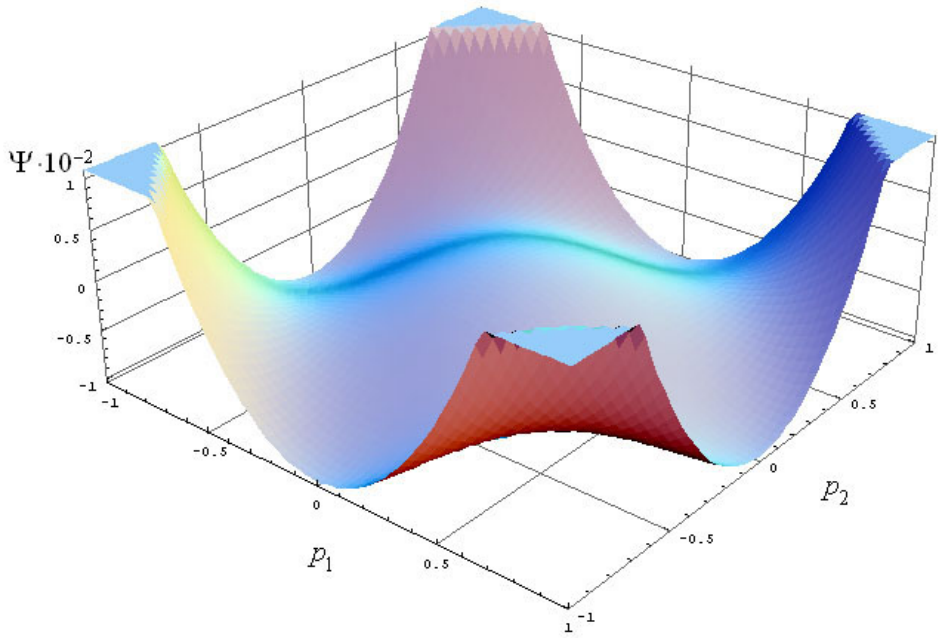

Figure 2.1: Phase separation energy

where γ_{ij} are the electrostrictive constants.

As concerns spontaneous quadrupole polarization tensor we assume a specific form of Eq. (2.16):

$$q^s_{ij} = \mu \begin{pmatrix} p_1 p_2 & \frac{1}{2}({p_1}^2 + {p_2}^2) \\ \frac{1}{2}({p_1}^2 + {p_2}^2) & p_1 p_2 \end{pmatrix}.$$

In the 2-D model, the internal motion Eq. (2.50) results in the simple form

$$\begin{aligned} \bar{\mu}\left(p_1\left(p_{1,2} + p_{2,1}\right) + p_2\left(p_{1,1} + p_{2,2}\right)\right) - \frac{\partial \Sigma}{\partial p_1} - \phi_{,1} = 0, \\ \bar{\mu}\left(p_2\left(p_{1,2} + p_{2,1}\right) + p_1\left(p_{1,1} + p_{2,2}\right)\right) - \frac{\partial \Sigma}{\partial p_2} - \phi_{,2} = 0, \end{aligned} \tag{2.62}$$

where $\bar{\mu}$ is a new parameter related to spontaneous quadrupoles.

Using all the above considerations and appropriate choices for the boundary conditions (2.39)–(2.41), one can formulate a specific boundary value problem in terms of displacement field u_i, electric potential ϕ and spontaneous polarization p_i.

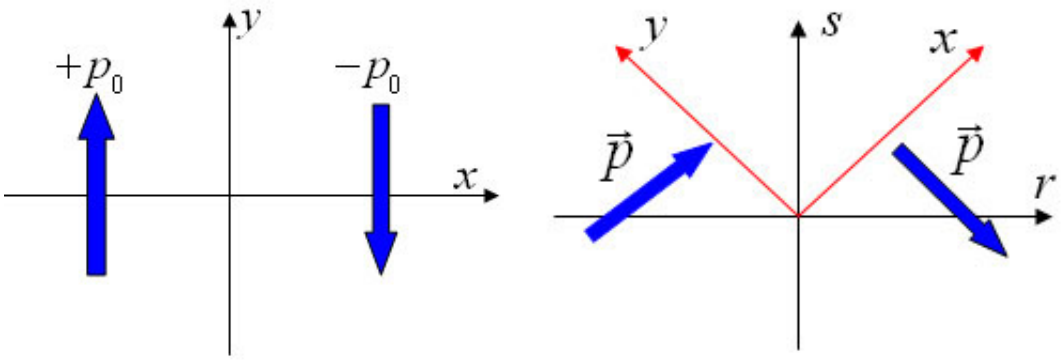

(a) 180° domain wall (b) 90° domain wall

Figure 2.2: Two types of domain walls in ferroelectrics with tetragonal crystal symmetry and the two coordinate systems

2.4 Analytical solutions

In the previous section, we have presented a two dimensional model accounting for quadrupole effects, which can be easily implemented in computer simulations. The key idea of the proposed theory is that in ferroelectrics one has to assume a spontaneous part for the quadrupole also. The reversible part of the quadrupole seems to play a minor role in the formation of domain walls. On the other hand, the spontaneous part of the quadrupole is essential for the microstructure of ferroelectrics, since it is proved to be responsible for the formation of domain walls with proper surface energy and thickness. In this section, analytical solutions for 1-D problem are provided to demonstrate this particular role of spontaneous quadrupoles.

Confining ourselves in rigid ferroelectrics, the system of Eqs. (2.51) becomes

$$\mu\, p_1(p_{1,2} + p_{2,1}) - \frac{\partial \Psi}{\partial p_1} - \frac{\partial \phi}{\partial x} = 0 \tag{2.63}$$

$$\mu\, p_2(p_{1,2} + p_{2,1}) - \frac{\partial \Psi}{\partial p_2} - \frac{\partial \phi}{\partial y} = 0 \tag{2.64}$$

$$p_{1,1} + p_{2,2} - \varepsilon_0 \epsilon \left(\frac{\partial^2 \phi}{\partial x^2} + \frac{\partial^2 \phi}{\partial y^2}\right) = 0 \tag{2.65}$$

Notice that in the above equations we have discarded the second terms in Eqs. (2.62) and the terms $q^s_{ij,ji}$ in Gauss equation so as to simplify the set of equations obtaining

exact analytical solutions (5). Also, the reversible part of quadrupole polarization is neglected.

2.4.1 The 180° Domain Wall

Consider an infinite strip $-\infty < x < \infty$, $-h/2 < y < h/2$ with a domain wall located at $x = 0$ as one can see in Figure 2.2a. In this simple problem the following boundary conditions are taken

$$\begin{aligned} & p_2(0) = 0, \\ & \lim_{x\to\pm\infty} p_2(x) = \mp p_0, \\ & \lim_{x\to\pm\infty} \frac{d\phi(x)}{dx} = 0, \\ & \lim_{x\to\pm\infty} p_1(x) = 0, \end{aligned} \tag{2.66}$$

where p_0 is the value of spontaneous polarization of the material under discussion.

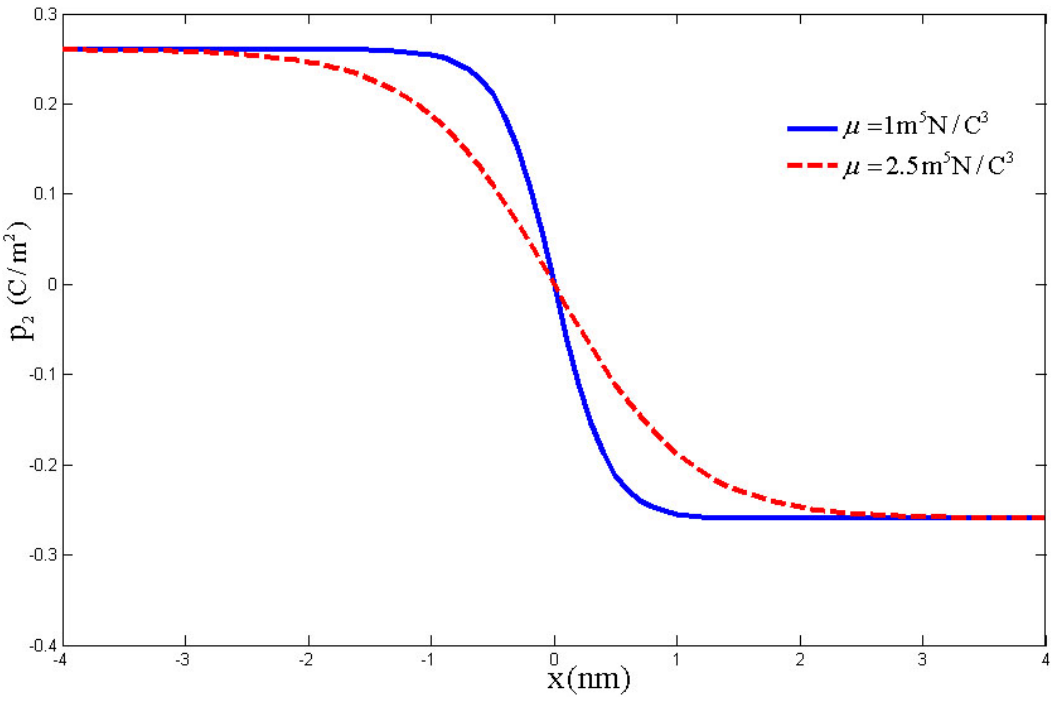

Figure 2.3: Normalized polarization profile for 180° domain wall.

The geometry of the body allows to assume that the partial derivative of all quantities

with respect to y vanish, thus the system of Eqs.(2.63)-(2.65) is transformed in an 1-D problem

$$\mu\, p_1 p_{2,1} - a_1 p_1 - a_2 p_1^3 - a_3 p_1 p_2^2 - \frac{d\phi}{dx} = 0 \tag{2.67}$$

$$\mu\, p_2 p_{2,1} - a_1 p_2 - a_2 p_2^3 - a_3 p_2 p_1^2 = 0 \tag{2.68}$$

$$p_{1,1} - \varepsilon_0 \epsilon \frac{d^2\phi}{dx^2} = 0. \tag{2.69}$$

One can easily notice that the solution $\phi = 0$ and $p_1 = 0$ satisfies Eqs. (2.67) and (2.69) simultaneously. What remains is Eq. (2.68) which takes the form

$$\mu\, p_2 \frac{dp_2}{dx} - a_1 p_2 - a_2 p_2^3 = 0. \tag{2.70}$$

Since $p_2 \neq 0$ the above equation becomes

$$\mu\, \frac{dp_2}{dx} - a_1 - a_2 p_2^2 = 0,$$

the general solution of which is

$$p_2(x) = -\sqrt{\frac{-a_1}{a_2}} \tanh\left(\frac{\sqrt{-a_1 a_2}}{\mu}(x - C)\right), \tag{2.71}$$

where C is a constant. From the boundary conditions one takes that $p_0 = \sqrt{-a_1/a_2}$ and $C = 0$, thus leading to the solution

$$p_2(x) = -p_0 \tanh\left(\frac{\sqrt{-a_1 a_2}}{\mu}\, x\right). \tag{2.72}$$

It is obvious from the polarization profile of an 180° domain wall that the quadrupole theory predicts domain walls with proper thickness as it is shown in Figure 2.3, where we have used the normalized values for the material parameters. It is remarked that the polarization gradient theories provide also such a profile for the 180° domain wall (17; 73). However, unlike the polarization gradient theories, here a first order differential equation has been used to obtain the same result. Also, of great interest is the domain wall energy which can be computed by the relation

$$E_{180^\circ} = \int_{-\infty}^{+\infty} (\Sigma - \Sigma_0) dx,$$

where Σ_0 is the energy density of the homogeneous system $(p_1, p_2) = (0, p_0)$. For $\mu = 1\,\mathrm{m^5N/C^3}$ the domain wall thickness is 2nm with surface energy $0.0058\,\mathrm{J/m^2}$ and for $\mu = 2.5\,\mathrm{m^5N/C^3}$ the domain wall thickness is approximately 4nm with surface energy $0.0146\,\mathrm{J/m^2}$.

2.4.2 The 90° Domain Wall

Similarly to the previous solution for 180° domain walls, it is possible to find analytical solutions for 90° domain walls. The 90° domain wall separates domains whose polarization axis are perpendicular. The current coordinate system i.e. (x, y) fits to the crystallographic symmetry of the material. This type of domain wall is oriented at 45° angle with respect to the crystallographic axes, so it is convenient to work in a new coordinate system (r, s), rotated at 45° from the (x, y) system, as shown in Figure 2.2b. The polarization vector in the new coordinate system is given by the relations

$$\begin{aligned} p_1 &= \frac{\sqrt{2}}{2}\left(p_r + p_s\right) \\ p_2 &= -\frac{\sqrt{2}}{2}\left(p_r - p_s\right). \end{aligned} \tag{2.73}$$

In the new coordinate system we consider an infinite strip $-\infty < r < \infty$, $-h/2 < s < h/2$, with h relatively small. The domain wall is located at $r = 0$ and the boundary conditions are

$$\begin{aligned} &p_s(0) = 0, \\ &\lim_{r\to\pm\infty} p_r\left(r\right) = \frac{p_0}{\sqrt{2}}, \\ &\lim_{r\to\pm\infty} p_s\left(r\right) = \mp\frac{p_0}{\sqrt{2}}, \\ &\lim_{r\to\pm\infty} \frac{d\phi\left(r\right)}{dr} = 0. \end{aligned} \tag{2.74}$$

Inserting Eqs. (2.73) to the phase separation energy Ψ (i.e. Eq. (2.60)), the latter is transformed to

$$\Psi' = \frac{a_1}{2}\left(p_r^2 + p_s^2\right) + \left(\frac{a_2}{8} + \frac{a_3}{4}\right)\left(p_r^4 + p_s^4\right) + \left(\frac{3a_2}{4} - \frac{a_3}{2}\right)p_r^2 p_s^2. \tag{2.75}$$

Taking all partial derivatives with respect to s to be zero, the system of equations in the new coordinate system takes the form

$$\begin{aligned} &\mu\, p_r p_{s,r} - \frac{\partial\Psi'}{\partial p_r} - \frac{d\phi}{dr} = 0, \\ &\mu\, p_s p_{s,r} - \frac{\partial\Psi'}{\partial p_s} = 0, \\ &p_{r,r} - \varepsilon_0\epsilon\frac{d^2\phi}{dr^2} = 0. \end{aligned} \tag{2.76}$$

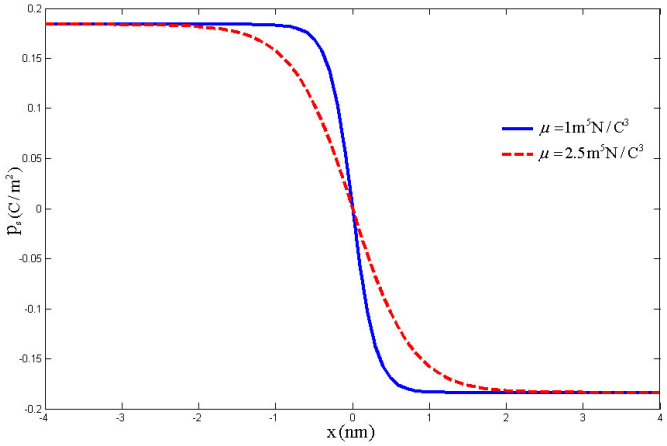

(a) Normalized polarization component p_s

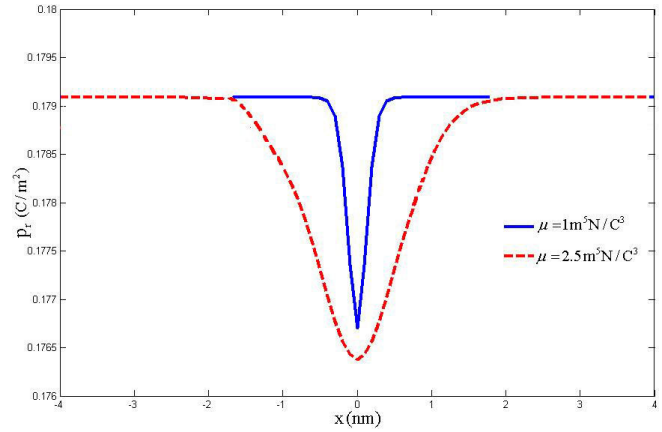

(b) Normalized polarization component p_r

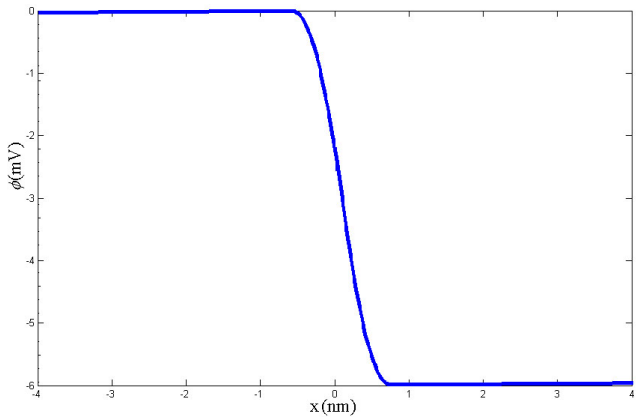

(c) Electric potential

Figure 2.4: Normalized polarization and electric potential profiles for 90° domain wall

Substituting Eq.(2.75) into Eq.(2.76) it is easy to arrive at the following set of equations

$$\mu\, p_r p_{s,r} - a_1 p_r - (\frac{a_2}{2} + a_3)p_r^3 - (\frac{3}{2}a_2 - a_3)p_r p_s^2 - \frac{d\phi}{dr} = 0 \tag{2.77}$$

$$\mu\, p_s p_{s,r} - a_1 p_s - (\frac{a_2}{2} + a_3)p_s^3 - (\frac{3}{2}a_2 - a_3)p_s p_r^2 = 0 \tag{2.78}$$

$$p_{r,r} - \varepsilon_0 \epsilon \frac{d^2\phi}{dr^2} = 0. \tag{2.79}$$

Specifically, if one sets

$$\frac{3}{2}a_2 - a_3 \Rightarrow a_3 = \frac{3}{2}a_2, \tag{2.80}$$

then Eq. (2.78) becomes

$$\mu\, p_s p_{s,r} - a_1 p_s - (\frac{a_2}{2} + a_3)p_s^3 = 0,$$

which, as before, can be solved analytically giving the general solution

$$p_s(r) = -\sqrt{\frac{-a_1}{a_2/2 + a_3}} \tanh\left(\frac{\sqrt{-a_1(a_2/2 + a_3)}}{\mu}(r - C)\right) \tag{2.81}$$

and after using Eq. (2.80) one obtains

$$p_s(r) = -\frac{1}{\sqrt{2}}\sqrt{\frac{-a_1}{a_2}} \tanh\left(\frac{\sqrt{-2a_1a_2}}{\mu}(r - C)\right). \tag{2.82}$$

Taking into account the boundary conditions, one may confirm that the quantity $\sqrt{-a_1/a_2}$ equals to p_0 and $C = 0$. Thus Eq. (2.82) may further be simplified to

$$p_s(r) = -\frac{p_0}{\sqrt{2}} \tanh\left(\frac{\sqrt{-2a_1a_2}}{\mu} r\right). \tag{2.83}$$

As concerns the other two under determination functions p_r and ϕ, one can start from Eq. (2.79) by writing it as

$$\frac{d}{dr}(p_r - \varepsilon_0 \epsilon \frac{d\phi}{dr}) = 0,$$

and after integrating

$$p_r - \varepsilon_0 \epsilon \frac{d\phi}{dr} = C,$$

where C is a constant. It is easy to confirm from Eqs. (2.74) that $C = p_0/\sqrt{2}$, leading to the form

$$p_r - \varepsilon_0 \epsilon \frac{d\phi}{dr} = \frac{p_0}{\sqrt{2}}. \tag{2.84}$$

Returning to Eq. (2.77), one can obtain a more convenient form

$$\mu\, p_r p_{s,r} - 2a_2 p_r^3 - a_1(p_r - \frac{1}{-a_1}\frac{d\phi}{dr}) = 0. \tag{2.85}$$

Comparing Eqs. (2.84) and (2.85), it is reasonable to choose $a_1 = -1/\varepsilon_0\epsilon$, thus concluding in

$$-\mu\sqrt{-a_1 a_2}\, p_0 \,\mathrm{Sech}^2\left(\sqrt{-2a_1 a_2}\, r\right) p_r - 2a_2 p_r^3 - a_1 \frac{p_0}{\sqrt{2}} = 0. \tag{2.86}$$

which is an algebraic equation because p_s has been already determined by Eq. (2.83). Substituting the latter in Eq. (2.86) one obtains

$$-\sqrt{-a_1 a_2}\, p_0 \,\mathrm{Sech}^2\left(\sqrt{-2a_1 a_2}\, r\right) p_r - 2a_2 p_r^3 - a_1 \frac{p_0}{\sqrt{2}} = 0. \tag{2.87}$$

The above equation is a third degree polynomial and can be solved analytically. Discarding the two complex roots, p_r is given by

$$p_r(r) = -\mu\,\frac{\sqrt{-a_1 a_2}\, p_0 \,\mathrm{Sech}^2\left(\frac{\sqrt{-a_1 a_2}}{\mu}\, r\right)}{3^{1/3}\left(-9\sqrt{2}\, a_1 a_2^2 p_0 + \sqrt{6}\, B(r)\right)^{1/3}} + \frac{\left(-9\sqrt{2}\, a_1 a_2^2 p_0 + \sqrt{6}\, B(r)\right)^{1/3}}{3^{2/3}\, 2a_2}, \tag{2.88}$$

where

$$B(r) = \sqrt{27\, a_1^2 a_2^4 p_0^2 + 4\, a_2^3 \left(-a_1 a_2\right)^{1/3} p_0^3 \mu^3 \,\mathrm{Sech}^6\left(\frac{\sqrt{-a_1 a_2}}{\mu}\, r\right)}. \tag{2.89}$$

After that, Eq. (2.84) can be solved by a simple numerical integration determining the electric potential. In Figure 2.4, the plots for the two polarization components and the electric potential are given. It is clear that across 90° domain wall there is an electric potential drop. Xiao (73) arrived at the same conclusion using the standard polarization gradient theory, remarking that this is the main difference between the two types of domain walls. As far as concerns the domain wall energy density, for $\mu = 1\,\mathrm{m^5N/C^3}$ the surface energy is $0.0018\,\mathrm{J/m^2}$ and for $\mu = 2.5\,\mathrm{m^5N/C^3}$ is approximately $0.046\,\mathrm{J/m^2}$. It is noted that this model predicts that the 90° domain walls are thinner than 180° domain walls.

2.5 Computations

Phase field theory provides a very powerful tool for studying the microstructural behavior of ferroelectric materials. The spontaneous dipole polarization is considered as the first order parameter of the dynamic process from a non-equilibrium state to the equilibrium, thus adopting a gradient flow argument one can write

$$m\dot{p_i} = -\frac{\delta I}{\delta p_i}, \tag{2.90}$$

where m denotes the mobility of the process, I is the energy free functional of the system. The thermodynamic driving force $\delta I/\delta p_i$ has been already determined. The two dimensional evolution equations for the first order parameter are (**?**)

$$\begin{aligned} m\dot{p}_1 &= \bar{\mu}\left(p_1\left(p_{1,2}+p_{2,1}\right)+p_2\left(p_{1,1}+p_{2,2}\right)\right)-\frac{\partial\Sigma}{\partial p_1}-\phi_{,1}, \\ m\dot{p}_2 &= \bar{\mu}\left(p_2\left(p_{1,2}+p_{2,1}\right)+p_1\left(p_{1,1}+p_{2,2}\right)\right)-\frac{\partial\Sigma}{\partial p_2}-\phi_{,2}. \end{aligned} \tag{2.91}$$

2.5.1 Material Parameters and normalization

In the applications of the next section barium titanate ($BaTiO_3$) was chosen to perform numerical simulations. The elastic parameters and the dielectric constant of the barium titanate are taken from (15)

$$c_{11} = 168 \text{ GPa}, \; c_{12} = 78 \text{ GPa}, \; c_{44} = 45 \text{ GPa}, \; \epsilon = 413.$$

The dielectric constant has been chosen relatively smaller according to a common practice (81). The material parameters for the polarization energy are taken to be

$$a_1 = -59.2 \cdot 10^7 \text{ C}^{-2}\text{m}^2\text{N}, \quad a_2 = 87.528 \cdot 10^8 \text{ C}^{-4}\text{m}^6\text{N},$$

$$a_3 = 26.259 \cdot 10^9 \text{ C}^{-4}\text{m}^6\text{N}.$$

The electrostrictive constants given by (59) are adopted:

$$\gamma_{11} = 0.11, \; \gamma_{12} = -0.045, \; \gamma_{44} = 0.059 \, (\text{C}^{-2}\text{m}^4).$$

The value of the mobility constant m^{-1} will be established indirectly, later on. What remains is to set values for the tensor α_{ijkl}, the material parameter, related with the

new term – the electric field gradient – added in this paper. For the particular case under study, given that the relation $\alpha_{12} = \alpha_{11}/2$ holds, we must solely choose the value for one parameter, i.e., for $\alpha_{11} = \alpha_0$.

To facilitate the presentation of the numerical results, we give a dimensionless version of the equations of the problem under study. Following (73), the energy density Σ is divided by a characteristic constant c_0 which has dimensions of mechanical load:

$$\bar{\Sigma} = \Sigma/c_0 = [W(e_{ij}, \phi_{,i}, \phi_{,ij}) + \Psi(p_i)]/c_0 = \bar{W} + \bar{\Psi}. \tag{2.92}$$

This results in a dimensionless stress tensor

$$\bar{\sigma}_{ij} = \frac{\partial \bar{W}}{\partial e_{ij}} = \sigma_{ij}/c_0, \tag{2.93}$$

where the fact that the strain tensor is a dimensionless quantity has been taken into account.

The spontaneous dipole polarization magnitude of $BaTiO_3$, in room temperature, takes the value $p_0 = 0.26\text{C/m}^2$ (16). Thus a dimensionless spontaneous polarization vector can be introduced as

$$\bar{p}_i = p_i/p_0, \tag{2.94}$$

for which $\|\bar{\mathbf{p}}\| = 1$. Furthermore, the rest unknown functions can be normalized as follows

$$\bar{u}_i = u_i/l_0, \quad \bar{\phi} = \phi/\phi_0, \tag{2.95}$$

while the independent variables are normalized as

$$\bar{x}_i = x_i/l_0, \quad \bar{t} = t/t_0. \tag{2.96}$$

The parameters, l_0, t_0 and ϕ_0 have dimensions of length, time and electric potential, respectively and the following relations hold

$$l_0 = \frac{\mu p_0^3}{c_0}, \quad t_0 = \frac{m p_0^2}{c_0}, \quad \phi_0 = \frac{c_0 l_0}{p_0} = \mu p_0^2. \tag{2.97}$$

With the aid of eqs. (2.92) and (2.94), one can write for the phase separation energy

$$\bar{\Psi}(\bar{p}_i) = \frac{\bar{a}_1}{2}\left(\bar{p}_1^2 + \bar{p}_2^2\right) + \frac{\bar{a}_2}{4}\left(\bar{p}_1^4 + \bar{p}_2^4\right) + \frac{\bar{a}_3}{2}\bar{p}_1^2\bar{p}_2^2, \tag{2.98}$$

where

$$\bar{a}_1 = a_1 p_0^2/c_0, \quad \bar{a}_2 = a_2 p_0^4/c_0, \quad \bar{a}_3 = a_3 p_0^4/c_0. \tag{2.99}$$

Similarly, the rest of the material parameters are transformed according to the relations:

$$\begin{array}{lll} \bar{c}_{11} = c_{11}/c_0, & \bar{c}_{12} = c_{12}/c_0, & \bar{m} = m p_0^2/(t_0 c_0), \\ \bar{\varepsilon}_0 = \varepsilon_0 c_0/p_0^2, & \bar{\gamma}_{ij} = \gamma_{ij} p_0^2, & \bar{\mu} = \mu p_0^3/c_0 l_0, \\ & \bar{\alpha}_0 = \alpha_0/l_0^2. & \end{array} \tag{2.100}$$

It is worth-noting that the parameters l_0 and α_0 appear always together in a non–dimensional fraction of the form $\sqrt{\alpha_0}/l_0$, this dictates to choose an appropriate value for this fraction. The parameter α_0 has dimension of $(\text{length})^2$, hence one may further suppose that the constant α_0 as well as the characteristic length l_0 are related with the microstructure of the material, that is the size of the domains and the domain walls, respectively (see also 75). In a similar manner, $c_0 = 1\text{GPa}$ is selected as the value for the characteristic stiffness so as the normalized elastic moduli to be a dimensionless quantity of range 10-100.

The transformation equation for $\bar{m}$, i.e. Eq. $(2.100)_3$, in conjunction with Eq. $(2.97)_2$ suggests that this parameter must be selected to be unity($\bar{m} = 1$). Furthermore notice that Eq. $(2.97)_2$ informs us that the characteristic time t_0 is inversely proportional to the mobility of the process. Thus one reasonably may assume that t_0 is related with the relaxation time of the process. In a similar spirit, the transformation equation for μ in conjunction with Eq. $(2.97)_1$ suggests that this parameter is also chosen to be unity, thus in this model the characteristic length l_0 is proportional to the parameter μ due to spontaneous quadrupoles. Choosing $\mu = 10\,\text{m}^5\text{N/C}^3$ the characteristic length becomes $l_0 = 1.75\,\text{nm}$. From experimental data and first principle calculation, it is generally admitted that the domain wall thickness is usually about $1 - 10\,\text{nm}$, although domain wall thickness as large as $150\,\text{nm}$ has been reported in $LiNbO_3$. Since the interest of this work focuses on electric field gradient effects on domain walls we have chosen wider domain walls. Certainly, this can be easily fixed by changing the value of the parameter μ.

Finally, after the above considerations, the dimensionless material parameters become:

$$\begin{array}{ccc} \bar{c}_{11} = 168, & \bar{c}_{12} = 78.2, & \bar{c}_{44} = 45, \\ \bar{a}_1 = -0.04, & \bar{a}_2 = 0.04, & \bar{a}_3 = 0.12, \\ \bar{\gamma}_{11} = 0.0074, & \bar{\gamma}_{12} = -0.003, & \bar{\gamma}_{44} = 0.0038, \\ \bar{\mu} = 1, & \bar{m} = 1, & \bar{\varepsilon}_0 = 0.133. \end{array} \tag{2.101}$$

Summing up, using the normalization described above, one concludes in the same set of partial differential equations, constitutive relations and boundary conditions derived in the previous sections with the sole difference that the material parameters should be replaced by those ones given in Eq. (2.101). For simplicity reason, hereafter we will denote the dimensionless quantities inserted above, without the bars over them as there is no danger of confusion.

2.5.2 The computational scheme

For the numerical results presented below, the set of governing equations accompanied with the proper boundary conditions are solved on a rectangular of normalized dimensions $w \times h$. To solve the problem, a finite element scheme for the space variables jointly with the finite difference method for the time are used. The number of degrees of freedom per node should be five, since we are solving for $(u_i, p_i, \phi), \quad i = 1, 2$. However, the fourth order Gauss equation is decomposed into a set of second order equations using Eq. $(2.57)_3$. This is a natural decomposition that allows to make use of the additional boundary conditions obtained in the previous section (see Eqs. $(2.41)_1$). This manipulation results in additional degrees of freedom per node (i.e. $(u_i, p_i, q^r_{ij}, \phi), \quad i, j = 1, 2$). To solve these equations Lagrange linear shape functions have been used. Time integration is accomplished using Backward Euler method with a normalized time step $\Delta t = 0.01$, which leads to converged solution. Finally, in order for the reaction - advection system to avoid breaking, a small amount of diffusion was added so as to provide a mechanism for maintenance of a slow wave speed (46). The system of equations solved is the following

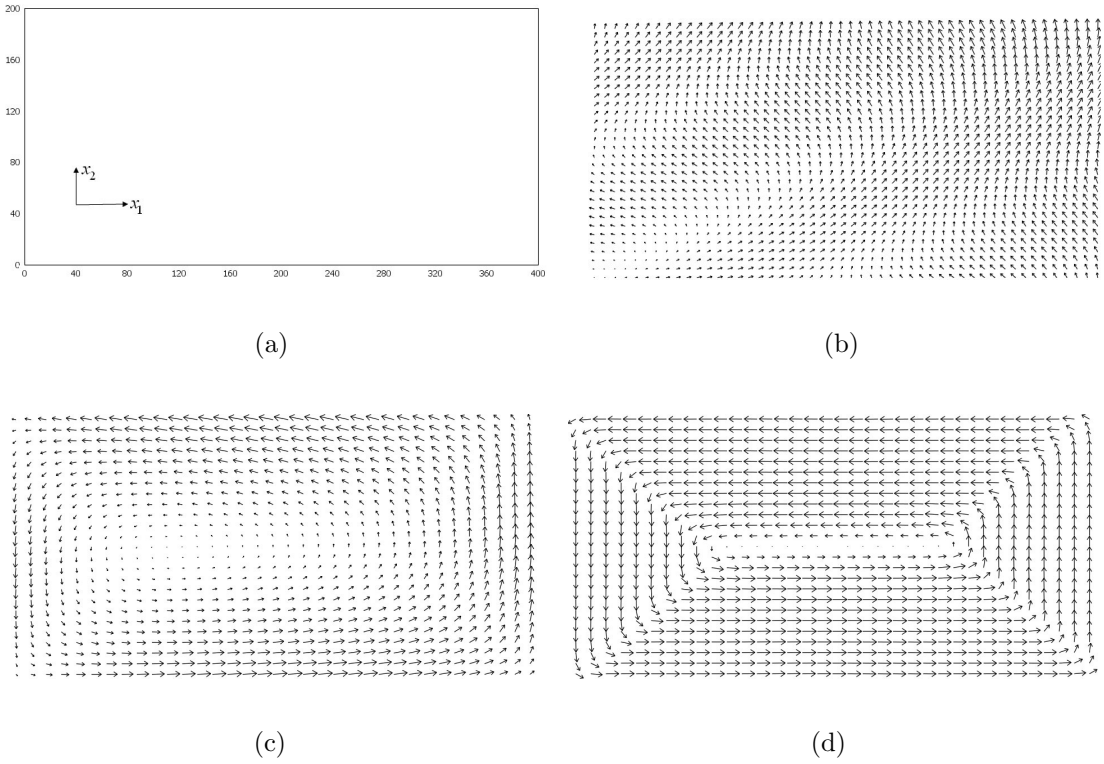

Figure 2.5: Domain formation in bulk ferroelectric: (a) computational geometry, (b) random initial data, (c) intermediate state, (d) final state

$$m\dot{p}_1 = \nu\nabla^2 p_1 + q^s_{11,1} + q^s_{12,2} - \frac{\partial\Sigma}{\partial p_1} - \phi_{,1}, \tag{2.102}$$

$$m\dot{p}_2 = \nu\nabla^2 p_2 + q^s_{21,1} + q^s_{22,2} - \frac{\partial\Sigma}{\partial p_2} - \phi_{,2} \tag{2.103}$$

$$q^r_{11} + \varepsilon_0\left(\alpha_{11}\phi_{,11} + \alpha_{12}\phi_{,22}\right) = 0 \tag{2.104}$$

$$q^r_{22} + \varepsilon_0\left(\alpha_{12}\phi_{,11} + \alpha_{11}\phi_{,22}\right) = 0 \tag{2.105}$$

$$q^r_{12} + 2\varepsilon_0\alpha_{66}\phi_{,12} = 0 \tag{2.106}$$

$$p_{i,i} - q^s_{ij,ji} - \varepsilon_0\epsilon\phi_{,ii} - q^r_{ij,ji} = 0, \tag{2.107}$$

where ν denotes the artificial diffusion parameter. This parameter is chosen $\nu = 0.01$, which is significantly smaller than the normalized parameter μ of the advective terms. In all simulations quadrilateral meshes were used selecting 1750 elements consisting of 1846 mesh points. The finite element implementation of the above equations was accomplished in the same spirit as in (60).

2.5.3 Microstructure in a single crystal

The first simulation concerns the domain formation under appropriate boundary conditions in a single crystal. The dimensions of a ferroelectric single crystal are in the micrometer length scale, thus it is reasonable to choose a rectangle with height $h = 200$ and length $w = 400$, as shown in Figure 2.5a. We assume that all boundaries are surface charge free ($\mathbf{D}\cdot\mathbf{n} = 0$) and traction free ($\sigma\cdot\mathbf{n} = 0$). The geometry of the computational sample suggests $q^r_{11} = 0$ for the left and right boundaries and $q^r_{22} = 0$ for the top and bottom boundaries as far as concerns the additional boundary conditions for electric quadrupoles.

In Figure 2.5b we start by posing a priori a random distribution of spontaneous polarization as initial data and we let the system evolve up to reach an equilibrium state. In Figure 2.5c the evolution still progresses and in Figure 2.5d attains the final configuration, where there exist four domains separated by four 90° domain walls and one 180° domain wall at the center. It is worth-mentioning that the final domain pattern strongly depends on the initial data. For another choice of initial spontaneous polarization distribution one can obtain different number of domains as well as different type of domain walls. This vortex domain structure is in agreement with the standard polarization gradient models (60), since this behavior is due to the boundary conditions and spontaneous polarization energy.

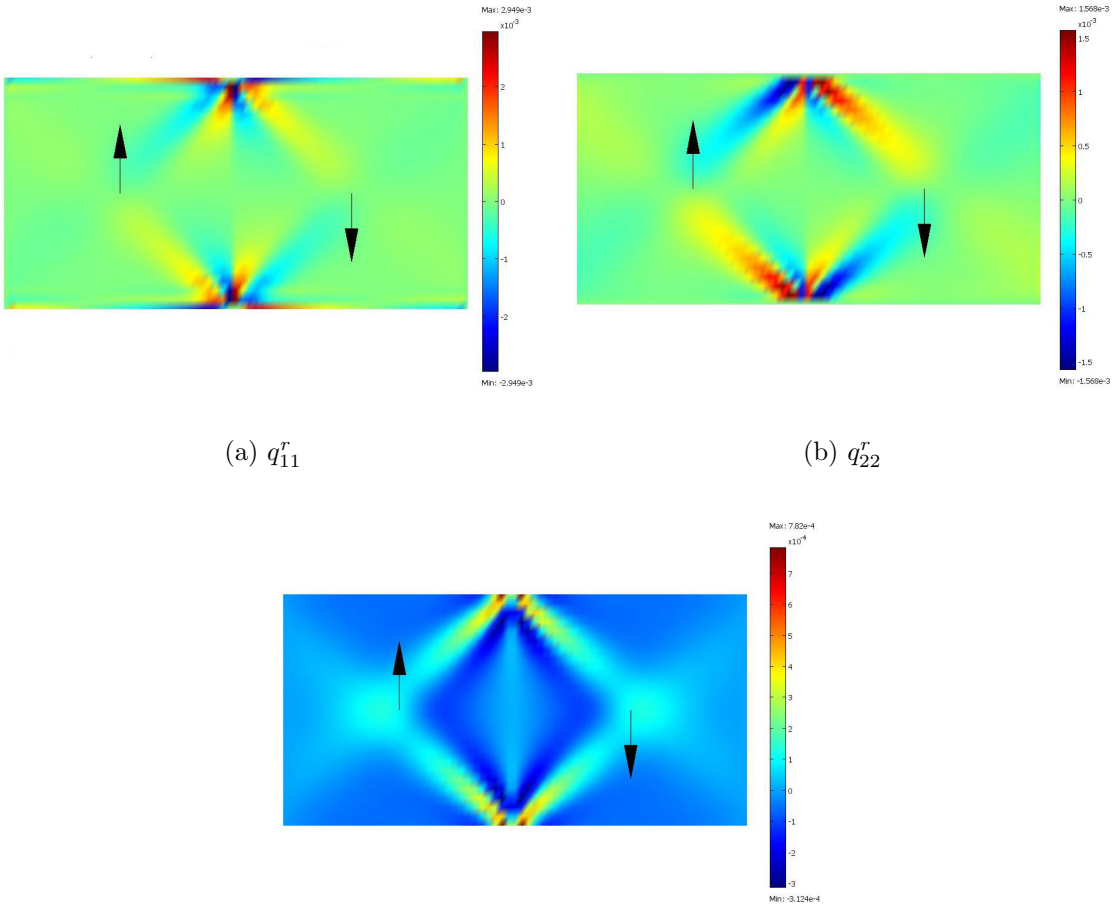

(a) q^r_{11} (b) q^r_{22}

(c) q^r_{12}

Figure 2.6: Reversible quadrupole polarization profile for 180° domain wall

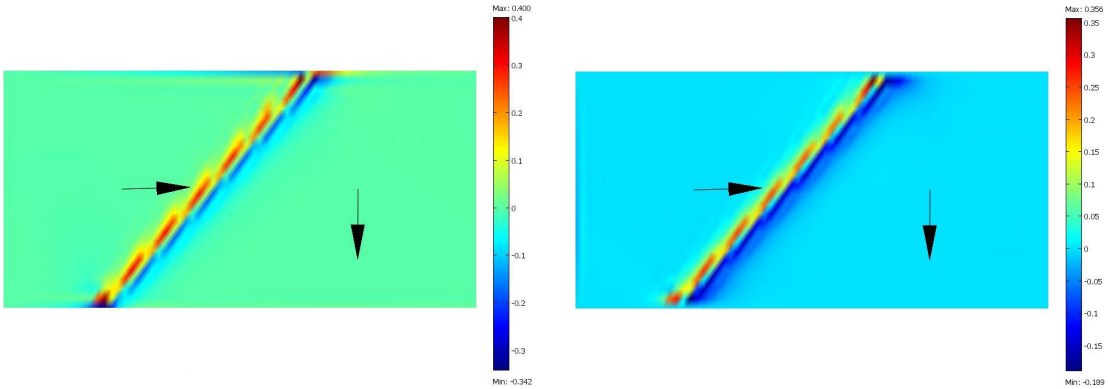

(a) q^r_{11} (b) q^r_{22}

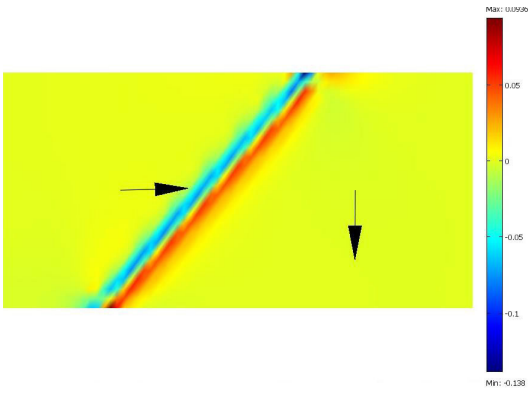

(c) q^r_{12}

Figure 2.7: Reversible quadrupole polarization profile for 90° domain wall

2.5.4 Domain walls

In Section 2.4, we have investigated the structure of domain walls under various simplifications of the governing equations and we were able to derive simple analytical solutions that describe the main aspects of 90° and 180° domain walls. It was shown that the domain wall thickness is due to the spontaneous part of the quadrupole polarization. At this point we are able to investigate the reversible part of the quadrupole polarization near domain walls, which was previously neglected. Imposing appropriate initial conditions we end up with a 180° or a 90° domain wall. In Figures 2.6,2.7 the profiles of the components of the reversible quadrupole tensor are shown for both types of domain walls. In these simulations we used various values of the parameter α_0 at a range 1-500 arriving at the conclusion that the influence of the reversible part of quadrupoles is minor to the formation of domain walls. One can notice that linear quadrupoles attain larger values on 90° domain walls than 180° domain walls and this can be explained due to the fact that across 90° domain walls there exists an electric potential drop as proved analytically in Section 2.4.

2.5.5 Electric field gradient effects in thin films

A ferroelectric thin film can be regarded to have a large value of the length w compared to the thickness h. In the context of phenomenological continuum models, appropriate boundary conditions need to be applied along the surfaces of the film. The standard polarization gradient models use the boundary condition (33; 71) $d\mathbf{P}/dn = -\mathbf{P}/\delta$ for the polarization flux on the surface, where δ denotes the extrapolation length. The introduction of the extrapolation length δ is the key concept to study nano-ferroelectrics in the framework of a phase field model. A positive δ means that spontaneous polarization is reduced as we approach the surface, while a negative δ implies that polarization is enhanced. A zero extrapolation length $\delta = 0$ indicates that spontaneous polarization vanishes on the boundary.

In the following simulations concerning thin films we use reduced dimensions of the computational sample of Figure 2.5a. The normalized length is taken to be $w = 60$, while the normalized thickness h is chosen at a range lower than 20. The boundary conditions are chosen accordingly. For the top and bottom boundaries we choose zero spontaneous polarization, i.e. $p_1 = p_2 = 0$ generating the most significant size effect in

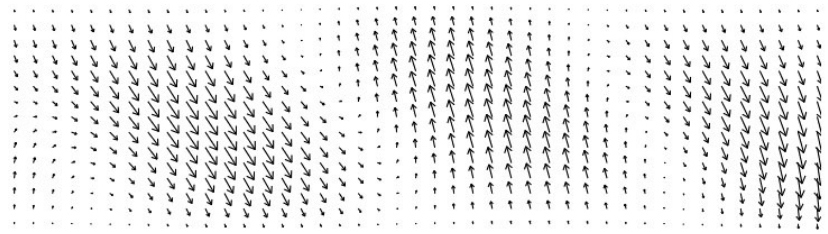

(a)

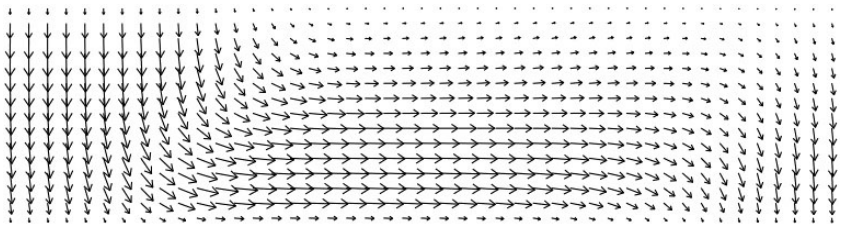

(b)

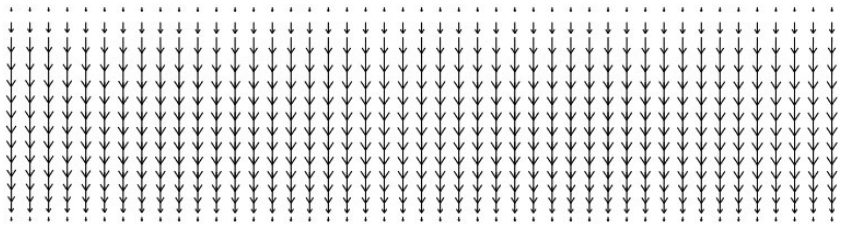

(c)

Figure 2.8: Domain formation in a thin film with normalized thickness $h = 16$: (a) initial data, (b) equilibrium state for $\alpha_0 = 1$, (c) equilibrium state for $\alpha_0 = 500$

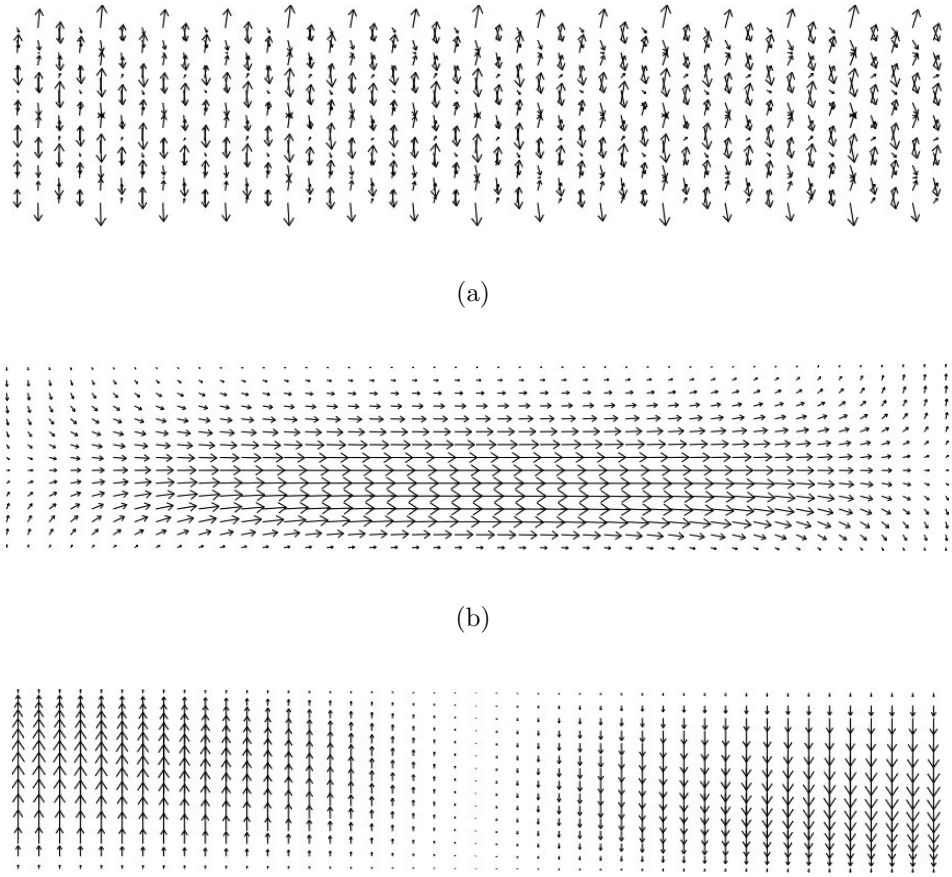

(a)

(b)

(c)

Figure 2.9: Domain formation in a thin film with normalized thickness $h = 12$: (a) initial data, (b) equilibrium state for $\alpha_0 = 1$, (c) equilibrium state for $\alpha_0 = 500$

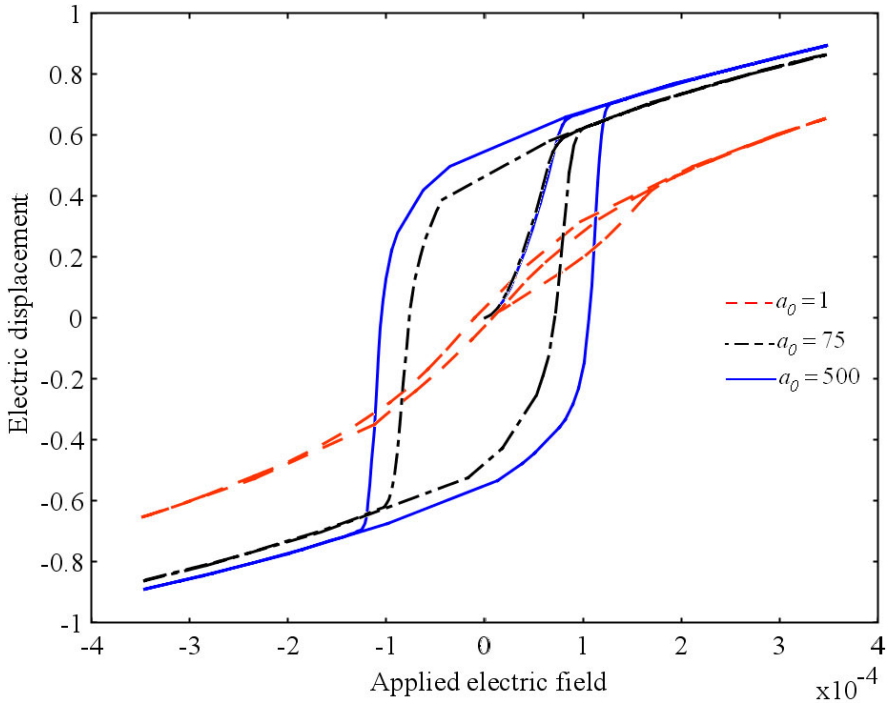

Figure 2.10: Hysteresis loop for various values of the electric field gradient coefficient α_0 at a normalized film thickness $h = 12$.

thin films corresponding to zero extrapolation length. This type of boundary condition is called the zero boundary condition (71) Also, for the top and bottom boundaries we choose Dirichlet boundary conditions for the electrostatic potential ϕ. Also, the three boundaries are taken traction free, while at the bottom boundary we set the constraint $u_2 = 0$ so as to account the influence of the substrate. It is noted that the influence of the substrate on the thin film is kept as simple as possible, since it is not the main aspect of this work. For electric quadrupoles the boundary conditions are the same as in the simulations of bulk single crystal described above. Finally, periodic boundary conditions along x_1 axis were applied for electric potential and mechanical strain in order to impose artificial periodicity in the crystal.

At first we study the domain formation starting from random initial data. In Figure 2.8 the normalized film thickness is chosen $h = 16$ and two equilibrium states are illustrated for two different values of the electric field gradient parameter α_0. For $\alpha_0 = 1$, Figure 2.8 b shows the formation of a polydomain structure containing three domains

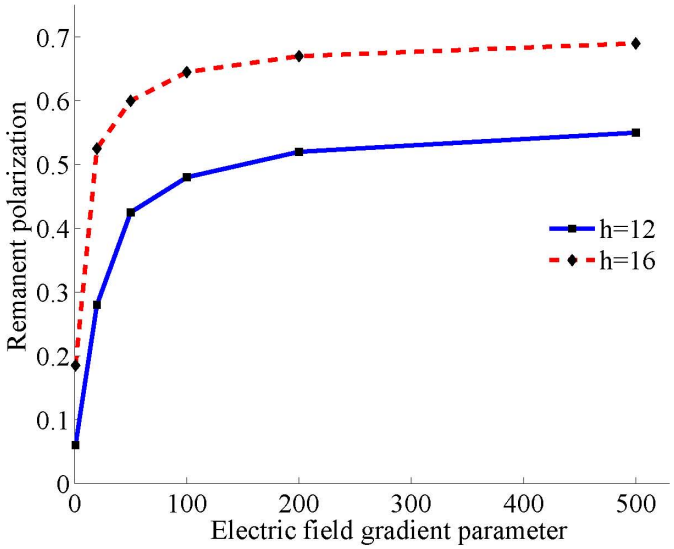

Figure 2.11: Remanent polarization as a function of the electric field gradient parameter α_0. The curves are drawn for clarity.

separated by two 90° domain walls. The existence of the specific structure is due to the reduction of the elastic energy in the thin film (71). Running the simulation for higher values of the parameter α_0 it is observed that domains of horizontal polarization are reduced and as one can see in Figure 2.8 c a vertical monodomain structure is predominant. For $h = 12$ and $\alpha_0 = 1$ the polydomain structure is still observed as shown in Figure 2.9 b, while in Figure 2.9 c using $\alpha_0 = 500$ two vertical domains separated by a 180° domain wall are observed. It is deduced that the electric field gradients can influence the microscopic behavior of the thin film, in contrast to bulk crystals. From a point of view this is acceptable, because higher electric field gradients indicate stronger electrical interactions between microscopic dipoles. Thus the elastic energy is unable to compensate the increased electrical energy in the film and structures of one or more vertical domains become predominant. Lowering the film thickness we notice the formation of a mono-domain status, which remains unchanged even for large values of the parameter α_0 until polarization finally vanishes.

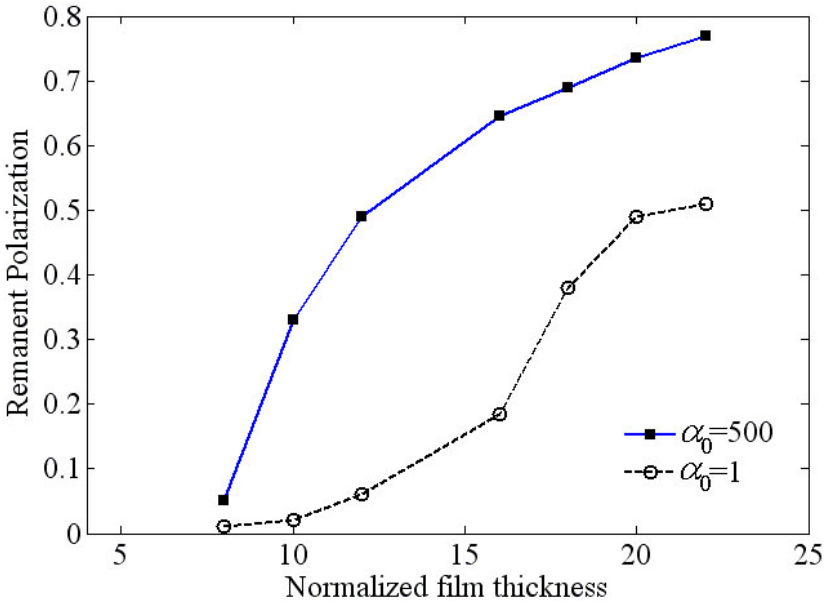

Figure 2.12: Size effect: the remanent polarization versus the normalized film thickness. Two different values of the electric field gradient parameter have been chosen.

The above simulations prove that electric field gradient effects are an important factor in the microstructure of thin films. Thus it is expected that electric field gradients consequently have an impact on the macroscopic behavior of the film as well. In Figure 2.10 we plot the hysteresis loop, which is the plot of the average electric displacement along x_2 direction for three different values of the parameter α_0 at a normalized thickness $h = 12$. To obtain the hysteresis loop an external electric field was applied along the x_2 axis, which is accomplished by imposing the condition $\phi = \phi_0\, sin(2\pi t/T)$ for the electrostatic potential at the upper boundary with $\phi_0 = 0.1$ and $T = 15000$. It is obvious that when electric field gradient effects become significant a larger hysteresis loop is obtained. In a sense, this indicates that ferroelectricity is enhanced, since comparing the loops the remanent polarization and the coercive field needed to switch the total polarization seem to increase. The remanent polarization is defined as the average polarization along the applied field direction when the applied field is reduced to zero from its high magnitude. In Figure 2.11 we plot the dependence of the remanent polarization as a function of the electric field gradient parameter α_0 for two different film thicknesses. It is observed that increased values of the parameter α_0

suggest higher remanent polarization and coercive field in the film.

Finally, to illustrate the size effect in thin films within the present phase field model, we plot the remanent polarization as a function of the film thickness shown in Figure 2.12. It is observed that the remanent polarization decreases with decreasing film thickness being in absolute accordance with thermodynamic calculations and other phase field models. It is interesting to notice that different values of the parameter α_0 result in different curves.

Chapter 3

The Level Set Approach to Phase Transitions in solids

"I was aware that there was supposed to be a difference between Faraday's way of conceiving phenomena and that of mathematicians, so that neither he nor they were satisfied with each other's language."

J.C. Maxwell

In contrast to the phase field theory presented in the previous section for ferroelectrics, the sharp interface theory treats phase boundaries as discontinuity surfaces of zero thickness (1; 2; 3; 7; 9; 10; 11; 12; 41). Certainly in these models the interfacial energy can be included in an explicit manner. Far away from the interface the basic equations of Continuum Mechanics are satisfied. However, across the interface certain quantities suffer discontinuity jumps that must obey specific conditions. These conditions can be taken by standard arguments and correspond to the famous Rankine-Hugoniot jump conditions. The problem of a moving interface in the context of sharp interface models remains ill-posed, thus additional constitutive information is needed. It seems that basic Continuum Mechanics gives us the potential to compute only the driving force on the interface and not its velocity. Abeyaratne and Knowles (3) proved that this drawback can be fixed by selecting a kinetic relation, namely a relation that determines the velocity of the phase boundary as a function of the exerted force. The selection of an

appropriate kinetic relation depends on experimental observations and in fact it is not easy to guess the correct one. It is generally admitted that the need for a kinetic relation is due to the fact that the motion of a phase boundary is a non-equilibrium process. Maugin and Berezovski (10; 11) introduced the so called contact quantities to study the motion of an interface in thermoelastic solids within the context of non-equilibrium thermodynamics (12). The authors were able to determine a kinetic relation, which provides the proper limit behavior of the kinetic curve. However, experimental results on the kinetics of a phase boundary are absent indicating that this research field is open.

In this chapter we use the level set method to describe the kinetics of a phase boundary. Level set methods have been introduced by Osher and Sethian (57; 58) and soon have become a very powerful tool for tracking a moving interface within a body. The method is based on an implicit representation of the interface by considering a smooth scalar function, which changes sign across the interface. Thus the zero level set of the implicit function coincides with the interface. The motion of the interface is accomplished by using an evolution equation for the level set function, which is of Hamilton-Jacobi type. It is remarked that the introduction of such an internal variable results in a regularization of the sharp interface model in solids. In level set methods the interfaces transform into thin transition layers where all discontinuous quantities take inhomogeneous but continuous expressions. However, as in sharp interface models it is essential to provide a kinetic relation as well. Here, at first we present a regularized version of the sharp interface theory in thermo-elastic solids within the framework of level set method. The effort focalizes in the derivation of the kinetic relation using simple minded phenomenology in the same spirit as Maugin and Berezovski (9; 11). Moreover, we derive useful relations which can be considered as the regularized versions of the Rankine-Hugoniot jump conditions. It is proved that the level set method is closely related to material mechanics, since it is proved that the force on the phase boundary is an inhomogeneity force obeying the canonical momentum or pseudo-momentum equation (30; 49).

Based on the theoretical analysis of this chapter, we focus on the kinetics of domain walls and on the domain formation in ferroelectric materials. The material force method is proved to be very useful in order to compute the driving forces on the domain walls. Thus it is proved that domain structures in ferroelectrics are due to inhomogeneity

forces entering the material momentum equation. The computations are based on a finite element scheme combined with an implicit time integration method. The final non-linear algebraic system is solved by the use of an iterative Newton-Raphson method.

3.1 Phase Transitions in a continuum

3.1.1 Sharp interface theory

Let us consider a continuous body occupying space Ω_R in the reference configuration containing a singular surface S_t separating the body in two distinct regions Ω_R^+ and Ω_R^-. Under the Lagrangian formulation of a continuous medium the governing equations at any regular material point $\mathbf{X}$ with no external supply of energy and external entropy are the following (49; 52):

(i) *The balance of mass*

$$\frac{d\rho_0}{dt} = 0, \quad \text{in} \quad \Omega_R^{\pm}, \tag{3.1}$$

where $\rho_0(\mathbf{X})$ is the referential matter density and d/dt denotes derivative with respect to time at fixed $\mathbf{X}$.

(ii) *The balance of physical momentum*

$$\frac{d\mathbf{p}}{dt} - \mathrm{div_R}\mathbf{T} = 0, \quad \text{in} \quad \Omega_R^{\pm}, \tag{3.2}$$

where $\mathbf{p} = \rho_0(\mathbf{X})\mathbf{v}(\mathbf{X}, t)$ is the physical momentum, $\mathbf{v}(\mathbf{X}, t)$ the physical velocity and $\mathbf{T}$ the first Piola-Kirrchoff stress tensor. The symbol $\mathrm{div_R}$ denotes the divergence differential operator.

(iii) *The balance of energy*

$$\frac{dH}{dt} - \mathrm{div_R}(\mathbf{T}\cdot\mathbf{v} - \mathbf{Q}) = 0, \quad \text{in} \quad \Omega_R^{\pm}, \tag{3.3}$$

where $H = K + E$, with $K = \rho_0\mathbf{v}^2/2$ corresponding to the kinetic energy density, $E(\mathbf{F}, \theta; \mathbf{X})$ is the internal energy density, $\mathbf{Q}$ is the material heat flux, $\mathbf{F}$ the deformation gradient tensor and θ the absolute temperature.

(iv) *The balance of angular momentum*

Neglecting polar effects, like rotary inertia and couple stress, the balance of angular momentum is reduced to the symmetry condition for the Piola-Kirrchoff stress, i.e.

$$\mathbf{T}\mathbf{F}^{\mathrm{T}} = \mathbf{F}\mathbf{T}^{\mathrm{T}}. \tag{3.4}$$

The above set of Eqs. (3.1)–(3.4) describe the behavior of any inhomogeneous material with appropriate boundary conditions. Certainly any combination of mechanical and thermic process in the body should be compatible with the second law of thermodynamics

$$\frac{dS}{dt} + \mathrm{div}_{\mathrm{R}}(\mathbf{Q}/\theta) = \sigma_S \geq 0, \quad \text{in} \quad \Omega_R^{\pm}, \tag{3.5}$$

where S is the entropy density. The term $\mathbf{Q}/\theta$ represents the entropy flux, where an extra entropy flux $\mathbf{K}$ can be added if necessary (see (52) for non-vanishing $\mathbf{K}$).
The deformation gradient $\mathbf{F}$ and the velocity vector $\mathbf{v}$ satisfy the compatibility condition

$$\frac{d\mathbf{F}}{dt} = \mathrm{grad}_{\mathrm{R}}\mathbf{v}, \quad \text{in} \quad \Omega_R^{\pm}, \tag{3.6}$$

where $\mathrm{grad}_{\mathrm{R}}$ stands for the gradient differential operator.

The existence of the sharp interface within the body suggests that certain quantities present discontinuities. Assuming homothermal and coherent front the corresponding jump conditions are the Rankine-Hugoniot jump conditions given as

$$V_n \, [\![\rho_0]\!] = 0, \tag{3.7}$$

$$V_n \, [\![\mathbf{p}]\!] + \mathbf{n} \cdot [\![\mathbf{T}]\!] = 0, \tag{3.8}$$

$$V_n \, [\![H]\!] + \mathbf{n} \cdot [\![\mathbf{T} \cdot \mathbf{v} - \mathbf{Q}]\!] = 0, \tag{3.9}$$

$$V_n \, [\![S]\!] - \mathbf{n} \cdot [\![\mathbf{Q}/\theta]\!] = 0, \tag{3.10}$$

where $[\![\bullet]\!] = \bullet^+ - \bullet^-$ is the jump of any field across the interface, $\mathbf{V}$ is the phase boundary velocity and $V_n = \mathbf{V} \cdot \mathbf{n}$ its normal component. Furthermore, the compatibility condition presents a jump condition given by the following relation

$$V_n \, [\![\mathbf{F}]\!] + [\![\mathbf{v}]\!] \otimes \mathbf{n} = 0, \quad \text{on} \quad S_t. \tag{3.11}$$

The above mentioned analysis sets the thermo-mechanical framework of any inhomogeneous continuum body in the physical space. Expressing the problem to the material space, i.e., by a canonical projection onto the material manifold, gives rise to

the notion of configurational or material forces. In the material manifold one is able to handle inhomogeneities or any kind of defects coming from changes of the reference configuration. Introducing the Helmholtz free energy function ($W = E - S\theta$) in combination with Eq. (3.3), the canonical (material) form of the energy equation in each phase is the following

$$\frac{d(\theta\, S)}{dt} + \mathrm{div}_{\mathrm{R}}\mathbf{Q} = 0, \quad \text{in} \quad \Omega_R^{\pm}, \tag{3.12}$$

Furthermore the constitutive relations for stress and entropy are the following

$$\mathbf{T} = \frac{\partial W}{\partial \mathbf{F}}, \quad S = -\frac{\partial W}{\partial \theta}. \tag{3.13}$$

The balance of physical momentum, i.e. Eq. (3.2) transforms to the canonical or pseudo-momentum equation in material space. This procedure is accomplished by a **pull-back** transformation of the physical momentum balance law to the material manifold (49). The pseudo-momentum balance law in Lagrangian description is the following

$$\frac{d\mathbf{P}}{dt} - \mathrm{div}_{\mathrm{R}}\boldsymbol{\Sigma} = \mathbf{f}^{int} + \mathbf{f}^{inh}, \quad \text{in} \quad \Omega_R^{\pm}, \tag{3.14}$$

where $\mathbf{P} = -\mathbf{F}^{\mathrm{T}} \cdot \mathbf{p}$ is the pseudo-momentum, $\boldsymbol{\Sigma} = -L\mathbf{I}_R - \mathbf{T} \cdot \mathbf{F}$ is the dynamical Eshelby stress tensor, L is the Lagrangian energy density function. The force terms on the right-hand side of Eq. (3.14) are material forces, where with $\mathbf{f}^{int}$ we denote the material internal forces and with $\mathbf{f}^{inh}$ the material inhomogeneity forces defined by the relations

$$\mathbf{f}^{int} = \mathbf{T} : (\mathrm{div}_{\mathrm{R}}\mathbf{F})^{\mathrm{T}} - \mathrm{grad}_{\mathrm{R}} W \mid_{impl}, \tag{3.15}$$

$$\mathbf{f}^{inh} = \left.\frac{\partial L}{\partial \mathbf{X}}\right|_{expl} = \frac{1}{2}\mathbf{v}^2 \mathrm{grad}_{\mathrm{R}}(\rho_0) - \left.\frac{\partial W}{\partial \mathbf{X}}\right|_{expl} \tag{3.16}$$

where the subscript notations *expl* and *impl* imply, respectively, the gradient keeping the fields fixed and taking the material gradient only through the fields present in the function. The first term of Eq. (3.16) represents forces due to mass density inhomogeneities usually called inertial inhomogeneities. The balance of pseudo-momentum is non-conservative, thus across the phase boundary S_t the jump condition for the pseudo-momentum is

$$V_n \left[\!\left[\mathbf{P}\right]\!\right] + \mathbf{n} \cdot \left[\!\left[\boldsymbol{\Sigma}\right]\!\right] + \mathbf{f} = 0, \tag{3.17}$$

where **f** is an unknown vector standing for the source term of the jump relation. Then the second law of thermodynamics dictates

$$\mathbf{f} \cdot \mathbf{V} = f_S \, V_n = \theta_S \sigma_S \geq 0, \tag{3.18}$$

where f_S is the driving force on the interface. Equation (3.18) indicates that the quantities f_S and V_n should have the same sign at all times implying that the interface will always move to the direction of the driving force. It can be proved that the driving force on S_t has the following expression

$$f_S = - \left[\!\left[W \right]\!\right] + \mathbf{n} \cdot < \mathbf{T} > \cdot \left[\!\left[F \right]\!\right] \cdot \mathbf{n}, \tag{3.19}$$

where $< \bullet >= (\bullet^+ + \bullet^-)/2$ denotes the mean value of any quantity across the interface. Thus it is made obvious that in a continuous thermoelastic body we are able to determine the force on the singularity, but the problem remains ill-posed since the velocity is still undetermined. To fix this drawback we have to select a kinetic relation of the form (3)

$$V_n = g(f_S, \mathbf{n}), \tag{3.20}$$

where g is the **kinetic response function** depending on the material. The explicit dependence of the velocity on the normal vector **n** of the interface accounts for anisotropic effects inside the material. According to Eq. (3.18) the kinetic response should obey the following inequality

$$f_S \, g(f_S, \mathbf{n}) \geq 0 \tag{3.21}$$

thus being consistent to the second thermodynamic law.

3.1.2 The level-set formulation

As it was mentioned previously, the key idea behind the level set method is to represent curves or surfaces as the zero level set of a continuous implicit function ψ, the so called level set function, as shown in Figure 3.1b. Then solving an appropriate partial differential equation of Hamilton–Jacobi type, the level set function is updated tracking the evolution of the interface. An impressive advantage of level set method is that one can handle easily topological changes of the interface, for instance it allows for the formation of cusps. For a given domain Ω with boundary $\partial\Omega$ we introduce a new field,

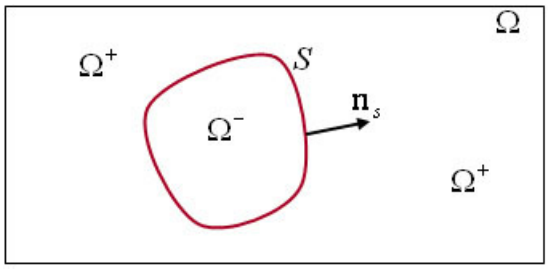

(a)

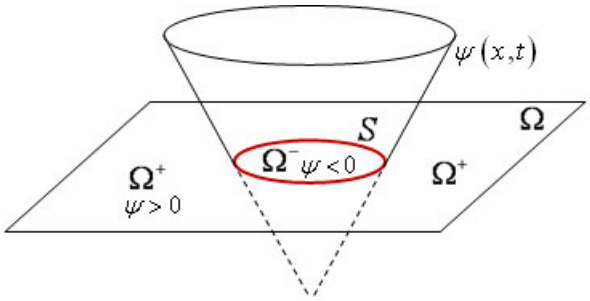

(b)

Figure 3.1: (a)The domain Ω separated in two regions by interface S and (b) the implicit representation via level set function

the level set function $\psi(\mathbf{x}, t)$ with the following properties

$$\begin{cases} \psi(\mathbf{x}, t) > 0, & \text{in} \quad \Omega^+, \\ \psi(\mathbf{x}, t) < 0, & \text{in} \quad \Omega^-, \\ \psi(\mathbf{x}, t) = 0, & \text{on} \quad S, \end{cases} \tag{3.22}$$

so that the zero level set of this function represents the interface S (see Figure 3.1b). The unit normal $\mathbf{n}_S$ to the interface and its curvature are given by the relations

$$\mathbf{n}_S = \frac{\nabla\psi}{|\nabla\psi|}, \quad \kappa = \nabla \cdot \left(\frac{\nabla\psi}{|\nabla\psi|} \right), \tag{3.23}$$

respectively.

The evolution of the level set function is determined by solving the partial differ-

ential equation (57)

$$\begin{cases} \dfrac{\partial \psi}{\partial t} + V|\nabla \psi| = 0, \quad \text{in} \quad \Omega \\ \psi\left(\mathbf{x}, 0\right) = \psi_0\left(\mathbf{x}\right), \end{cases} \tag{3.24}$$

where $\psi_0\left(\mathbf{x}\right)$ is the initial value of the level set function usually chosen as a signed distance function from the interface.

A signed distance function has the property $|\nabla \psi| = 1$, or every function obeying this property is a signed distance function (57; 58). Solving Eq. (3.24) numerically is not a straightforward task since the function ψ will not remain a signed distance function after several time steps leading to instabilities. To avoid such drawbacks it is necessary to keep level set function as a signed distance from the interface. To do that, a re-initialization procedure has to be applied. In traditional level set methods the re-initialization scheme concludes in the solution of the following initial value problem (57),

$$\begin{cases} \dfrac{\partial \psi}{\partial t} = \text{sign}\left(\psi_0\right)\left(1 - |\nabla \psi|\right), \quad \text{in} \quad \Omega \\ \psi\left(\mathbf{x}, 0\right) = \psi_0\left(\mathbf{x}\right). \end{cases} \tag{3.25}$$

However, in practice it is not easy to handle re-initialization, since one must find out the right time step and how often to apply it. Furthermore, it is computationally expensive. In this work, a variational level set formulation (37; 38; 45) is adopted which completely eliminates the need for re-initialization and can be easily implemented in a finite element scheme.

3.1.3 Building a phase transition problem by using the level set method

We assume two different thermo-elastic problems defined in the same region (6). These problems correspond to two different phases of a material capable of undergoing phase transformation at a specific temperature. This means that one has to deal with two given problems with different material behavior as in martensite–austenite case. Treating separately these problems it is apparent that the two solutions will differ, providing different values for every field. Now, using a level set function we can interpolate between the computed fields of the two problems in Ω_R, building a two phase problem (see Figure 3.2). The interpolated fields shall obey the equations of thermoelasticity in region Ω_R, as shown in Table 3.1. It becomes evident that making such an assumption,

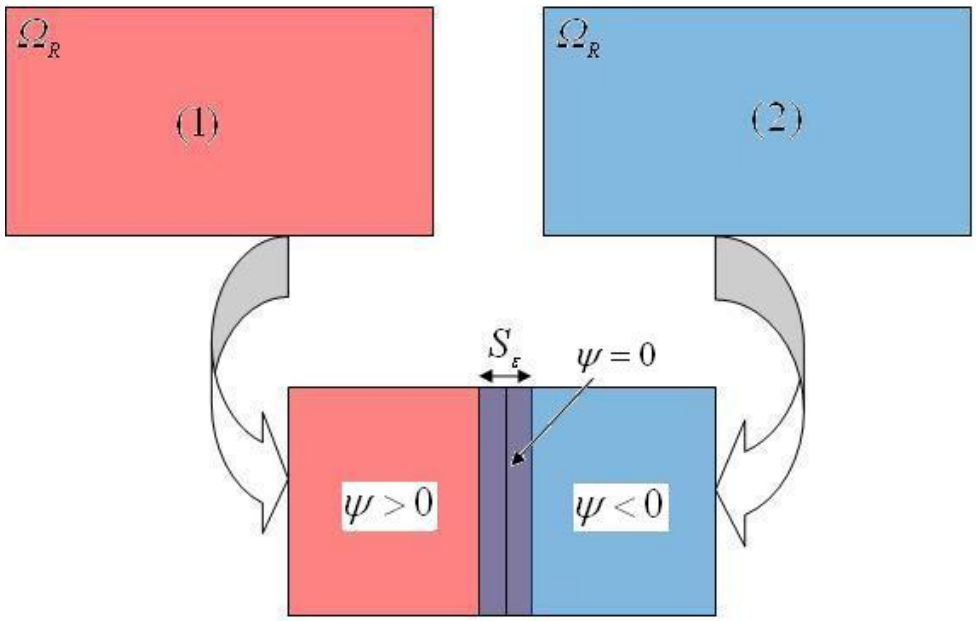

Figure 3.2: Blending two different problems defined in the same region Ω_R by a level set function

on the interface certain conditions should be valid that can drive the singularity and consequently determine the exact position of the interface in the domain.

Let us assume the arbitrary quantities A^1, A^2 (scalar, vectorial or higher-order tensorial denoting deformation gradient, velocity, stress e.t.c.) which are continuous in region Ω_R and correspond to similar fields, but computed on the distinct problems 1 and 2, respectively. For the needs of the level set one can write A as an interpolation between the computed fields

$$A = A^1 + h(A^2 - A^1), \tag{3.26}$$

where h is the Heaviside function defined as

$$h = H(\psi) = \begin{cases} 1, & \psi \geq 0, \\ 0, & \psi < 0, \end{cases} . \tag{3.27}$$

The next step is to introduce a continuous version of Eq. (3.27), i.e.,

$$A_\varepsilon = A^1 + h_\varepsilon(A^2 - A^1), \tag{3.28}$$

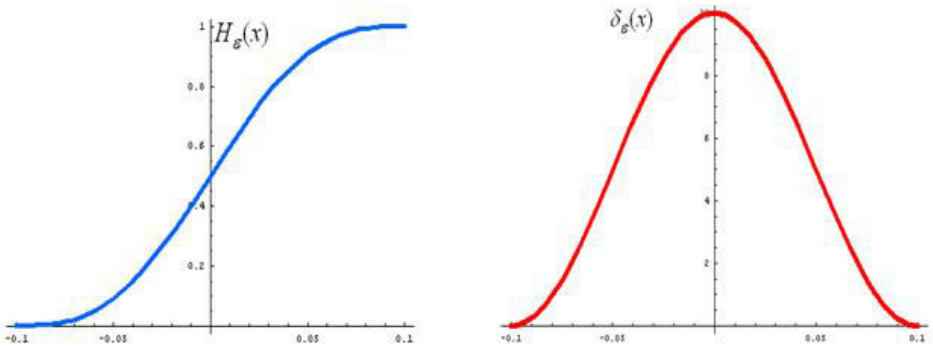

Figure 3.3: Plots of the smoothed Heaviside and Dirac delta functions for $\varepsilon = 0.1$. The transition width is 2ε.

where

$$h_\varepsilon = H_\varepsilon(\psi) = \begin{cases} 1, & \psi > \varepsilon, \\ 0, & \psi < -\varepsilon, \\ \frac{1}{2}\left(1 + \frac{\psi}{\varepsilon} + \frac{1}{\pi}\sin\left(\frac{\pi\psi}{\varepsilon}\right)\right), & |\psi| \leq \varepsilon. \end{cases} \quad . \tag{3.29}$$

It is apparent that h_ε is a regularized version of the Heaviside function. Notice that the field A is transformed into a continuous, but inhomogeneous, function in a narrow layer $S_\varepsilon = \{\mathbf{X} \in \Omega_R, |\psi(\mathbf{X}, t)| \leq \varepsilon\}$ around the interface. The parameter ε controls the thickness of the interface called regularization parameter. Furthermore, the regularized Dirac delta function is the derivative of the Heaviside step function

$$\delta_\varepsilon(\psi) = h_\varepsilon^{'}(\psi). \tag{3.30}$$

In Figure 3.3 we plot the regularized versions of Dirac delta and Heaviside functions for thickness $\varepsilon = 0.1$, where it is easily deduced that the interface has thickness 2ε.

For further development, we make the following computation for the time derivative of any inhomogeneous field A_ε applying the chain rule

$$\frac{dA_\varepsilon}{dt} = \frac{\partial A^{(1)}}{\partial t} + h_\varepsilon\left(\frac{\partial A^{(2)}}{\partial t} - \frac{\partial A^{(1)}}{\partial t}\right) + \frac{\partial A_\varepsilon}{\partial \psi}\dot{\psi} \tag{3.31}$$

and after using Eqs. $(3.24)_1$ and (3.30) the above derivative takes the form

$$\begin{aligned} \frac{dA_\varepsilon}{dt} &= \frac{\partial A^{(1)}}{\partial t} + h_\varepsilon\left(\frac{\partial A^{(2)}}{\partial t} - \frac{\partial A^{(1)}}{\partial t}\right) - \frac{\partial A_\varepsilon}{\partial \psi} V|\nabla\psi| \\ &= \frac{\partial A^{(1)}}{\partial t} + h_\varepsilon\left(\frac{\partial A^{(2)}}{\partial t} - \frac{\partial A^{(1)}}{\partial t}\right) - \frac{\partial A_\varepsilon}{\partial h_\varepsilon}\delta_\varepsilon(\psi) V|\nabla\psi|. \end{aligned} \tag{3.32}$$

Table 3.1: The governing equations for the two distinct problems and the two phase problem

Phase 1	*Phase* 2	*Two phase problem*
$\frac{d\rho_0^{(1)}}{dt} = 0$	$\frac{d\rho_0^{(2)}}{dt} = 0$	$\frac{d\rho_\varepsilon}{dt} = 0$
$\frac{d\mathbf{p}^{(1)}}{dt} - \mathrm{div}_\mathrm{R}\mathbf{T}^{(1)} = 0$	$\frac{d\mathbf{p}^{(2)}}{dt} - \mathrm{div}_\mathrm{R}\mathbf{T}^{(2)} = 0$	$\frac{d\mathbf{p}_\varepsilon}{dt} - \mathrm{div}_\mathrm{R}\mathbf{T}_\varepsilon = 0$
$\frac{dH^{(1)}}{dt} - \mathrm{div}_\mathrm{R}(\mathbf{T}\cdot\mathbf{v} - \mathbf{Q})^{(1)} = 0$	$\frac{dH^{(2)}}{dt} - \mathrm{div}_\mathrm{R}(\mathbf{T}\cdot\mathbf{v} - \mathbf{Q})^{(2)} = 0$	$\frac{dH_\varepsilon}{dt} - \mathrm{div}_\mathrm{R}(\mathbf{T}\cdot\mathbf{v} - \mathbf{Q})_\varepsilon = 0$
$\frac{dS^{(1)}}{dt} + \mathrm{div}_\mathrm{R}(\mathbf{Q}/\theta)^{(1)} = \sigma_S^{(1)}$	$\frac{dS^{(2)}}{dt} + \mathrm{div}_\mathrm{R}(\mathbf{Q}/\theta)^{(2)} = \sigma_S^{(2)}$	$\frac{dS_\varepsilon}{dt} + \mathrm{div}_\mathrm{R}(\mathbf{Q}/\theta)_\varepsilon = \sigma_S^\epsilon$
$\frac{d\mathbf{F}^{(1)}}{dt} = \mathrm{grad}_\mathrm{R}\mathbf{v}^{(1)}$	$\frac{d\mathbf{F}^{(2)}}{dt} = \mathrm{grad}_\mathrm{R}\mathbf{v}^{(2)}$	$\frac{d\mathbf{F}_\varepsilon}{dt} = \mathrm{grad}_\mathrm{R}\mathbf{v}_\varepsilon$

In a similar manner we can write for the spatial derivative of the quantity A_ε which depends on ψ *explicitly*

$$\begin{aligned}\frac{dA_\varepsilon}{d\mathbf{X}} &= \frac{\partial A^{(1)}}{\partial \mathbf{X}} + h_\varepsilon\left(\frac{\partial A^{(2)}}{\partial \mathbf{X}} - \frac{\partial A^{(1)}}{\partial \mathbf{X}}\right) + \frac{\partial A_\varepsilon}{\partial \psi}\frac{\partial \psi}{\partial \mathbf{X}} \\ &= \frac{\partial A^{(1)}}{\partial \mathbf{X}} + h_\varepsilon\left(\frac{\partial A^{(2)}}{\partial \mathbf{X}} - \frac{\partial A^{(1)}}{\partial \mathbf{X}}\right) + \frac{\partial A_\varepsilon}{\partial h_\varepsilon}\delta_\varepsilon(\psi)\nabla\psi. \qquad (3.33)\end{aligned}$$

With Eqs. (3.32) and (3.33) at hand we can determine the field equations of the mixed two phase problem as they given in the third column of Table 3.1. Consequently, the mass density is written

$$\frac{d\rho_\varepsilon}{dt} = \frac{\partial \rho_0^{(1)}}{\partial t} + h_\varepsilon\left(\frac{\partial \rho_0^{(2)}}{\partial t} - \frac{\partial \rho_0^{(1)}}{\partial t}\right) - \frac{\partial \rho_\varepsilon}{\partial h_\varepsilon}\delta_\varepsilon(\psi)V|\nabla\psi| = 0, \quad \text{in} \quad \Omega_R. \qquad (3.34)$$

According to Table 3.1 the first and second terms vanish, thus the equation is true outside the thin transition layer since $\delta_\varepsilon(\psi) = 0$, but within the layer Eq. (3.34) reads

$$V\frac{\partial \rho_\varepsilon}{\partial h_\varepsilon} = 0, \quad \text{in} \quad S_\varepsilon, \qquad (3.35)$$

where one can notice the similarity of the above relation to the jump condition (3.7). In a similar spirit the balance of the interpolated momentum provides the following condition in the thin layer S_ε

$$-\frac{\partial \mathbf{p}_\varepsilon}{\partial h_\varepsilon}\delta_\varepsilon(\psi)V|\nabla\psi| - \frac{\partial \mathbf{T}_\varepsilon}{\partial h_\varepsilon}\delta_\varepsilon(\psi)\nabla\psi = 0, \qquad (3.36)$$

or

$$\left(V\frac{\partial \mathbf{p}_\varepsilon}{\partial h_\varepsilon}+\frac{\partial \mathbf{T}_\varepsilon}{\partial h_\varepsilon}\frac{\nabla\psi}{|\nabla\psi|}\right)\delta_\varepsilon(\psi)=0. \tag{3.37}$$

and using Eq. $(3.23)_1$ we end up with the following relation within the transition layer

$$V\frac{\partial \mathbf{p}_\varepsilon}{\partial h_\varepsilon}+\frac{\partial \mathbf{T}_\varepsilon}{\partial h_\varepsilon}\cdot\mathbf{n}_s=0,\quad \text{in}\quad S_\varepsilon. \tag{3.38}$$

Following the same procedure we can write the other two balance laws

$$V\frac{\partial H_\varepsilon}{\partial h_\varepsilon}+\frac{\partial(\mathbf{T}\cdot\mathbf{v}-\mathbf{Q})_\varepsilon}{\partial h_\varepsilon}\cdot\mathbf{n}_s=0,\quad \text{in}\quad S_\varepsilon \tag{3.39}$$

and

$$V\frac{\partial(\theta S)_\varepsilon}{\partial h_\varepsilon}-\frac{\partial \mathbf{Q}_\varepsilon}{\partial h_\varepsilon}\cdot\mathbf{n}_s=0,\quad \text{in}\quad S_\varepsilon. \tag{3.40}$$

Finally, the compatibility equation within the transition layer must obey the following condition

$$-V\frac{\partial \mathbf{F}_\varepsilon}{\partial h_\varepsilon}=\frac{\partial \mathbf{v}_\varepsilon}{\partial h_\varepsilon}\otimes\mathbf{n}_s,\quad \text{in}\quad S_\varepsilon \tag{3.41}$$

Concluding our analysis we can claim that Eqs. (3.35), (3.38), (3.39) and (3.40) are the regularized versions of the Rankine-Hugoniot jump conditions of the standard sharp interface theory. In other words the standard jump conditions are recovered after taking the limit $\varepsilon\to 0$, since the relation "$\lim_{\varepsilon\to 0}\partial A/\partial h_\varepsilon=[\![A]\!]$" holds. These conditions should be fulfilled within the transition layer in order to ensure a coherent and homothermal phase boundary.

3.1.4 Material-Inhomogeneity forces

The introduction of the level set function induces explicit material inhomogeneities as was mentioned in the previous section. We assume a priori constant mass density, constant temperature and the following energy functional dependency (6)

$$W_\varepsilon(\mathbf{F}^1,\mathbf{F}^2,\psi)=W^1(\mathbf{F}^1)+h_\varepsilon(W^2(\mathbf{F}^2)-W^1(\mathbf{F}^1)), \tag{3.42}$$

where W^1 and W^2 correspond to the energy of each phase and the constitutive relations are given by Eq. (3.13). Note that selecting the specific type of energy yields a simpler form for the pseudo-momentum equation which now takes the form (52)

$$\frac{d\mathbf{P}}{dt}-\mathrm{div}_{\mathrm{R}}\boldsymbol{\Sigma}=\mathbf{f}^{inh},\quad \text{in}\quad \Omega_R, \tag{3.43}$$

with the difference that the equation contains regularized versions of the pseudo-momentum vector and the Eshelby stress tensor within the level set framework. The force term in the right hand side of Eq. (3.43) corresponds to the material inhomogeneity force given as

$$\mathbf{f}^{inh} = -\left.\frac{\partial W_\varepsilon}{\partial \mathbf{X}}\right|_{expl} = -\frac{\partial W_\varepsilon}{\partial \psi}\frac{\partial \psi}{\partial \mathbf{X}}. \tag{3.44}$$

or in the form

$$\mathbf{f}^{inh} = -\frac{\partial W_\varepsilon}{\partial h_\varepsilon}\delta_\varepsilon(\psi)\nabla\psi = -f_\varepsilon\delta_\varepsilon(\psi)\nabla\psi, \tag{3.45}$$

where we have set

$$f_\varepsilon = \frac{\partial W_\varepsilon}{\partial h_\varepsilon}. \tag{3.46}$$

Notice in Eq. (3.45) the crucial role of the Dirac delta function that confines material force to act only inside the thin transition layer where inhomogeneities are present. It is remarked that Eq. (3.46) is similar to the expression of the driving force for isothermal medium, as shown by Hou et al. (34) using a thermodynamical argument. Combining Eq. $(3.23)_1$ and Eq. (3.45) one can write

$$F_n = -\int_{\Omega_R} f_\varepsilon\delta_\varepsilon(\psi)|\nabla\psi|dv = \int_{\Omega_R} \mathbf{f}^{inh}\cdot\mathbf{n}_s dv, \tag{3.47}$$

where F_n is the resultant driving force on the layer S_ε.

It becomes evident that as in the sharp interface theory, the level set formulation provides us with the potential to determine only the driving force within the transition layer. Thus it seems reasonable to select an appropriate kinetic relation given by

$$V = g(f_\varepsilon, \mathbf{n}_s), \tag{3.48}$$

where V is computed globally inside the whole region of the body and the values within the layer S_ε correspond to the velocity of the interface. However, in the next section we present a simple one dimensional problem where the kinetic relation is derived and not taken by assumption.

3.1.5 A simple example: Phase transition in a bar

In this section we consider the simple case of a phase boundary propagation inside a one dimensional alloy bar separated in two phases within the level set framework, as

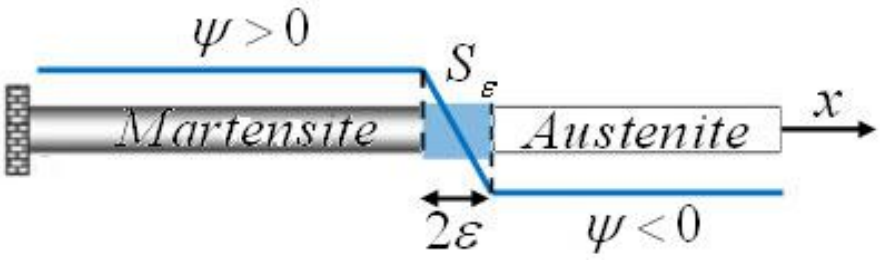

Figure 3.4: One-dimensional bar with two phases and the implicit representation of the phase boundary by the level set curve.

shown in Figure 3.4. We assume that the bar has constant temperature θ_0 and constant mass density ρ_0. It is assumed that we have two distinct problems to solve in the entire region: a martensite and an austenite. Using the level set method we give an implicit representation of the interface. In this problem the level set function $\psi(x,t)$ has the following property

$$\begin{cases} \psi\,(x,t) > 0, & Martensite, \\ \psi\,(x,t) < 0, & Austenite, \\ \psi\,(x,t) = 0, & S_t. \end{cases} \tag{3.49}$$

Within the level set framework the strain and velocity fields transform into inhomogeneous, but continuous functions through the whole bar. Thus based on the previous analysis we can write

$$e_\varepsilon = e^A + h_\varepsilon(e^M - e^A), \tag{3.50}$$

$$v_\varepsilon = v^A + h_\varepsilon(v^M - v^A) \tag{3.51}$$

where e^A, e^M denote the strain in each phase and the same applies for the energy of the bar written in the following form

$$W_\varepsilon(e^A, e^M, \psi) = W^A(e^A) + h_\varepsilon(W^M(e^M) - W^A(e^A)), \tag{3.52}$$

where the superscripts A and M stand for austenite and martensite, respectively. Note that the energy density of each phase is globally defined in the whole body. The stress tensor within the bar is then determined by the relation

$$\sigma_\varepsilon = \frac{\partial W^A}{\partial e^A} + h_\varepsilon(\frac{\partial W^M}{\partial e^M} - \frac{\partial W^A}{\partial e^A}) = \sigma^A + h_\varepsilon(\sigma^M - \sigma^A), \tag{3.53}$$

The field equations for the proposed simple problem are the physical momentum balance laws, the kinematic compatibility equations and the level set equation which governs the evolution of the interface

$$\rho_0 \frac{\partial \upsilon^{A,M}}{\partial t} = \frac{\partial \sigma^{A,M}}{\partial x}, \tag{3.54}$$

$$\frac{\partial e^{A,M}}{\partial t} = \frac{\partial \upsilon^{A,M}}{\partial x}, \tag{3.55}$$

$$\frac{\partial \psi}{\partial t} = -V \left| \frac{\partial \psi}{\partial x} \right|. \tag{3.56}$$

Moreover we can provide the regularized versions of the jump conditions which are very important for our further analysis. According to Eqs. (3.38) and (3.41) the following conditions within the transition layer S_ε should be valid

$$-\rho_0 V \frac{\partial \upsilon_\varepsilon}{\partial h_\varepsilon} = \frac{\partial \sigma_\varepsilon}{\partial h_\varepsilon}, \tag{3.57}$$

$$-V \frac{\partial e_\varepsilon}{\partial h_\varepsilon} = \frac{\partial \upsilon_\varepsilon}{\partial h_\varepsilon}. \tag{3.58}$$

Combining Eqs. (3.57) and (3.58) we end up with the following equation

$$\rho_0 V^2 \frac{\partial e_\varepsilon}{\partial h_\varepsilon} = \frac{\partial \sigma_\varepsilon}{\partial h_\varepsilon} \quad \text{or} \quad \rho_0 V^2 (e^M - e^A) = \sigma^M - \sigma^A, \quad \text{in} \quad S_\varepsilon. \tag{3.59}$$

It is remarked that Eq. (3.59) is the regularized version of the equation used in the standard sharp interface models (1; 9; 10; 11). This equation is convenient to determine the velocity of the front.

To derive the kinetic relation we need to determine the driving force acting in the transition layer. For this kind of problem the driving force is given by Eq. (3.46), which here takes the form

$$f_\varepsilon = W^M(e^M) - W^A(e^A). \tag{3.60}$$

We continue our analysis by selecting the characteristics of each phase. Specifically for the energy of each phase we adopt the expressions (1; 7; 8)

$$W^A = \frac{E}{2} e^{A2}, \quad W^M = \frac{E}{2}(e^M - e_{sp})^2 + \tau_0 \, e_{sp} \tag{3.61}$$

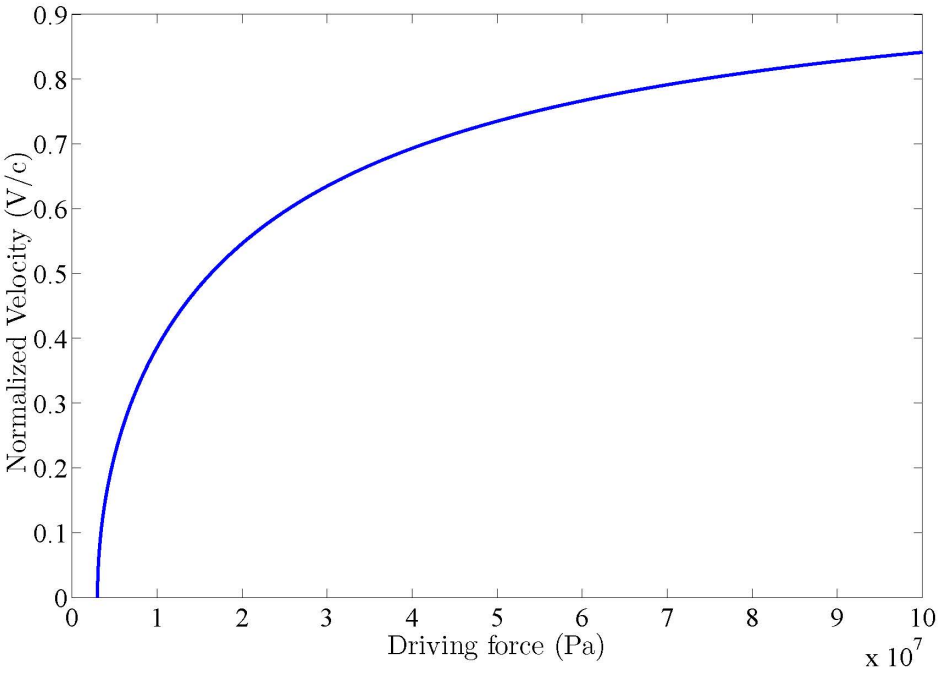

Figure 3.5: Plot of the proposed kinetic relation.

where the modulus E and the Maxwell stress τ_0 are positive constants and e_{sp} denotes the spontaneous strain in the absence of stresses in the martensite phase. The stress in each phase are given by

$$\sigma^A = Ee^A, \quad \sigma^M = E(e^M - e_{sp}), \tag{3.62}$$

which can be used to extract the following useful relation

$$e^M - e^A = \frac{\sigma^M - \sigma^A}{E} + e_{sp}. \tag{3.63}$$

According to Eq. (3.60) the driving force for the two phase problem takes the form

$$f_\varepsilon = \frac{E}{2}(e^M - e_{sp})^2 + \tau_0\, e_{sp} - \frac{E}{2}e^{A^2}. \tag{3.64}$$

A combination of Eqs. (3.59) and (3.63) yields the following relation

$$\rho_0 V^2 = E\frac{\sigma^M - \sigma^A}{\sigma^M - \sigma^A + Ee_{sp}}. \tag{3.65}$$

In order to find the desirable relation between the velocity of the front and the driving force we start by writing Eq. (3.64) with respect to stresses. Thus using Eq. (3.62) we can express the driving force as

$$\begin{aligned} f_\varepsilon &= \frac{1}{2E}(\sigma^{M\,2} - \sigma^{A\,2}) + \tau_0 e_{sp} \\ &= \frac{\sigma^M - \sigma^A}{E} \cdot \frac{\sigma^M + \sigma^A}{2} + \tau_0 e_{sp}, \end{aligned} \tag{3.66}$$

where the term $(\sigma^M + \sigma^A)/2$ represents the mean value of the stress in the thin transition layer S_ε. We identify the mean value of the stress at the phase boundary with the transformation stress (10) σ_{tr} leading to the relation

$$\sigma^M - \sigma^A = \frac{E}{\sigma_{tr}}(f_\varepsilon - \tau_0 e_{sp}), \tag{3.67}$$

which is in agreement with thermodynamical considerations (9). Substituting Eq. (3.67) into Eq. (3.65) we can finally determine the velocity of the front

$$\left(\frac{V}{c}\right)^2 = \frac{f_\varepsilon - \tau_0 e_{sp}}{f_\varepsilon - \tau_0 e_{sp} + \sigma_{tr} e_{sp}}, \tag{3.68}$$

where $c = \sqrt{E/\rho_0}$ corresponds to the shock wave velocity. If the material on both sides of the discontinuity belong to the same phase then the discontinuity is a shock wave (1). The above equation indicates $f_\varepsilon \geq \tau_0 e_{sp}$ meaning that there exists a critical value for the force. Also, it is easily deduced that $V < c$, which is expected, because phase boundaries propagate at subsonic speeds. It is noted that a similar equation was derived in (9; 11). The critical value of the force is obviously $f_{crt} = \tau_0 e_{sp}$ and it is in accordance with experimental observations of the existence of a threshold in the initiation of the martensitic phase transformation (2).

For the specific problem the material constants have been chosen as $E = 1\,\text{GPa}$, $\tau_0 = 30\,\text{MPa}$, $e_{sp} = 0.1$ and $\sigma_{tr} = 400\,\text{MPa}$. In Figure 3.5 we plot the kinetic relation resulting from the consideration of an implicit representation of the interface by the level set function. We point out that the kinetic curve exhibits the proper limit behavior for all values of the driving force as in other works. Indeed, if in Eq. (3.68) we set $f_\varepsilon = f_{crt}$, then $V = 0$ and if we assume $f_\varepsilon \gg f_{crt}$ then $V \to c$.

3.2 Phase Transitions in ferroelectrics

3.2.1 Sharp interface formulation

Consider an elastic ferroelectric body occupying the region $\Omega \subset \mathrm{IR}^2$. Ω is separated by a domain wall S in two subregions Ω^- and Ω^+ corresponding to domains of different oriented polarization. The unit normal $\mathbf{n}_S$ to the domain wall is directed from the domain Ω^- to Ω^+ as shown in Figure 3.1a. Notice that no care is taken on the nature of the domain wall, so as both 90° and 180° domain wall cases to be examined.

It is assumed that the constitutive response of the body is fixed in each domain. Moreover, limiting to quasi-static processes, the momentum and Gauss equations are

$$\begin{aligned} &\mathrm{div}\boldsymbol{\sigma} = 0, \quad \text{in} \quad \Omega^{\pm}, \\ &\mathrm{div}\mathbf{D} = 0, \quad \text{in} \quad \Omega^{\pm}, \end{aligned} \tag{3.69}$$

where $\boldsymbol{\sigma}$ is the Cauchy stress tensor and $\mathbf{D}$ is the electric displacement vector. In the above description inertial forces and electric charges within the body are ignored. The boundary conditions for the mechanical and electrical problem are

$$\begin{aligned} &\mathbf{u} = \bar{\mathbf{u}}, \quad \text{on} \quad \partial\Omega_u \\ &\boldsymbol{\sigma}\cdot\mathbf{n} = \mathbf{t}, \quad \text{on} \quad \partial\Omega_t, \end{aligned} \tag{3.70}$$

and

$$\begin{aligned} &\phi = \bar{\phi}, \quad \text{on} \quad \partial\Omega_\phi \\ &\mathbf{D}\cdot\mathbf{n} = q, \quad \text{on} \quad \partial\Omega_D, \end{aligned} \tag{3.71}$$

where $\mathbf{u}$ and ϕ are the mechanical displacement and the electric potential, $\bar{\mathbf{u}}$ and $\bar{\phi}$ denote their prescribed values on the boundary and last, $\mathbf{t}$ and q are the traction and the surface charge density. Also, the different parts of the boundary satisfy the following relations

$$\begin{aligned} &\partial\Omega_t \cup \partial\Omega_u = \partial\Omega \quad \text{and} \quad \partial\Omega_t \cap \partial\Omega_u = \emptyset, \\ &\partial\Omega_\phi \cup \partial\Omega_D = \partial\Omega \quad \text{and} \quad \partial\Omega_\phi \cap \partial\Omega_D = \emptyset. \end{aligned}$$

The stress tensor and the electric displacement vector satisfy the following jump conditions

$$\begin{aligned} &[\![\boldsymbol{\sigma}]\!]\cdot\mathbf{n}_S = 0, \quad \text{on} \quad S, \\ &[\![\mathbf{D}]\!]\cdot\mathbf{n}_S = 0, \quad \text{on} \quad S, \end{aligned} \tag{3.72}$$

where $[\![\bullet]\!] = \bullet^+ - \bullet^-$ denotes the jump of any field. The superscripts $+$ and $-$ indicate limits of the corresponding quantities as domain wall S is approached from Ω^+ or Ω^-, respectively.

Furthermore, on the domain wall the displacement $\mathbf{u}$ and electric potential ϕ are assumed continuous and piecewise differentiable

$$\begin{array}{lll} [\![\mathbf{u}]\!] = 0, & \text{on} & S, \\ [\![\phi]\!] = 0, & \text{on} & S. \end{array} \tag{3.73}$$

The first relation in Eq.(3.73) implies that interpenetration, sliding and separation of the domains are prohibited. The electric field and strain are given by the equations

$$\begin{aligned} \mathbf{E} &= -\nabla\phi, \\ \mathbf{e} &= \frac{1}{2}\left(\nabla\mathbf{u} + (\nabla\mathbf{u})^{\mathrm{T}}\right). \end{aligned} \tag{3.74}$$

Within each domain, the body exhibits the behavior of a linear piezoelectric material, thus the energy in each domain takes the general form

$$\begin{aligned} W(\mathbf{e},\mathbf{E}) = \frac{1}{2}(\mathbf{e}-\mathbf{e}^{\circ}) : [\mathbf{C}(\mathbf{e}-\mathbf{e}^{\circ})] \quad & -(\mathbf{e}-\mathbf{e}^{\circ}) : [\mathbf{d}^{\mathrm{T}}\mathbf{E}] - \\ & \tfrac{1}{2}\mathbf{E}\cdot(\mathbf{k}\mathbf{E}) - \mathbf{P}^{\circ}\cdot\mathbf{E}, \end{aligned} \tag{3.75}$$

where $\mathbf{P}^{\circ}$ is the spontaneous polarization of the domain, $\mathbf{C}$ the elastic stiffness matrix, $\mathbf{d}$ the piezoelectric tensor, $\mathbf{k}$ the dielectric tensor and $\mathbf{e}^{\circ}$ the spontaneous strain. Obviously one may distinguish the energy in each domain according to the spontaneous polarization orientation (55; 61). Thus, one can set

$$W = \left\{ \begin{array}{lll} W_1, & \text{in} & \Omega^{+} \\ W_2, & \text{in} & \Omega^{-} \end{array} \right. , \tag{3.76}$$

where

$$\begin{aligned} W_i(\mathbf{e},\mathbf{E}) = \frac{1}{2}(\mathbf{e}-\mathbf{e}_i^{\circ}) : [\mathbf{C}(\mathbf{e}-\mathbf{e}_i^{\circ})] - (\mathbf{e}-\mathbf{e}_i^{\circ}) : [\mathbf{d}_i^{\mathrm{T}}\mathbf{E}] - \\ \frac{1}{2}\mathbf{E}\cdot(\mathbf{k}\mathbf{E}) - \mathbf{P}_i^{\circ}\cdot\mathbf{E}, \quad i=1,2. \end{aligned} \tag{3.77}$$

In the above relations, the spontaneous strain and the piezoelectric tensor depend on spontaneous polarization vector, i.e., $\mathbf{e}_i^{\circ} = \mathbf{e}_i^{\circ}(\mathbf{P}_i^{\circ})$ and $\mathbf{d}_i = \mathbf{d}_i(\mathbf{P}_i^{\circ})$.

Using Eq. (3.77), the constitutive relations for stress and electric displacement are given by

$$\begin{aligned} \boldsymbol{\sigma}^i &= \frac{\partial W_i}{\partial \mathbf{e}} = \mathbf{C}\,(\mathbf{e}-\mathbf{e}_i^{\circ}) - \mathbf{d}_i^{\mathrm{T}}\mathbf{E}, \\ \mathbf{D}^i &= -\frac{\partial W_i}{\partial \mathbf{E}} = \mathbf{d}_i\,(\mathbf{e}-\mathbf{e}_i^{\circ}) + \mathbf{k}\mathbf{E} + \mathbf{P}_i^{\circ}. \end{aligned} \tag{3.78}$$

As mentioned above, the domain wall movement is accompanied by energy dissipation, which is nothing but the excess of the external work rate over the rate of change of stored energy

$$\Delta = \int_{\partial\Omega} \boldsymbol{\sigma}\mathbf{n} \cdot \boldsymbol{\upsilon} ds - \int_{\Omega} \mathbf{D} \cdot \dot{\mathbf{E}} d\Omega - \frac{d}{dt} \int_{\Omega} W d\Omega, \tag{3.79}$$

where $\boldsymbol{\upsilon}$ is the particle velocity. The first term accounts for the power due to external mechanical forces, the second for the power due to external electric field and the third is the rate of change of stored energy. In sharp interface theories it is proved (3) that

$$\Delta = \int_{S} f V ds \geq 0. \tag{3.80}$$

Following (55), (51), the driving force is proved to be

$$f = -\mathbf{n}_S \cdot \left([\![\boldsymbol{\Sigma}]\!] \, \mathbf{n}_S \right), \tag{3.81}$$

where $\boldsymbol{\Sigma}$ is the Eshelby stress tensor (49), (51) for electro-elasticity given by

$$\boldsymbol{\Sigma} = W\mathbf{I} - (\nabla \mathbf{u})\boldsymbol{\sigma} + \mathbf{E} \otimes \mathbf{D}. \tag{3.82}$$

In the above relation $\otimes$ denotes the classic tensorial product. Equation (3.80) expresses the second law of thermodynamics implying that the interface will always move to the direction of the driving force.

However, the problem is not yet well defined, thus additional constitutive information is needed. We have already discussed the fact that the solution uniqueness of such problems needs a kinetic relation between the driving force on the domain wall and its normal velocity,

$$V = V\left(f, \mathbf{n}_S\right), \quad \text{on} \quad S. \tag{3.83}$$

It becomes evident that for a given domain pattern inside a ferroelectric material, one has to solve the mechanical equilibrium and the Gauss equation as a coupled boundary value problem. The driving force exerted on domain walls is computed by Eq. (3.81), and the velocity from Eq. (3.83). The velocity then updates the domain pattern for the next time step. This approach is referred to as "local approach" (48), but its numerical implementation is not an easy task. For instance, in a finite element scheme the mesh needs refinement at each time step so as to keep tracking the interface.

3.2.2 Continuous Energy and Material Forces in the Level Set Framework

3.2.2.1 Continuous Energy

For the needs of the level set method, one can write Eq. (3.76) as an interpolation between the two branches

$$W(\mathbf{e},\mathbf{E}) = W_1(\mathbf{e},\mathbf{E}) + h(W_2(\mathbf{e},\mathbf{E}) - W_1(\mathbf{e},\mathbf{E})), \tag{3.84}$$

where h is the Heaviside function. The next step is to introduce a continuous version of Eq. (3.84), i.e.,

$$W_\varepsilon(\mathbf{e},\mathbf{E},h_\varepsilon) = W_1(\mathbf{e},\mathbf{E}) + h_\varepsilon(W_2(\mathbf{e},\mathbf{E}) - W_1(\mathbf{e},\mathbf{E})), \tag{3.85}$$

where h_ε is a regularized version of the Heaviside function given by Eq. (3.29). Notice that the non-continuous energy in Eq. (3.76) is transformed into a continuous, but inhomogeneous, function in a narrow layer $S_\varepsilon = \{\mathbf{x} \in \mathbf{\Omega}, |\psi(\mathbf{x},\mathbf{t})| \leq \varepsilon\}$ around the interface. The parameter ε controls the thickness of the interface.

> **Remark 3.1:** *It is noted that the treatment of a moving singularity in a ferroelectric crystal is much simpler than that presented in the previous section. Here, we do not assume two different problems solved in the same region and apparently there is no need to talk about conditions within the thin transition layer (strain field and electric potential are taken to be continuous).*

3.2.2.2 A variational principle

To study domain wall kinetics in elastic ferroelectrics, it is necessary to derive the appropriate field equations and boundary conditions corresponding to the above energy. To this end a variational principle will be used. Consider the energy functional

$$I[\mathbf{u},\phi,\psi] = \frac{p}{2}\int_\Omega (|\nabla\psi| - 1)^2 d\Omega + \int_\Omega W_\varepsilon d\Omega - \int_{\partial\Omega_t} \mathbf{t}\cdot\mathbf{u} ds - \int_{\partial\Omega_D} q\phi ds, \tag{3.86}$$

where p is a new parameter penalizing the deviation from the signed distance function. The first integral in Eq. (3.86) is an energy term used as a metric (45) to characterize how close to a signed distance function is the level set function ψ. For arbitrary variations of the independent variables $\mathbf{u}, \phi, \psi$, the energy functional should vanish leading to an extremum for the energy of the system

$$\delta I[\mathbf{u}, \phi, \psi; \delta\mathbf{u}, \delta\phi, \delta\psi] = 0. \tag{3.87}$$

Taking variations for the displacement field $\mathbf{u}$ and the electric potential ϕ, one derives the mechanical equilibrium equation and Gauss law, respectively

$$\mathrm{div}\boldsymbol{\sigma}_\varepsilon = 0, \quad \mathrm{div}\mathbf{D}_\varepsilon = 0, \quad \text{in} \quad \Omega. \tag{3.88}$$

In addition the following boundary conditions can be obtained

$$\begin{array}{l} \boldsymbol{\sigma}_\varepsilon \cdot \mathbf{n} = \mathbf{t} \quad \text{on} \quad \partial\Omega_t, \\ \mathbf{D}_\varepsilon \cdot \mathbf{n} = q, \quad \text{on} \quad \partial\Omega_D, \end{array} \tag{3.89}$$

where $\boldsymbol{\sigma}_\varepsilon$ and $\mathbf{D}_\varepsilon$ are the regularized versions of Cauchy stress tensor and electric displacement vector given by the constitutive relations

$$\boldsymbol{\sigma}_\varepsilon = \frac{\partial W_\varepsilon}{\partial \mathbf{e}}, \quad \mathbf{D}_\varepsilon = -\frac{\partial W_\varepsilon}{\partial \mathbf{E}}. \tag{3.90}$$

Combining Eqs. (3.85), (3.90), one can further determine the Cauchy stress tensor and electric displacement vector:

$$\begin{aligned} \mathbf{D}_\varepsilon &= -\frac{\partial W_1}{\partial \mathbf{E}} + h_\varepsilon(-\frac{\partial W_2}{\partial \mathbf{E}} + \frac{\partial W_1}{\partial \mathbf{E}}) = \mathbf{D}^1 + h_\varepsilon(\mathbf{D}^2 - \mathbf{D}^1), \\ \boldsymbol{\sigma}_\varepsilon &= \frac{\partial W_1}{\partial \mathbf{e}} + h_\varepsilon(\frac{\partial W_2}{\partial \mathbf{e}} - \frac{\partial W_1}{\partial \mathbf{e}}) = \boldsymbol{\sigma}^1 + h_\varepsilon(\boldsymbol{\sigma}^2 - \boldsymbol{\sigma}^1). \end{aligned} \tag{3.91}$$

Notice that the jump conditions in Eq. (3.72) no longer hold and the transition from one region to the other is smooth. In other words, Eq. (3.91) is the continuous version of Eq. (3.78).

To complete the analysis, arbitrary variations of the energy functional I with respect

to ψ are considered

$$\begin{aligned}
\frac{\delta I}{\delta \psi} &= p \int_{\Omega} \left(|\nabla \psi| - 1\right) \delta \left(|\nabla \psi|\right) d\Omega + \int_{\Omega} \frac{\partial W_{\varepsilon}}{\partial \psi} \delta \psi d\Omega \\
&= p \int_{\Omega} \left(|\nabla \psi| - 1\right) \left[\frac{\nabla \psi \cdot \nabla \left(\delta \psi\right)}{|\nabla \psi|}\right] d\Omega \\
&+ \int_{\Omega} \frac{\partial W_{\varepsilon}}{\partial h_{\varepsilon}} h_{\varepsilon}^{'} \delta \psi d\Omega \\
&= p(\int_{\Omega} \nabla \psi \cdot \nabla \left(\delta \psi\right) d\Omega - \int_{\Omega} \frac{\nabla \psi}{|\nabla \psi|} \cdot \nabla \left(\delta \psi\right) d\Omega) \\
&+ \int_{\Omega} \frac{\partial W_{\varepsilon}}{\partial h_{\varepsilon}} \delta_{\varepsilon}(\psi) \delta \psi d\Omega,
\end{aligned}$$

where $\delta_{\varepsilon} = h_{\varepsilon}^{'}$. After applying the divergence theorem in both integrals and using Eq. $(3.23)_2$, one obtains

$$\begin{aligned}
\frac{\delta I}{\delta \psi} &= p(\int_{\partial\Omega} \left(\nabla \psi \cdot \mathbf{n}\right) \delta \psi dS - \int_{\Omega} \left[\nabla \cdot \left(\nabla \psi\right)\right] \delta \psi d\Omega) \\
&- p(\int_{\partial\Omega} \frac{\left(\nabla \psi \cdot \mathbf{n}\right)}{|\nabla \psi|} \delta \psi dS - \int_{\Omega} \left[\nabla \cdot \left(\frac{\nabla \psi}{|\nabla \psi|}\right)\right] \delta \psi d\Omega) \\
&+ \int_{\Omega} \frac{\partial W_{\varepsilon}}{\partial h_{\varepsilon}} \delta_{\varepsilon}(\psi) \delta \psi d\Omega \\
&= p \int_{\partial\Omega} \left(1 - \frac{1}{|\nabla \psi|}\right) \left(\nabla \psi \cdot \mathbf{n}\right) \delta \psi dS - \int_{\Omega} p \left(\Delta \psi - \kappa\right) \delta \psi d\Omega \\
&+ \int_{\Omega} \frac{\partial W_{\varepsilon}}{\partial h_{\varepsilon}} \delta_{\varepsilon}(\psi) \delta \psi d\Omega \\
&= - \int_{\Omega} [p(\Delta \psi - \kappa) - \frac{\partial W_{\varepsilon}}{\partial h_{\varepsilon}} \delta_{\varepsilon}(\psi)] \delta \psi d\Omega \\
&+ p \int_{\partial\Omega} \left(1 - \frac{1}{|\nabla \psi|}\right) \left(\nabla \psi \cdot \mathbf{n}\right) \delta \psi dS.
\end{aligned}$$

Adopting a gradient flow argument, thus attributing an evolution character to the extremum problem, one may take

$$\int_{\Omega} \frac{\partial \psi}{\partial t} d\Omega = -M \frac{\delta I}{\delta \psi}, \tag{3.92}$$

where M is the mobility of the process. Furthermore, based on the work of Zhao *et al.* (85), the function $\delta_\varepsilon(\psi)$ is replaced by $|\nabla\psi|$. According to these authors, this is a time re-scaling that does not affect the steady state solution, since only the speed of gradient flow is affected and not its direction. The above considerations result in the evolution equation of the level set function

$$\frac{\partial\psi}{\partial t} = \mu(\Delta\psi - \kappa) - M\frac{\partial W_\varepsilon}{\partial h_\varepsilon}|\nabla\psi|, \quad \text{in} \quad \Omega, \tag{3.93}$$

where $\mu = pM$ and the boundary condition

$$\nabla\psi \cdot \mathbf{n} = 0, \quad \text{on} \quad \partial\Omega. \tag{3.94}$$

Comparing Eqs. (3.93) and (3.24), one deduces that the above variational principle defines indirectly the kinetic relation. Indeed, defining

$$f_\varepsilon = -\frac{\partial W_\varepsilon}{\partial h_\varepsilon}, \quad \text{in} \quad S_\varepsilon \tag{3.95}$$

as the driving force moving the zero level set of ψ, the following kinetic relation emerges

$$V = V(f_\varepsilon, \mathbf{n}_S) = M\, f_\varepsilon, \tag{3.96}$$

where $M = M(\mathbf{n}_S)$ is the mobility of the domain wall which in general depends on the normal unit vector $\mathbf{n}_S$ and accounts for anisotropic effects. It is remarked that Hou *et al.* (34) derived the same expression for the driving force by the use of thermodynamical argument. Finally, our analysis concludes in the following equation and boundary condition

$$\begin{array}{l} \dfrac{\partial\psi}{\partial t} = \mu(\Delta\psi - \kappa) + V|\nabla\psi|, \quad \text{in} \quad \Omega \\ \nabla\psi \cdot \mathbf{n} = 0, \quad \text{on} \quad \partial\Omega. \end{array} \tag{3.97}$$

The first term of the evolution equation keeps the level set function as a signed distance function, while the second term moves the level set function with velocity determined by the kinetic relation. It is obvious that no need for re-initialization is necessary anymore. Variational level set methods can be found in other interesting problems (26; 27).

Remark 3.2: *It is remarked that no surface energy was included in the sharp interface theory adopted in this work. If such energy was taken into*

account, then the resulting driving force would include an extra term related explicitly to the curvature of the interface (30), (48). For instance, if a surface energy of the form $\int_S \gamma ds$ *is assumed for the sharp interface model where* γ *is the energy per unit surface on the interface, then the driving force in Eq. (3.81) will be given as* (30), (48)

$$f = \gamma\kappa - \mathbf{n}_S \cdot (\llbracket \boldsymbol{\Sigma} \rrbracket \, \mathbf{n}_S), \quad \text{on} \quad S. \tag{3.98}$$

In the level set method, accounting for the surface energy γ *will modify our result for the level set equation, i.e. Eq. (3.93). The latter will take the form*

$$\frac{\partial \psi}{\partial t} = \mu(\Delta\psi - \kappa) - M(\frac{\partial W_\varepsilon}{\partial h_\varepsilon} - \gamma\kappa)|\nabla\psi|, \quad \text{in} \quad \Omega, \tag{3.99}$$

as one could extract from the work of Zhang et al. *(83) and Esedoglu and Smereka (29). This finally results in a smooth driving force of the form*

$$f_\varepsilon = \gamma\kappa - \frac{\partial W_\varepsilon}{\partial h_\varepsilon}, \quad \text{in} \quad S_\varepsilon. \tag{3.100}$$

Please notice that in Eq. (3.99) *the interface curvature emerges in two distinct terms coming from two distinct sources: the re-initialization procedure and the surface energy. It is worth noting that the curvature of the interface, as it appears in the present work, i.e. Eq.* (3.93)*, is exclusively due to the re-initialization procedure and has nothing to do with the surface energy. Nevertheless, in a level set approach one could consider a surface energy term as Hou* et al. *(34) did, accounting for that part of the bulk energy contained in the layer* S_ε*. In that case one must be warned that this term vanishes at the sharp interface limit as thoroughly explained in Ref. (34).*

3.2.2.3 Material forces

The sharp interface theory presented previously shows that on domain walls the driving force is given by Eq. (3.81), where the Eshelby stress tensor is involved. In the level set framework the driving force is determined by Eq. (3.95), thus it is reasonable to

wonder on the role that material forces might play in that case. Equation (3.85) is written in the following form (37; 38)

$$\bar{W}(\mathbf{e}, \mathbf{E}, \mathbf{x}) = W_\varepsilon(\mathbf{e}, \mathbf{E}, h_\varepsilon(\psi(\mathbf{x}))), \tag{3.101}$$

so as to underline the explicit dependence of the energy function on $\mathbf{x}$. Then, the equilibrium equation for configurational forces holds (7; 8; 30; 49)

$$\mathrm{div}\boldsymbol{\Sigma} + \mathbf{f}_{\mathrm{inh}} = 0, \quad \text{in} \quad \Omega, \tag{3.102}$$

where $\mathbf{f}_{\mathrm{inh}}$ represents the inhomogeneity forces and $\boldsymbol{\Sigma}$ the Eshelby tensor given by

$$\boldsymbol{\Sigma} = \bar{W}\mathbf{I} - (\nabla\mathbf{u})\boldsymbol{\sigma}_\varepsilon + \mathbf{E} \otimes \mathbf{D}_\varepsilon. \tag{3.103}$$

A simple calculation gives

$$\mathbf{f}_{\mathrm{inh}} = -\frac{\partial \bar{W}}{\partial \mathbf{x}} = -\frac{\partial W_\varepsilon}{\partial h_\varepsilon} h_\varepsilon' \frac{\partial \psi}{\partial \mathbf{x}} = -\frac{\partial W_\varepsilon}{\partial h_\varepsilon} \delta_\varepsilon(\psi) \nabla\psi. \tag{3.104}$$

Combining Eq. $(3.23)_1$ and Eq. (3.104) one can write

$$F_n = \int_\Omega f_\varepsilon \delta_\varepsilon(\psi) |\nabla\psi| d\Omega = \int_\Omega \mathbf{f}_{\mathrm{inh}} \cdot \mathbf{n}_S d\Omega, \tag{3.105}$$

where F_n is the resultant driving force on the layer S_ε. Also, using the equilibrium of the material forces in Eq. (3.102) the resultant driving force can be written

$$F_n = -\int_\Omega \mathrm{div}\boldsymbol{\Sigma} \cdot \mathbf{n}_S d\Omega. \tag{3.106}$$

The above Eqs. (3.105) and (3.106) show that the concept of material force can be naturally inserted in the framework of the level set method. Moreover, Eq. (3.106) shows that the Eshelby stress tensor can be used for the computation of the driving force.

3.2.3 Two level set functions

So far we have studied the dynamics of a single domain wall in a ferroelectric by the use of one level set function thus being limited only to two distinct phases. However, there are domain patterns with more than two phases. Motivated by this fact, two

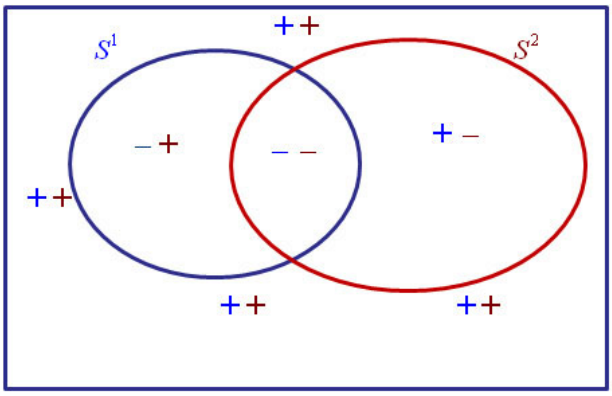

Figure 3.6: The domain Ω separated in four regions by the interfaces S^1 and S^2

distinct level set functions ψ_1 and ψ_2 are introduced in this section. In this way, it is possible to form four different phases of the material corresponding to the four possible orientations of the polarization in 2-D ferroelectrics with tetragonal crystal symmetry. According to Figure 3.6, one can write for the implicit representation of the interfaces S^1 and S^2 via level set functions ψ_1 and ψ_2

$$S^1 = \{\mathbf{x} \in \Omega | \psi_1(\mathbf{x}, t) = 0\}, \quad S^2 = \{\mathbf{x} \in \Omega | \psi_2(\mathbf{x}, t) = 0\}. \tag{3.107}$$

The domains arisen from ψ_1 and ψ_2 are given as

$$\begin{aligned}
\Omega^{++} &= \{\mathbf{x} \in \Omega \,|\, \psi_1(\mathbf{x}, t) > 0 \text{ and } \psi_2(\mathbf{x}, t) > 0\}, \\
\Omega^{--} &= \{\mathbf{x} \in \Omega \,|\, \psi_1(\mathbf{x}, t) < 0 \text{ and } \psi_2(\mathbf{x}, t) < 0\}, \\
\Omega^{+-} &= \{\mathbf{x} \in \Omega \,|\, \psi_1(\mathbf{x}, t) > 0 \text{ and } \psi_2(\mathbf{x}, t) < 0\}, \\
\Omega^{-+} &= \{\mathbf{x} \in \Omega \,|\, \psi_1(\mathbf{x}, t) < 0 \text{ and } \psi_2(\mathbf{x}, t) > 0\}.
\end{aligned} \tag{3.108}$$

The above regions correspond to the polarization phases $\mathbf{P}^{++} = (p_0 \quad 0)^{\mathrm{T}}$, $\mathbf{P}^{--} = (-p_0 \quad 0)^{\mathrm{T}}$, $\mathbf{P}^{-+} = (0 \quad -p_0)^{\mathrm{T}}$ and $\mathbf{P}^{+-} = (0 \quad p_0)^{\mathrm{T}}$, where p_0 is the spontaneous polarization magnitude. Unlike the work of Zhao *et al.* (85), in this paper overlapping is not prohibited and in fact intersecting area corresponds to an additional phase of the material. To study the multiphase problem, it is necessary to formulate an appropriate expression for the energy of the material containing the above four phases (37). As before a regularized version of the energy is adopted

$$\begin{aligned}
W_\varepsilon(\mathbf{e}, \mathbf{E}, h_\varepsilon^1, h_\varepsilon^2) \quad &= (W_2 - W_1)h_\varepsilon^1 + (W_3 - W_1)h_\varepsilon^2 \\
&+(W_4 + W_1 - W_2 - W_3)h_\varepsilon^1 h_\varepsilon^2 + W_1,
\end{aligned} \tag{3.109}$$

where W_1, W_2, W_3, W_4 are the energy expressions for each region and $h_\varepsilon^1 = H_\varepsilon(\psi_1)$ and $h_\varepsilon^2 = H_\varepsilon(\psi_2)$.

The next step is to determine the driving forces moving the two level sets. As it has been proved, they are inhomogeneity forces and it makes sense to use a procedure similar to that presented previously,

$$\begin{aligned} -\frac{\partial \bar{W}}{\partial \mathbf{x}} &= -\frac{\partial W_\varepsilon}{\partial h_\varepsilon^1}\delta_\varepsilon(\psi_1)\nabla\psi_1 - \frac{\partial W_\varepsilon}{\partial h_\varepsilon^2}\delta_\varepsilon(\psi_2)\nabla\psi_2 \\ &= \mathbf{f}_{\text{inh}}^1 + \mathbf{f}_{\text{inh}}^2. \end{aligned} \tag{3.110}$$

One can notice the crucial role of the delta function δ_ε which confines the material forces to act within the thin layer S_ε^1 and S_ε^2 where the inhomogeneities are present. According to Eq. (3.110) the driving forces on the interface layers are

$$f_\varepsilon^1 = -\frac{\partial W_\varepsilon}{\partial h_\varepsilon^1}, \quad f_\varepsilon^2 = -\frac{\partial W_\varepsilon}{\partial h_\varepsilon^2} \tag{3.111}$$

that must be used in the kinetic relations to determine the velocities of the zero level sets. In a general theoretical framework the kinetic relations are assumed to be of the form

$$V_i = V_i(f_\varepsilon^1, f_\varepsilon^2, \mathbf{n}_{S^1}, \mathbf{n}_{S^2}), \quad i = 1, 2, \tag{3.112}$$

to account for the interaction between the surface layers S_ε^1 and S_ε^2.

In concluding, the field equations and boundary conditions for the problem under study take the final form

$$\begin{aligned} &\nabla \cdot \boldsymbol{\sigma}_\varepsilon = 0, \quad \nabla \cdot \mathbf{D}_\varepsilon = 0, \quad \text{in} \quad \Omega \\ &\frac{\partial \psi_i}{\partial t} = \mu_i \left(\Delta\psi_i - \kappa_i\right) + V_i \left|\nabla\psi_i\right|, \quad \text{in} \quad \Omega, \quad i = 1, 2 \\ &\boldsymbol{\sigma}_\varepsilon \cdot \mathbf{n} = 0, \quad \mathbf{D}_\varepsilon \cdot \mathbf{n} = 0, \quad \nabla\psi_i \cdot \mathbf{n} = 0, \quad \text{on} \quad \partial\Omega. \end{aligned} \tag{3.113}$$

Certainly, in order the above system to be solvable, one must consider the constitutive relations given by Eq. (3.90) and a specific selection for the kinetic relations provided by Eq. (3.112).

3.3 Computational results

3.3.1 Finite element implementation and parameter selection

In this subsection, the finite element implementation of the level set equation coupled with the Gauss law and the mechanical equilibrium equation is presented. To apply

the finite element method one has to derive the weak forms of the governing equations. Following the standard procedure from the strong forms one can obtain

$$\int_\Omega \boldsymbol{\sigma}_\varepsilon \nabla(\delta\mathbf{u}) d\Omega - \int_{\partial\Omega_t} \mathbf{t}\cdot\delta\mathbf{u} ds = 0, \tag{3.114}$$

$$\int_\Omega \mathbf{D}_\varepsilon \nabla(\delta\phi) d\Omega - \int_{\partial\Omega_D} q\,\delta\phi\, ds = 0, \tag{3.115}$$

$$\int_\Omega [(\tfrac{\partial\psi}{\partial t} - V|\nabla\psi|)\delta\psi + \mu(1-|\nabla\psi|^{-1})\nabla\psi\cdot\nabla(\delta\psi)] d\Omega = 0, \tag{3.116}$$

where with $\delta\mathbf{u}, \delta\phi, \delta\psi$ we denote the test functions. Consider a discretization of the domain Ω consisting of n_{el} finite elements

$$\Omega = \bigcup_{e=1}^{n_{el}} \Omega_e, \tag{3.117}$$

where $\Omega_e, e = 1, \ldots, n_{el}$, denote the finite elements of the mesh. In element level, the finite element solution of the unknown fields is taken to be of the form

$$\mathbf{u} = \mathbf{N}_u(\mathbf{x})\tilde{\mathbf{u}}(t), \quad \phi = \mathbf{N}_\phi(\mathbf{x})\tilde{\boldsymbol{\phi}}(t), \quad \psi = \mathbf{N}_\psi(\mathbf{x})\tilde{\boldsymbol{\psi}}(t), \tag{3.118}$$

where $\mathbf{N_u}$,$\mathbf{N}_\phi$, $\mathbf{N}_\psi$ are the appropriate matrices of the shape functions for the displacements, the electric potential and the level set function, respectively. The vectors $\tilde{\mathbf{u}}$, $\tilde{\boldsymbol{\phi}}$ and $\tilde{\boldsymbol{\psi}}$ consist of the unknown nodal parameters of the fields $\mathbf{u}, \phi$ and ψ, respectively. The same shape functions are used to interpolate the test functions as well as the space and time derivatives

$$\begin{aligned} &\delta\mathbf{u} = \mathbf{N}_u\delta\tilde{\mathbf{u}}, \quad \delta\phi = \mathbf{N}_\phi\delta\tilde{\boldsymbol{\phi}}, \quad \delta\psi = \mathbf{N}_\psi\delta\tilde{\boldsymbol{\psi}}, \\ &\nabla\mathbf{u} = \mathbf{B}_u\tilde{\mathbf{u}}, \quad \nabla\phi = \mathbf{B}_\phi\tilde{\boldsymbol{\phi}}, \quad \nabla\psi = \mathbf{B}_\psi\tilde{\boldsymbol{\psi}}, \; \dot{\psi} = \mathbf{N}_\psi\dot{\tilde{\boldsymbol{\psi}}}, \end{aligned} \tag{3.119}$$

where $\mathbf{B}_u$, $\mathbf{B}_\phi$ and $\mathbf{B}_\psi$ denote the spatial derivatives of the shape function matrices $\mathbf{N}_u$, $\mathbf{N}_\phi$ and $\mathbf{N}_\psi$, respectively.

Substitution of Eqs. (3.118) and (3.119) into Eqs. (3.114), (3.115) yields the following discretized equations

$$\begin{aligned} &\int_{\Omega_e} \mathbf{B}_u^{\mathrm{T}}\tilde{\boldsymbol{\sigma}}_\varepsilon d\Omega - \int_{\partial\Omega_t^e} \mathbf{N}_u\mathbf{t} ds = 0 \\ &\int_{\Omega_e} \mathbf{B}_\phi^{\mathrm{T}}\tilde{\mathbf{D}}_\varepsilon d\Omega - \int_{\partial\Omega_D^e} q\,\mathbf{N}_\phi\, ds = 0, \end{aligned} \tag{3.120}$$

where $\tilde{\boldsymbol{\sigma}}_\varepsilon$ and $\tilde{\mathbf{D}}_\varepsilon$ are the discretized stress and electric displacement, respectively.

The discetized level set equation can be written in a more specific form. After substitution of Eqs. (3.118), (3.119) into Eq. (3.116) the following equation can be obtained

$$\tilde{\mathbf{C}}\dot{\tilde{\boldsymbol{\psi}}} + \tilde{\mathbf{K}}\tilde{\boldsymbol{\psi}} + \mathbf{f} = 0, \tag{3.121}$$

where

$$\tilde{\mathbf{C}} = \int_{\Omega_e} \mathbf{N}_\psi^{\mathrm{T}} \mathbf{N}_\psi d\Omega, \quad \mathbf{f} = -\int_{\Omega_e} \mathbf{N}_\psi^{\mathrm{T}} \tilde{V} \sqrt{\tilde{\boldsymbol{\psi}}^{\mathrm{T}} \mathbf{B}_\psi^{\mathrm{T}} \mathbf{B}_\psi \tilde{\boldsymbol{\psi}}} d\Omega$$

$$\tilde{\mathbf{K}} = \mu \int_{\Omega_e} (1 - (\tilde{\boldsymbol{\psi}}^{\mathrm{T}} \mathbf{B}_\psi^{\mathrm{T}} \mathbf{B}_\psi \tilde{\boldsymbol{\psi}})^{-1/2}) \mathbf{B}_\psi^{\mathrm{T}} \mathbf{B}_\psi d\Omega.$$

Employing the standard assembly procedure one can conclude to the overall system of equations. In this work, the finite element solution of the coupled field problem is accomplished by the use of FEMLAB. Time discetization is accomplished by the use of an implicit time integration scheme and at each time step the nonlinear algebraic system is linearized through Newton-Raphson method. The FEMLAB uses the direct UMFPACK solver, which is a set of routines to solve the final linear system of equations, by performing LU factorization. Here, triangular meshes were used with Lagrange quadratic shape functions. The interested reader is referred to a standard text book on finite element method (86) and to the FEMLAB handbook for more details.

To solve numerically the system of equations, the ferroelectric soft lead zirconate titanate has been selected. In the 2-D setting, plane strain and plane polarization conditions were considered. Also, the material is assumed to be transversally isotropic with axis of anisotropy coinciding with the corresponding polarization axis, so when the material is poled in the positive x_2 direction the material parameters are chosen (61)

$$\mathbf{C} = \begin{pmatrix} 12.6 & 5.3 & 0 \\ 5.3 & 11.7 & 0 \\ 0 & 0 & 3.53 \end{pmatrix} 10^{10}\,\mathrm{Pa},$$

$$\mathbf{d} = \begin{pmatrix} 0 & 0 & 17 \\ -6.5 & 23.3 & 0 \end{pmatrix} \tfrac{\mathrm{C}}{\mathrm{m}^2}, \quad \mathbf{e}^\circ = \begin{pmatrix} -0.0039 \\ 0.0076 \\ 0 \end{pmatrix},$$

$$\mathbf{P}^0 = \begin{pmatrix} 0 \\ 0.2 \end{pmatrix} \tfrac{\mathrm{C}}{\mathrm{m}^2}, \quad \mathbf{k} = \begin{pmatrix} 1.51 & 0 \\ 0 & 1.3 \end{pmatrix} 10^{-8}\, \tfrac{\mathrm{C}}{\mathrm{Vm}}.$$

To describe the other three phases, changes have to be made to the above material parameters so as to conform to the spontaneous polarization. If the material is poled

in the negative x_2 direction (180° domain wall) only the piezoelectric tensor will change inverting the sign of all entries. For a 90°-rotation of the x_2 axis (90° domain wall) all materials tensors have to change accordingly.

3.3.2 Domain growth under electromechanical loading

The evolution of a domain within a single ferroelectric crystal is examined. It is considered as a two phase problem, thus according to our analysis one must use only one level set function to represent the interface. In what follows, two distinct cases of a single domain evolution within a large parent domain are examined. The first case concerns the development of a domain with polarization opposite to the surrounding domain while the second a domain with polarization vertical to the parent domain polarization. Notice that the interest of this work is focused on the domain evolution and no care is taken on the nucleation mechanism. As it is mentioned in subsection 3.2.2.2, the kinetic relation for the two–phase problem is given by Eq. (3.96). In the case of 180° and 90° domain nucleus, it is assumed a specific relation of the form

$$V = M_1\, f_\varepsilon + M_2\, f_\varepsilon\, |n_S^2 - n_S^1|, \tag{3.122}$$

where M_1, M_2 are the mobilities of the isotropic and anisotropic terms, respectively. Also, n_S^1 and n_S^2 are the components of the normal unit vector $\mathbf{n}_S$ given by Eq. $(3.23)_1$.

Consider a mono-domain sample of rectangular shape with dimensions 200nm × 100nm. An elliptic inclusion with opposite spontaneous polarization is set as initial value for the level set function. The right and left boundaries are chosen to be surface charge free ($\mathbf{D}_\varepsilon \cdot \mathbf{n} = 0$), while the bottom and top boundaries are set $\phi = 0$ and $\phi = -0.05\,\mathrm{V}$, respectively. Also, all boundaries are assumed to be traction free. The mobility parameters are chosen $M_1 = 2 \cdot 10^{-4}\,\mathrm{m^3/s\,N}$ and $M_2 = 0$, while the rest parameters are selected as $\varepsilon = 0.01$ and $\mu = 10^{-6}$. In Figure 3.7, it is shown that the domain grows vertically until it reaches the boundary. Then under the motion of 180° domain walls it expands to cover the whole region of the sample.

In the 90° domain nucleus an elliptic inclusion is taken with horizontal polarization as initial value for the level set function. All boundaries are chosen with zero electric potential $\phi = 0$, while the left and right boundaries are traction free. At the bottom and top boundaries compressive mechanical loading is applied. The parameters for

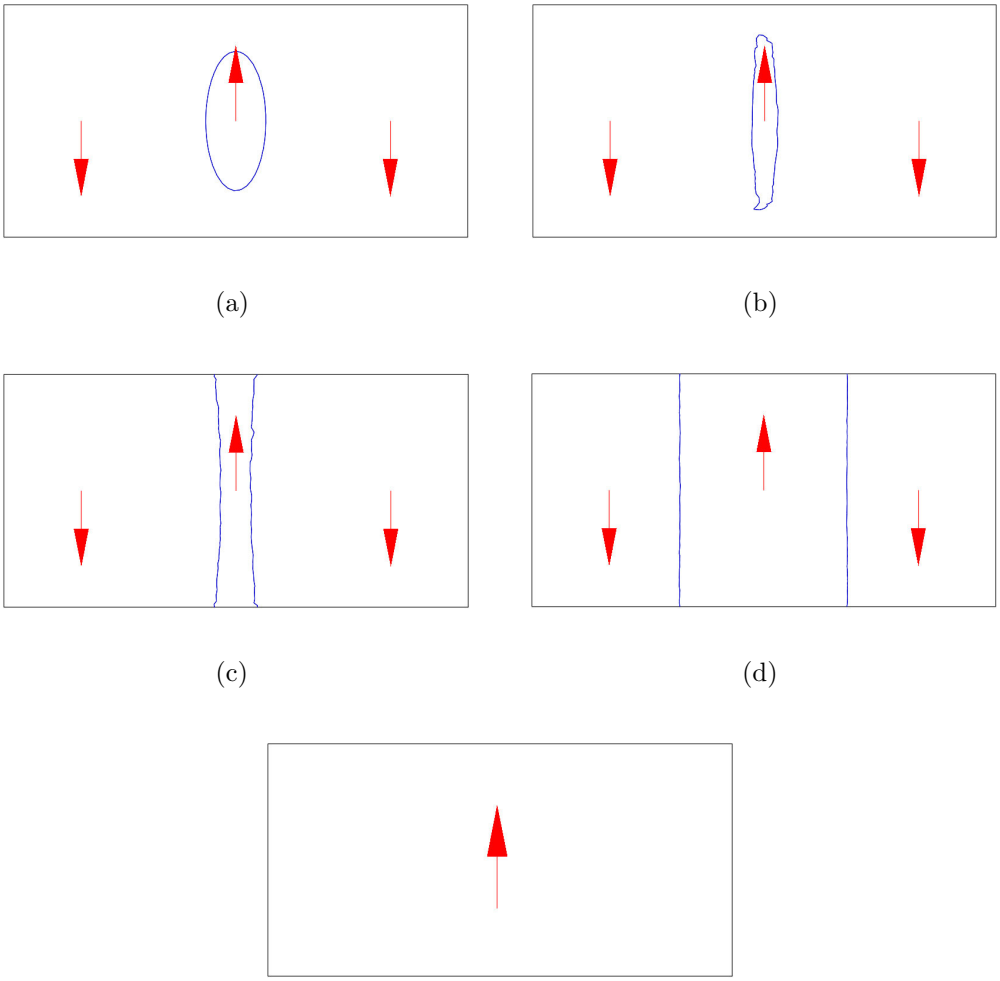

Figure 3.7: 180° domain nucleus

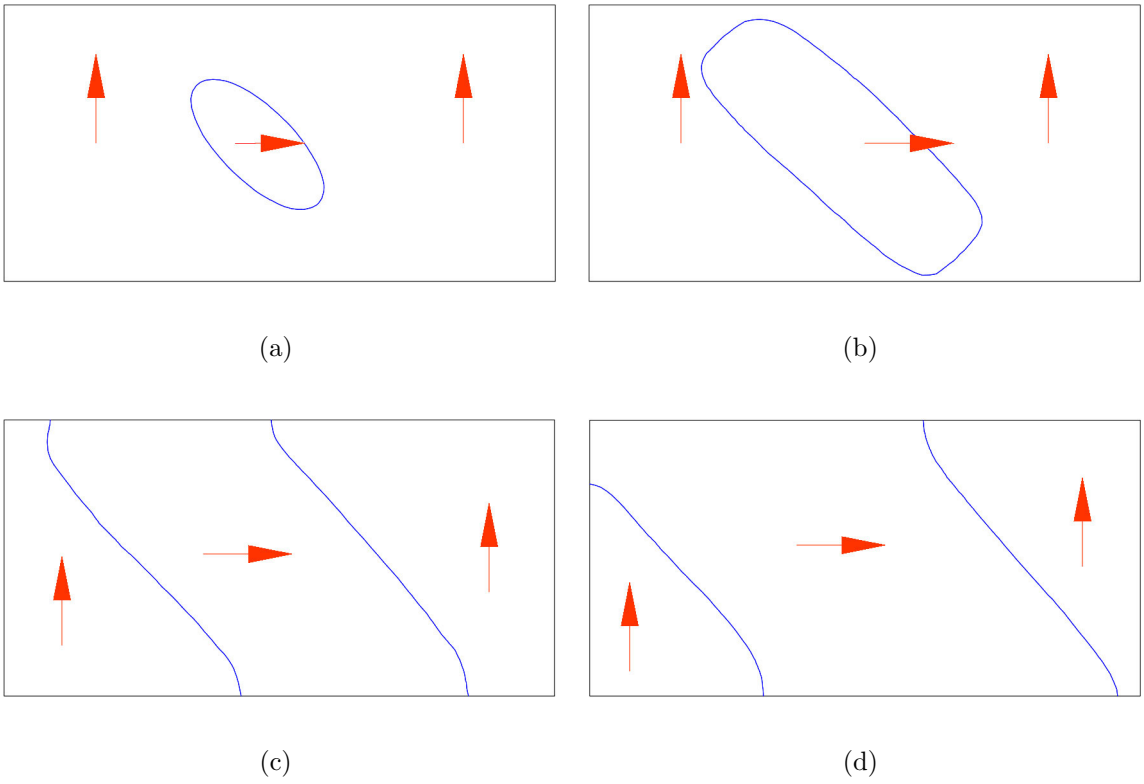

Figure 3.8: 90° domain nucleus

the kinetic relation are chosen as $M_1 = 2 \cdot 10^{-4}\,\mathrm{m^3/s\,N}$ and $M_2 = 20 \cdot 10^{-4}\,\mathrm{m^3/s\,N}$ and the parameters $\varepsilon = 0.01, \mu = 10^{-6}$, as before. This type of kinetic relation forces the domain to grow faster at 45° angle from the applied stress axis, so as to be in agreement with the behavior experimentally observed. In Figure 3.8 the 90° domain nucleus process is illustrated. It is worth noticing that under compressive stress, the interior domain grows until it reaches the boundary, then under the motion of 90° domain walls it expands inside the crystal.

3.3.3 Material forces on 180° domain wall

This subsection is devoted to the computation of material forces within the body. The kinetics of 180° domain wall is considered to present a specific example of material forces computation. It is assumed that the computational sample is separated in two phases of opposite spontaneous polarization as it is illustrated in Figure 3.9a. Practically, this can be achieved by appropriate selection of the initial value for the level set function. Moreover, an external electric field is applied in the upward direction so as the left domain to expand to cover the whole region of the sample. The same parameters are selected as in the previous example of 180° domain nucleus. There is only a slight difference concerning the domain wall thickness, which here is selected to be $\varepsilon = 0.2$. In Figure 3.9a, the norm of material forces within the sample is depicted. The computation of material forces is accomplished through the Eshelby stress tensor, as described in subsection 3.2.2.3. It is evident that non–vanishing material forces only exist within the transition layer, where one reasonably should expect to be present. In Figure 3.9b the norm of material forces at the middle point $x_2 = 50\,\mathrm{nm}$ is computed for different times to demonstrate that the interface is moving to the right end driven by the external electric field.

3.3.4 Typical microstructures of ferroelectrics

In this subsection, attention is paid on the computational reproduction of the microstructure for a sample with four phases. The computation is based on the theoretical analysis developed in detail in Section 3.2.3. First, one has to assume an appropriate form for the kinetic relations. For the sake of simplicity the mechanical part of the

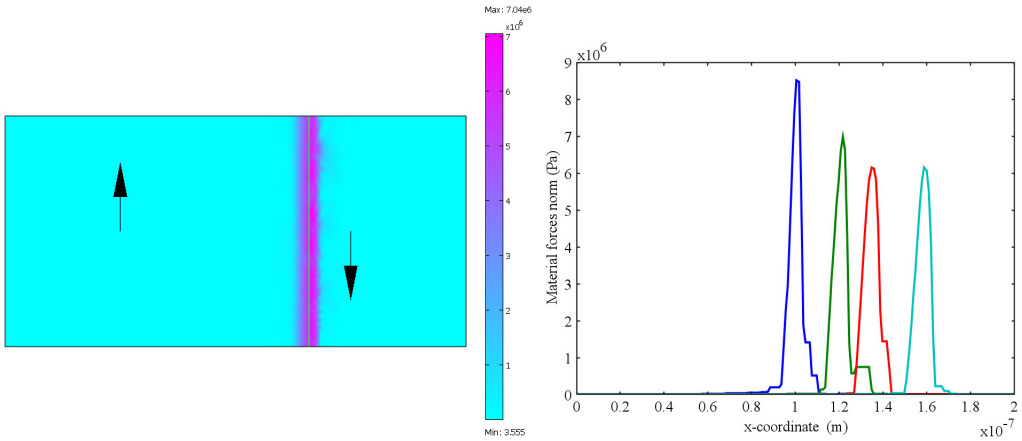

(a) (b)

Figure 3.9: Material forces on a moving 180° domain wall (a) Norm distribution profile, (b) Cross-section at $x_2 = 50\,\text{nm}$ at different time steps

problem is currently neglected, i.e., the analysis is restricted to rigid body ferroelectrics. An appropriate assumption, in the sense it reproduces successfully the microstructure, is given by the following forms

$$V_1 = M\frac{f_\varepsilon^1 + f_\varepsilon^2}{2}\,,\ V_2 = M\frac{f_\varepsilon^1 - f_\varepsilon^2}{2}. \tag{3.123}$$

The material parameters were selected as in the previous simulations, apart from the the mobility parameter, which is now taken $M = 2.5 \cdot 10^{-4}\,\text{m}^3/\text{s}\,\text{N}$. Also the regularization parameter is taken $\varepsilon = 0.01$. The initial structure is chosen by two intersecting ellipses as shown in Figure 3.10. The boundary conditions are surface charge free ($\mathbf{D}_\varepsilon \cdot \mathbf{n} = 0$). As one can see in Figure 3.11, the initial structure evolves up to its steady state configuration. This vortex-like domain structure is due to the choice of the boundary conditions which forces the normal component of the polarization vector to vanish on the boundary and it is in agreement with the results of the phase field model presented in the previous chapter. In Figure 3.12, the three dimensional plots of the two level set functions in equilibrium state are presented. It is obvious that their intersections with the sample provide the zero level sets of these functions. Also, for this simulation, the resultant material forces on the interfaces versus time are

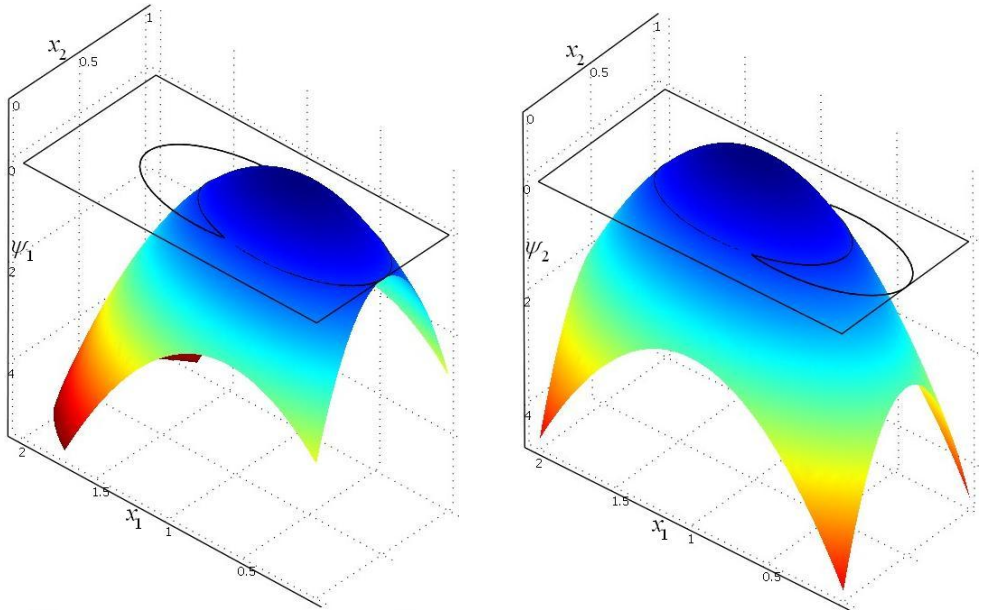

(a) (b)

Figure 3.10: Three dimensional plots of the two level set functions in the initial state and their zero levels (a) ψ_1, (b) ψ_2.

illustrated in Figure 3.13a. Notice that the material forces tend to zero, i.e., they are finite and drive the movement of the interfaces up to the equilibrium configuration of the microstructure, where they finally vanish. The behavior of the total energy with time is presented in Figure 3.13b. As it is expected, the energy of the system attains a minimum indicating equilibrium state.

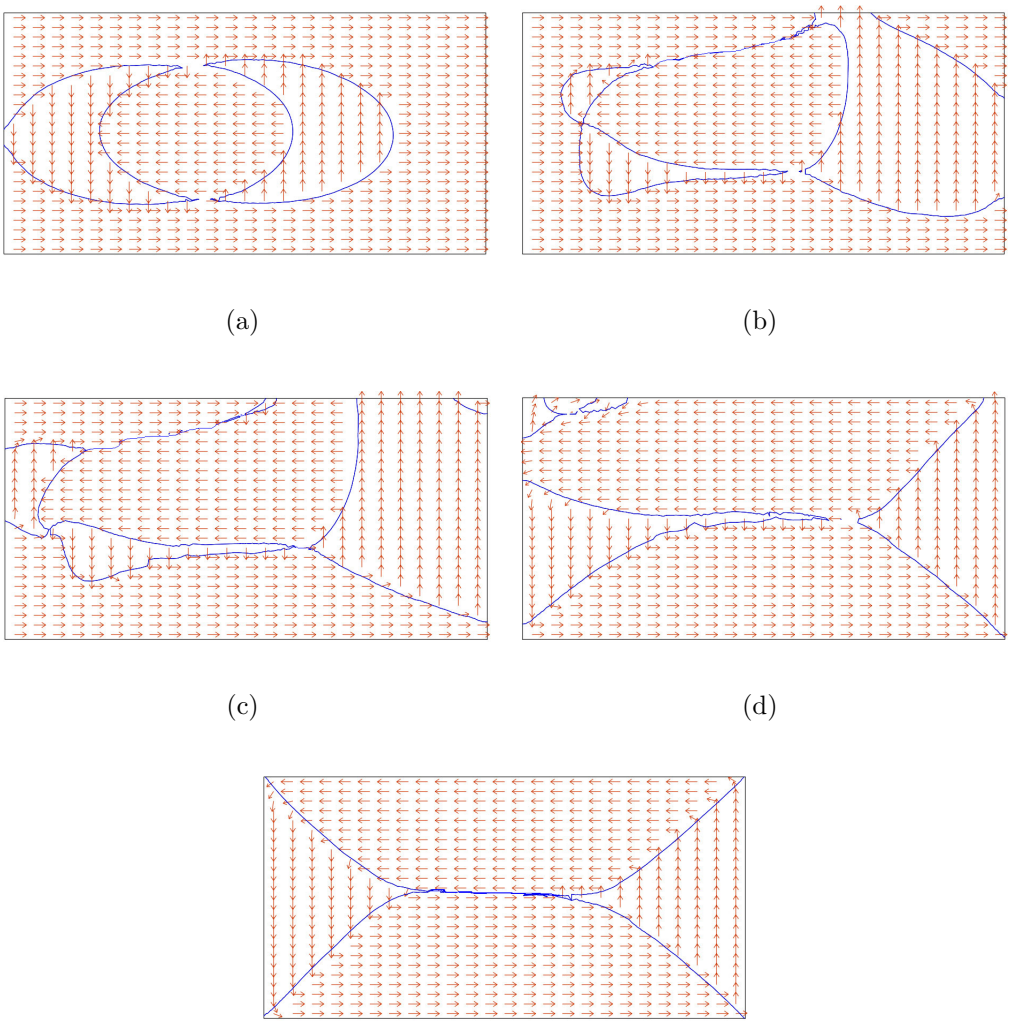

(a) (b)

(c) (d)

(e)

Figure 3.11: Domain formation

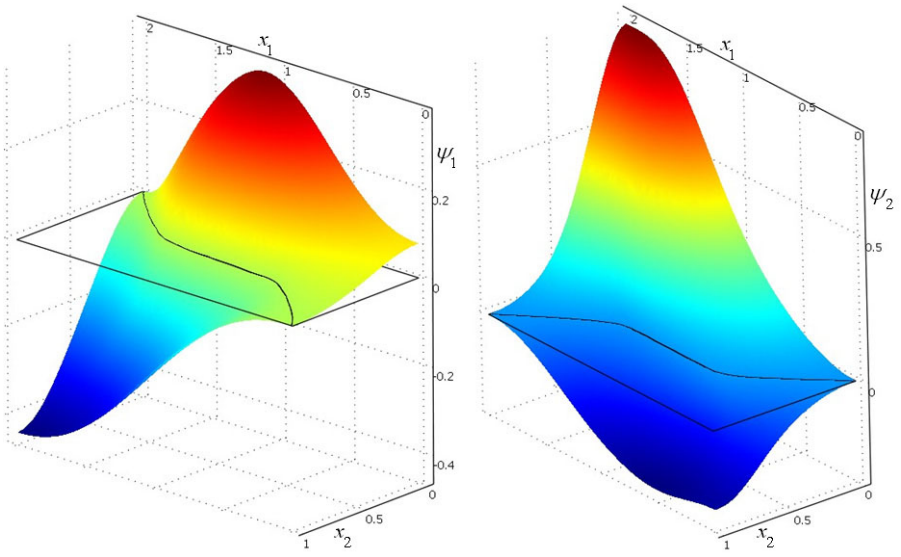

(a) (b)

Figure 3.12: Three dimensional plots of the two level set functions in the final state and their zero levels (a) ψ_1, (b) ψ_2.

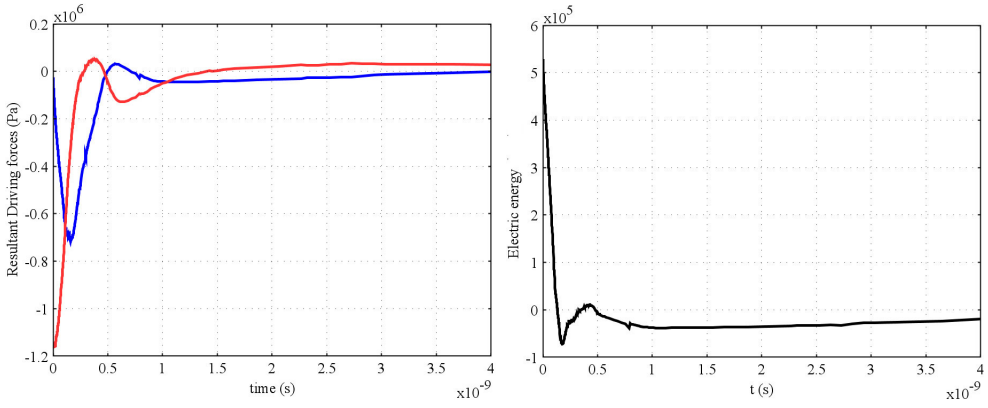

(a) (b)

Figure 3.13: (a) Resultant driving forces on the two zero level sets and (b) the total system energy as functions of time.

Chapter 4

Special topics in ferroelectrics

4.1 Damage in ferroelectrics

Defects play a crucial role in explaining important aspects of ferroelectric behavior since they interact with domain walls at sub - micron scales. Yang *et al.* (78) provide experimental observations on the pinning and bowing of domain walls near defects in ferroelectric crystals. Scott and Dawber (62) study the role of oxygen vacancies on the pinning of domain walls. Brennan (13; 14) presented a theoretical description of the effect of charged defects in stabilizing domain configurations and in blocking their motion. Numerical simulations have been performed by Su and Landis (65), provide values for the critical applied electric field and shear stress which required for the domain wall to break through an array of charged defects. The role of dislocations in ferroelectric thin film behavior has been studied experimentally by Dai *et al.* (23). Kontsos and Landis (43) provide a theoretical and numerical framework to investigate the interactions between domain walls and arrays of dislocations in ferroelectric single crystals.

The appearance of defects within a ferroelectric crystal results in degradation of material properties and fatigue of the material. Fatigue in ferroelectrics is triggered by two important defect mechanisms: (1) domain wall pinning due to charged point defects and (2) aging due to doping or radiation damage. Fatigue is very common in all ferroelectrics and it is an issue that has attracted much attention over the last decade. Until now, there is not any satisfying explanation for this time dependent alteration

of material properties, since the basic theory of ferroelectricity does not predict it. According to Zhang and Ren (84), fatigue can be safely assumed to be caused by a certain relaxation process. In the same work, the authors discuss whether the two types of defects come from a boundary effect or a volume effect. It is noted that the effect of electrodes or surface defects is also known to cause fatigue in ferroelectrics (56).

Domain wall pinning mechanism admits that point defects, possibly coming from charges injected by electrodes or oxygen vacancies, migrate to the domain walls. The strong electromechanical interaction between these defects and the domain walls causes the pinning of the latter, making switching of the total macroscopic polarization difficult or even impossible. Experimental observations have shown distorted hysteresis loops and asymmetric butterfly loops. Several continuum models simulate successfully the microscopic and macroscopic behavior under the presence of point defects e.g. (65; 80) and accept domain wall pinning as a significant damage mechanism. In this work, a similar analysis is performed and emphasis is paid on the distortion of domain walls by point charges and the appropriate electric field (coercive field) needed to overcome the defect.

Aging in ferroelectrics is attributed to the stabilization of domains within the material due to polar lattice defects making polarization switching hard. In general, dipole defects show the tendency to align with the surrounding spontaneous polarization following the crystal symmetry. For more details on the doping mechanism one is referred to the work of Damjanovic (24). There are several continuum models that accumulate dipole defects, i.e. (4; 47; 79). Here, a simple example accounting for dipole defects is proposed based on electric field gradient effects within the framework of the new phase field model presented in Section 2. It is assumed that a distribution of dipole defects on an interior surface of a single crystal interacts strongly with a domain wall resulting in the pinning of the domain wall. In this work we do not consider alignment of dipole defects.

4.1.1 Point charges

Consider a two dimensional ferroelectric sample where an array of two charges at a certain distance h has been placed. Furthermore, It is assumed that the sample is separated in two phases by a 180° domain wall by imposing an appropriate initial

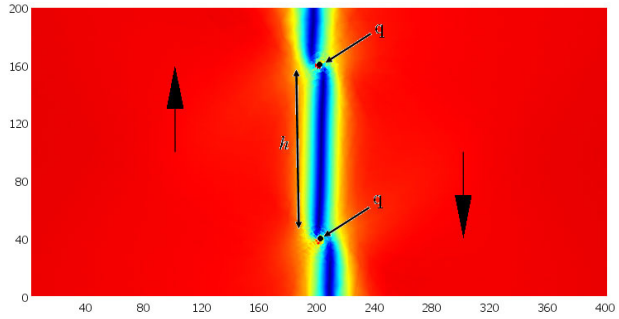

(a) Zero electric field

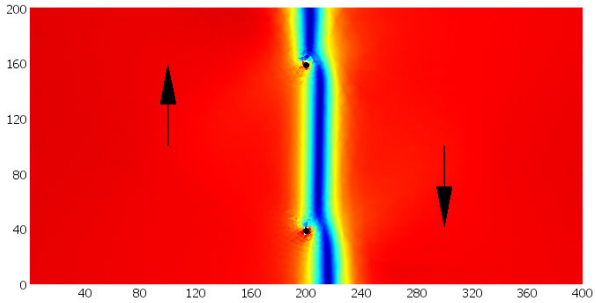

(b) Non zero electric field

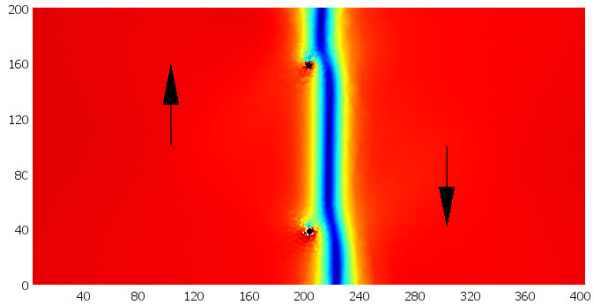

(c) Coersive field

Figure 4.1: 180^0 Domain wall interaction with two negative point charges $q = -10$ at distance $h = 120$

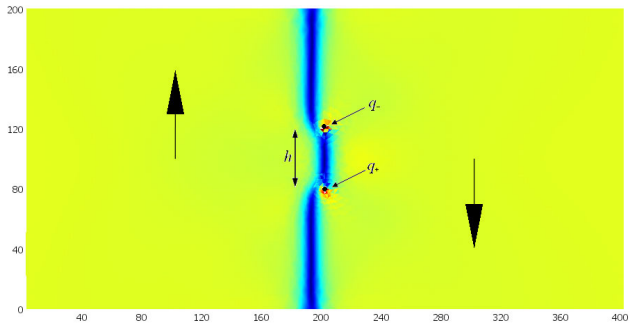

(a) Zero electric field

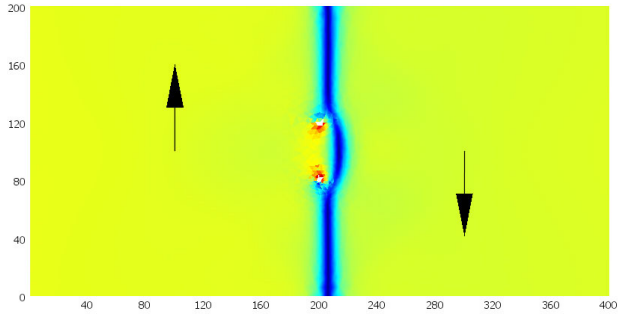

(b) Non zero electric field

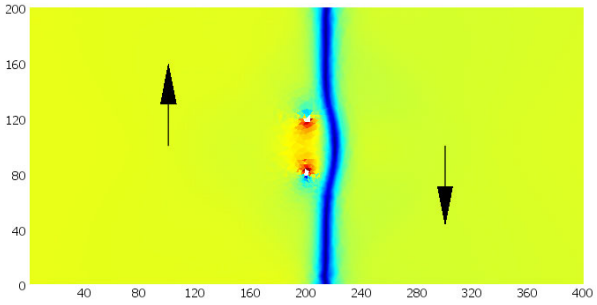

(c) Coersive field

Figure 4.2: 180^0 Domain wall interaction with two point charges with $q_- = -10, \quad q_+ = +10$ at distance $h = 40$

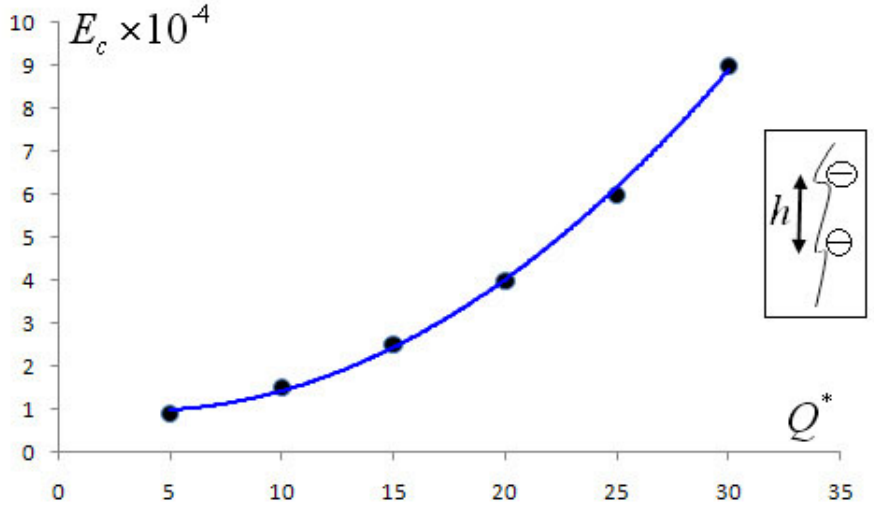

(a) Two negative point charges

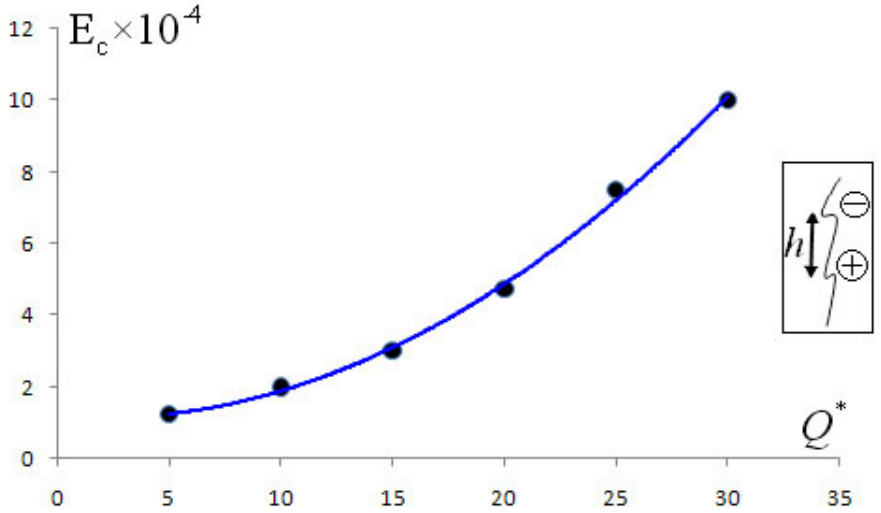

(b) Two charges with opposite signs

Figure 4.3: Plots of the coercive field as function of the absolute value of charge at distance $h = 40$.

condition for spontaneous dipole polarization. All boundaries are taken traction free and electric potential free. The additional boundary conditions for quadrupoles imply $q^r_{22} = 0$ for the top and bottom boundaries and $q^r_{11} = 0$ for the left and right boundaries. We are interested in the interaction of the domain wall with the array of charges. The influence of n point charges in the system of equations is taken into account by choosing the density of volume charges in the form

$$Q^* = \sum_{i=1}^{n} Q_i \delta(\mathbf{x} - \mathbf{x}^i), \tag{4.1}$$

where Q_i is the value of a point charge at position $\mathbf{x}^i$ and $\delta(\mathbf{x})$ denotes the Dirac delta function.

The first example concerns the interaction of the domain wall with two negative charges, as shown in Figure 4.1. The configurations illustrate equilibrium states at very large times. In Figure 4.3a, a 180° domain wall has been posed in the middle of the sample where exactly the defects are also present and no external electric field is applied. After many time steps it becomes evident that the strong interactions between the domain wall and the charges creates kinks in the domain wall. According to (65) who have used the standard polarization gradient theory, these kinks are important features of the interaction between the 180° domain wall and isolated charges. In Figure 4.1b, an upward electric field is applied so as to move the domain wall increasing the domain area with upward spontaneous polarization. It is remarked that the electric field is not able to move the domain wall over the array of charges, thus the domain wall is pinned by the defects. Increasing slowly the electric field it is observed that the domain wall stays pinned, until one reaches a critical field, called coercive field, where the domain wall starts moving surpassing the defected area, as shown in Figure 4.1c.

We turn now to a second example concerning the interaction between a domain wall and an array of two charges, a positive and a negative one in a finite distance h as shown in Figure 4.2. It should be emphasized that the behavior of such an array is far from the impact of a dipolar defect on the domain wall. In Figure 4.2a, the equilibrium state of the domain wall interacting with the two opposite charges is illustrated. Once again the strong interaction creates kinks in the domain wall slightly different with the ones of the array of negative charges. As before, the domain wall stays pinned while

raising the applied electric field, as shown in Figure 4.2b. In Figure 4.2c the coercive field moving the domain wall over the defect has been reached.

In Figure 4.3 the coercive field as a function of the absolute value of the electric charge is plotted for the two cases under discussion. As expected the coercive field increases with raising values of charge. It is worth mentioning that the function is non-linear and this can be explained from the finite thickness of the domain wall (65) as such behavior cannot be captured by sharp interface models.

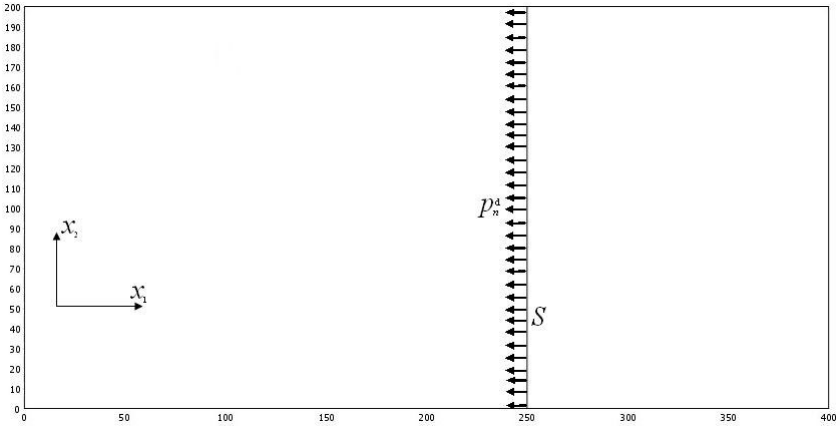

Figure 4.4: An array of dipole defects on S.

4.1.2 Dipole defects

Consider a surface S within the ferroelectric body with a fixed distribution of dipoles, p_i^{d} as shown in Figure 4.4. According to Eq. (2.41), the reversible part of quadrupoles result in a contribution to the surface dipole density on S as well. Thus one may write the total surface dipole polarization Π_i on S as follows

$$\Pi_i = q_{ij}^r n_j + p_i^{\mathrm{d}}. \tag{4.2}$$

As any surface vector field, Π may be resolved into a normal (to S) and a tangent component, $\Pi_n = (\Pi \mathbf{n}) \cdot \mathbf{n}$ and $\Pi_t = \Pi - \Pi_n$, respectively. The quadrupole theory developed in this paper obligates the normal component of the total dipole density on S to vanish (see Eq. $(2.31)_1$), i.e., one has to impose the restriction

$$\Pi_n = 0 \Rightarrow q_{ij}^r n_i n_j = -p_i^{\mathrm{d}} n_i = -p_n^{\mathrm{d}}, \text{ on } S. \tag{4.3}$$

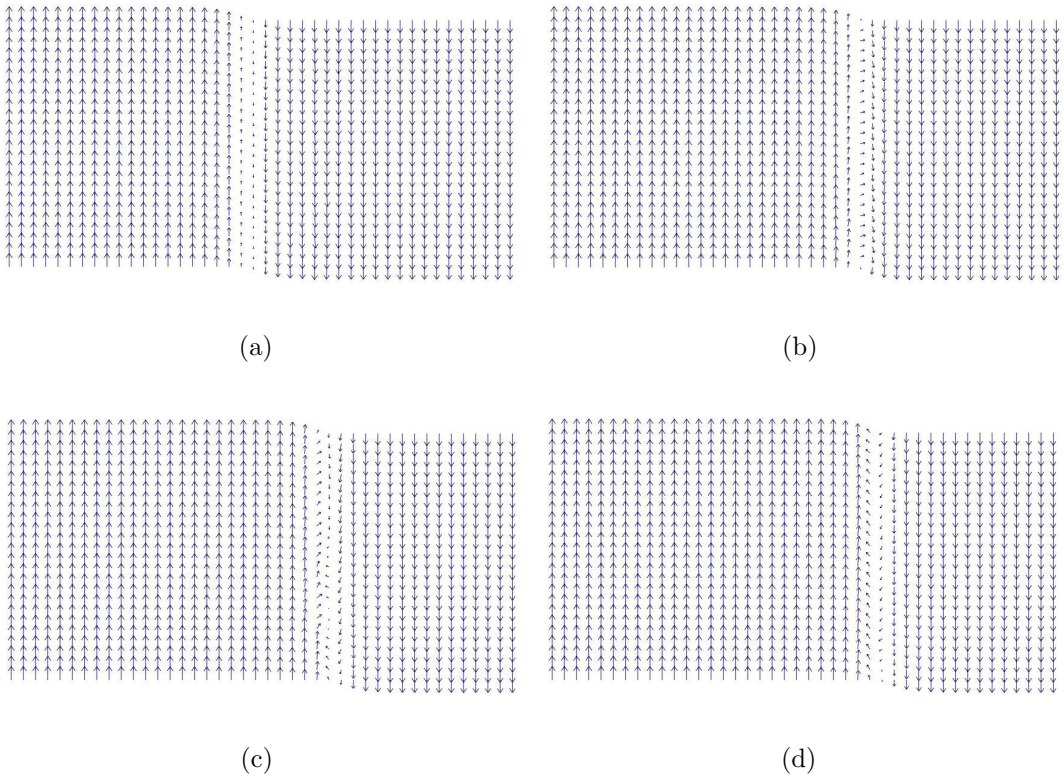

Figure 4.5: Interaction of a domain wall with a homogeneous distribution of dipole defects, (a) initial configuration, (b,c) intermediate states, (d) pinned domain wall

For the specific geometry of the 2-D example discussed here the boundary condition (4.3) takes the simple form (36)

$$q^r_{11} = -p^{\mathrm{d}}_n \quad \text{on} \quad S.$$

We start with a domain wall moving to the right direction under the influence of an external electric field. The left and right boundaries are taken charge free ($\mathbf{D} \cdot \mathbf{n} = 0$). The bottom is set at zero electric potential while the top edge is set at a non - zero electric potential. Also, all boundaries are taken traction free. As concerns the quadrupole polarization, the condition $q^r_{11} = 0$ holds for the left and right edge, while for the top and bottom the condition $q^r_{22} = 0$ is imposed.

In Figure 4.5 the interaction of a single domain wall with a distribution of dipole defects is illustrated. In Figure 4.5a the domain wall driven by the external electric

field is approaching the defected area. Notice in Figure 4.5b that the inhomogeneous electric field results in the enhancement of the spontaneous polarization in the x_1 direction within the domain wall. In Figure 4.5c the spontaneous polarization inside the domain wall rotates following the direction of dipole defects. Finally in Figure 4.5d the domain wall stops moving, thus it is pinned. To overcome the defected surface, a higher electric field must be applied.

4.2 Phase field modeling of ferroelectric polycrystals with an implicit representation of grain boundaries by using the level set method

Until now, we have restricted our analysis to ferroelectric single crystals. Ferroelectric ceramics are a collection of grains separated by firm boundaries, called grain boundaries. Each grain has different orientation with respect to one another. The grain boundary and grain boundary phases, grain orientation has been found to play a significant role in polarization switching. The preferential orientation of grains has been shown to affect the properties in ferroelectric ceramics. Zhang and Bhattacharya (82) presented a phase field model for domain switching in single and bi-crystals. It has been shown that the domain switching behavior was dependent on the misorientation of the two half crystals in the bi-crystal. Choudhury *et al.* (21) conducted phase field simulations for studying the effect of the grain orientation, grain boundary and a low ferroelectric transition temperature at the grain boundary on the domain structure, stress distribution and switching behavior in ferroelectric materials.

In this thesis we follow the work of Zhang and Bhattacharya (see subsection 2.1.2) by presenting the same phase field model in bi-crystals but the grain boundary is assumed to be the zero level set of an implicit function ψ. This treatment ensures continuity of the displacements, the traction and the electric potential across the grain boundary as in Section 3. It becomes obvious that domains and domain walls are controlled by the phase field model, while grain boundaries are controlled by the level set method. Thus for bi-crystals we propose a combined phase field–level set model, which can be easily extended to poly-crystals.

4.2.1 Phase field–Level set model for bi-crystals

As it has been mentioned in (21), there are two levels of structure for describing the microstructure in ferroelectric ceramics, i.e. the grain structure and the domain structure of each individual grain. Therefore, it is possible to introduce two coordinate systems, the laboratory frame and the material frame (82), and denote by $\boldsymbol{O}$ the transformation (rotation) that takes the laboratory frame to the material frame. $\boldsymbol{O}$ is constant in each grain but changes from one grain to another and has the property that

$$\boldsymbol{O}^{\mathrm{T}}\boldsymbol{O} = \boldsymbol{O}\boldsymbol{O}^{\mathrm{T}} = \mathbf{I}, \tag{4.4}$$

where $\mathbf{I}$ is the identity matrix. Naturally we can write the following relations

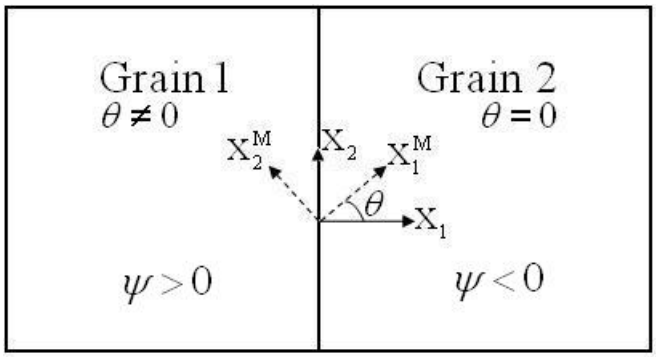

Figure 4.6: A bi-crystal and the two coordinate systems.

$$\begin{aligned} \mathbf{p}^M &= \boldsymbol{O}\mathbf{p}, \\ \mathbf{e}^M &= \boldsymbol{O}\mathbf{e}\boldsymbol{O}^{\mathrm{T}}, \end{aligned} \tag{4.5}$$

where $\mathbf{p}$ and $\mathbf{e}$ denote the polarization vector and strain tensor in the laboratory frame and $\mathbf{p}^M$ and $\mathbf{e}^M$ in the material frame. Specifically in two dimensions and assuming that the rotation matrix $\boldsymbol{O}$ describes rotation by an angle θ about the x_3 axis, Eq.

(4.5) takes the form

$$
\begin{aligned}
p_1^M &= p_1\cos\theta + p_2\sin\theta, && (4.6)\\
p_2^M &= p_2\cos\theta - p_1\sin\theta, && (4.7)\\
e_{11}^M &= e_{11}\cos^2\theta + e_{22}\sin^2\theta + e_{12}\sin 2\theta, && (4.8)\\
e_{22}^M &= e_{22}\cos^2\theta + e_{11}\sin^2\theta - e_{12}\sin 2\theta, && (4.9)\\
e_{12}^M &= e_{12}\cos 2\theta + \frac{1}{2}(e_{22} - e_{11})\sin 2\theta. && (4.10)
\end{aligned}
$$

Now we turn to the energy densities f_G and W (see Eq. (2.10)) which correspond to the domain wall and the Landau-Devonshire energy densities, respectively. These functions are directly affected by the rotation matrix $\boldsymbol{O}$. In the two dimensional setting and assuming plane polarization and plane strain conditions, these functions are chosen

$$
\begin{aligned}
f_G^M &= \frac{\alpha_0}{2}\left(\left(\frac{\partial p_1^M}{\partial x_1^M}\right)^2 + \left(\frac{\partial p_1^M}{\partial x_2^M}\right)^2 + \left(\frac{\partial p_2^M}{\partial x_1^M}\right)^2 + \left(\frac{\partial p_2^M}{\partial x_2^M}\right)^2\right), && (4.11)\\
W^M &= \frac{\alpha_1}{2}\left((p_1^M)^2 + (p_2^M)^2\right) + \frac{\alpha_2}{4}\left((p_1^M)^4 + (p_2^M)^4\right) + \frac{\alpha_3}{2}(p_1^M)^2(p_2^M)^2\\
&+ \frac{\alpha_4}{6}\left((p_1^M)^6 + (p_2^M)^6\right) + \frac{\alpha_5}{4}(p_1^M)^4(p_2^M)^4 - \frac{b_1}{2}\left(e_{11}^M(p_1^M)^2 + e_{22}^M(p_2^M)^2\right)\\
&- \frac{b_2}{2}\left(e_{11}^M(p_2^M)^2 + e_{22}^M(p_1^M)^2\right) - 2b_3 e_{12}^M p_1^M p_2^M + \frac{c_1}{2}\left((e_{11}^M)^2 + (e_{22}^M)^2\right)\\
&+ c_2 e_{11}^M e_{22}^M + c_3(e_{12}^M)^2. && (4.12)
\end{aligned}
$$

A substitution of Eqs. (4.6)–(4.10) in the above energy functions provides their expressions in the laboratory coordinate system. For instance, the domain wall energy density can be easily proved to be

$$
f_G^M = \frac{\alpha_0}{2}\left(\left(\frac{\partial p_1}{\partial x_1}\right)^2 + \left(\frac{\partial p_1}{\partial x_2}\right)^2 + \left(\frac{\partial p_2}{\partial x_1}\right)^2 + \left(\frac{\partial p_2}{\partial x_2}\right)^2\right) = f_G, \qquad (4.13)
$$

which means that the function f_G remains the same for all grains of various orientations. However, the expression for the Landau-Devonshire energy density W^M is complicated and for more details one is referred to (82). In this way we are able to work and perform computer simulations in the laboratory coordinate system.

With the above considerations we assume a ferroelectric bi-crystal consisting of two grains, as shown in Figure 4.6. The energy density of the system is written with the

help of the level set function ψ as

$$W_\varepsilon(\mathbf{e},\mathbf{p},\psi) = W_2(\mathbf{p},\mathbf{e}) + h_\varepsilon(\psi)(W_1(\mathbf{p},\mathbf{e}) - W_2(\mathbf{p},\mathbf{e})), \tag{4.14}$$

where W_1^M is the energy of grain 1 ($\theta \neq 0$) and W_2^M is the energy of grain 2 ($\theta = 0$) both written in the laboratory coordinate system. Then, the total energy functional I of the system may be written as

$$I[u_i,\phi,p_i] = \int_\Omega \left[f_G(p_{i,j}) + W_\varepsilon(e_{ij},p_i,\psi)\right] d\Omega + \frac{\varepsilon_0}{2}\int_{\mathbb{R}^3} \phi_{,i}^2 d\Omega. \tag{4.15}$$

Following the same procedure as in (82), we can conclude to the system of governing equations

$$\mu\dot{p}_i = \left(\frac{\partial f_G}{\partial p_{i,j}}\right)_{,j} - \frac{\partial W_2}{\partial p_i} - h_\varepsilon(\psi)(\frac{\partial W_1}{\partial p_i} - \frac{\partial W_2}{\partial p_i}) - \phi_{,i} \tag{4.16}$$

$$p_{i,i} - \varepsilon_0\phi_{,ii} = 0, \tag{4.17}$$

$$\left(\frac{\partial W_2}{\partial e_{ij}} + h_\varepsilon(\psi)(\frac{\partial W_1}{\partial e_{ij}} - \frac{\partial W_2}{\partial e_{ij}})\right)_{,j} = 0, \tag{4.18}$$

accompanied by appropriate boundary conditions (see subsection 2.1.2).

> **Remark 4.1:** *It is noted that arbitrary variations with respect to ψ were not considered, since the motion of the grain boundary is prohibited. Certainly, one can apply this model to grain boundary evolution of poly-crystalline ferroelectrics by extracting the level set equation as well. However, grain boundary evolution is complicated and for more details one is referred to the work of Zhang* et al. *(83).*

Following the theoretical analysis of Section 3, we can apply the material force method to compute the forces acting on the grain boundary due to the grain mismatch. According to Eq. (3.44) we take

$$\mathbf{f}_{\text{mat}} = -\frac{\partial \bar{W}}{\partial \mathbf{x}} = -\frac{\partial W_\varepsilon}{\partial h_\varepsilon} h_\varepsilon' \frac{\partial \psi}{\partial \mathbf{x}} = -\frac{\partial W_\varepsilon}{\partial h_\varepsilon}\delta_\varepsilon(\psi)\nabla\psi, \tag{4.19}$$

or the resultant force

$$F_n = -\int_\Omega \text{div}\boldsymbol{\Sigma}\cdot\mathbf{n}_S d\Omega = \int_\Omega \mathbf{f}_{\text{mat}}\cdot\mathbf{n}_S d\Omega, \tag{4.20}$$

where $\boldsymbol{\Sigma}$ denotes the Eshelby stress tensor for electro-elasticity.

4.2.2 Switching under electrical loading

To solve the system of Eqs. (4.16)–(4.18) we consider the same parameter normalization as in (82). The normalized material properties are chosen:

$$\begin{array}{ccccccc} c_1 = 185, & c_2 = 111, & c_3 = 74, & b_1 = 1.4282, & b_2 = -0.185, & b_3 = 0.8066, \\ \alpha_1 = -0.007, & \alpha_2 = 0.009, & \alpha_3 = 0.018, & \alpha_4 = 0.0261, & \alpha_5 = 5 \end{array}$$

for barium titanate. The mobility μ^{-1} is chosen unity and the gradient parameter $\alpha_0 = 1$.

A rectangular sample with normalized dimensions 1000×400 is considered and in order to separate it into two grains we chose the level set function as $\psi(x_1, x_2) = 500 - x_1$ (see Figure 4.6) and the regularizing parameter $\varepsilon = 1$. All simulations were performed by the use of the finite element method combined with an implicit time integration scheme with normalized time step $\Delta t = 1$. As for the boundary conditions we do not enforce periodic boundary conditions for electric potential, polarization and strain along x_1 direction. Specifically, for the bottom, right and left boundary we impose $\phi = 0$, while the top boundary is taken $\phi = \phi_0 \sin(2\pi t/T)$, with $\phi_0 = -12$ and $T = 30000$. Also, the system was taken mechanically clamped and for the polarization we have set $\nabla \mathbf{P}\mathbf{n} = 0$.

In Figure 4.7 we plot the hysteresis loop, which is the plot of the average electric displacement along x_2 direction as a function of the applied electric field. As one can notice, this is a typical hysteresis loop similar to the loop in a single crystal. In Figure 4.8 a series of domain structures are shown at time instants where the electric field is close to zero. A direct conclusion is that near the grain boundary we have noticed the nucleation of 90° domain propagating towards the grain interior. This is in agreement with other phase field models (21; 82) and experiments. It is apparent that the model produces the behavior of ferroelectric bi-crystals and can be easily modified to describe more complicated aspects. For instance we can construct a ferroelectric containing four grains oriented differently to each other by writing the energy as in Eq. (3.109). Also, we can easily assume defects or any kind of failure on the grain boundaries.

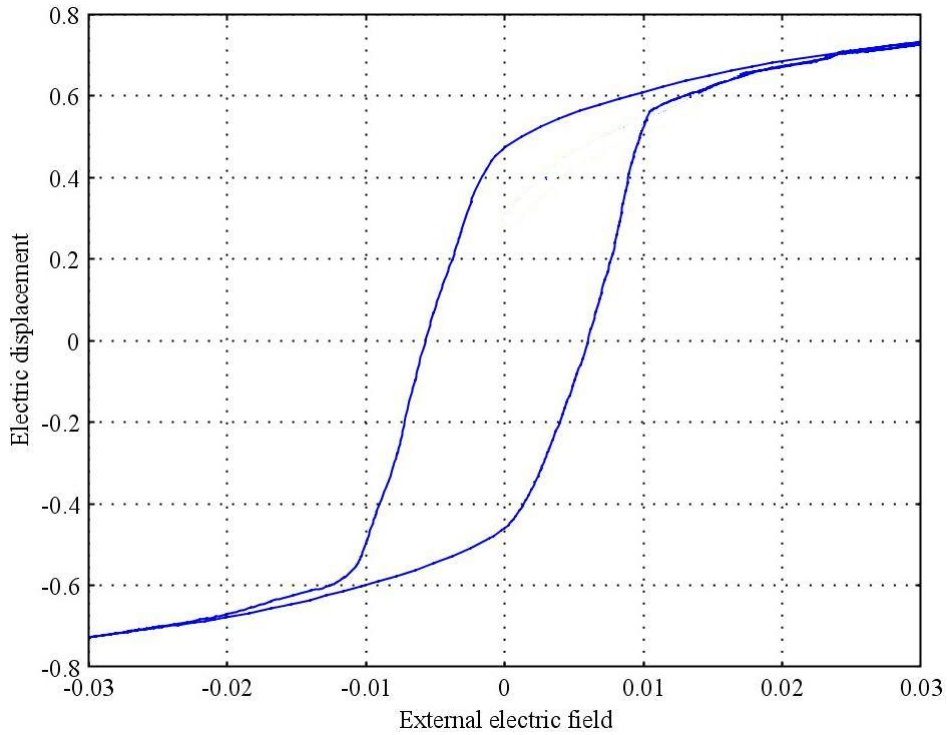

Figure 4.7: Hysteresis loop for a ferroelectric bi-crystal with grain 1 oriented at angle $\theta = 22.5°$ and grain 2 at an angle $\theta = 0°$.

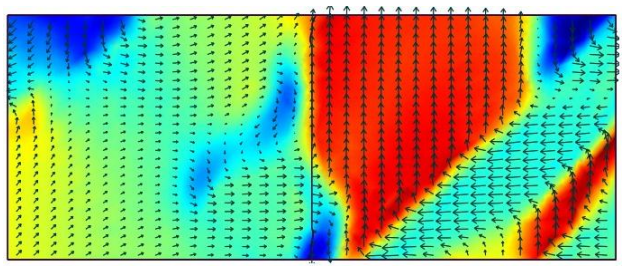

(a)

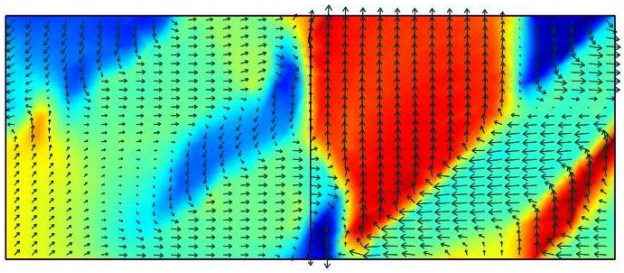

(b)

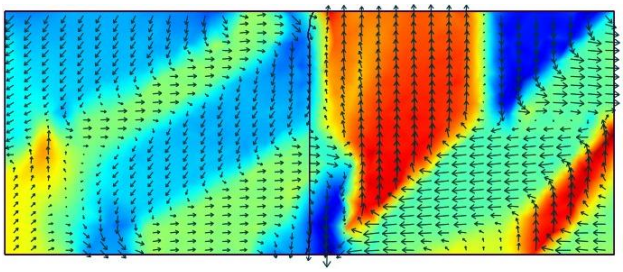

(c)

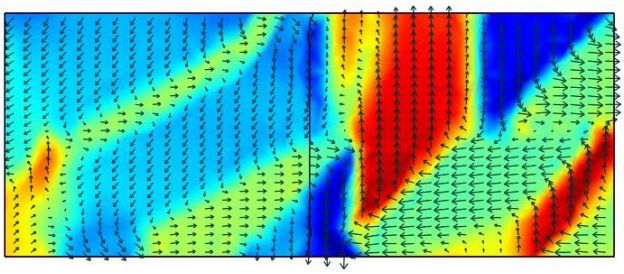

(d)

Figure 4.8: Domain switching under cyclic electric field. Snapshots were taken at (a) t=15511, (b) t=15660, (c) t=15948, (d) t=16060

Chapter 5

Conclusions

The phase-field models are more than capable of reproducing the microstructure as well as the macroscopic behavior of ferroelectric materials. The most important feature of phase field models is the introduction of a first order parameter, which governs the evolutionary process leading the system from a non-equilibrium state (energetically unfavorable) to an equilibrium one (energetically favorable). The transition from one phase to the other is continuous attributing a certain thickness and surface energy to the phase boundary. The first order parameter obeys an internal equation of motion of Landau-Ginzburg type coupled with the fundamental equilibrium equations of continuum mechanics. The information about the formation of the domain structure resides in the time evolution of the spontaneous polarization within the material. In Chapter 2, we outlined the standard phase-field models that are under the umbrella of Mindlin's polarization gradient theory, only to introduce the reader to the current state-of-the-art modeling of ferroelectrics. Moreover, we proposed a new phase-field model based on a newly developed electric field gradient theory. Our contribution can be seen as a model accumulating electric quadrupole moments and our effort focalizes in exploring the role of quadrupole moments in the overall behavior of ferroelectrics. The additional boundary conditions of the model seem useful enough to introduce dipolar defects in a natural way. Dipole defects represent an important damage mechanism in these materials resulting in an overall degradation of their ferroelectric properties, i.e. fatigue of the material. Our computational simulations prove that dipole defects have their way of blocking the motion of domain walls making polarization switching hard or even

impossible. Furthermore, based on the fact that gradient theories are closely related to size effect phenomena we conduct simulations on low dimensional ferroelectrics, i.e. thin films. Our results indicate that electric field gradients have a major impact on the domain structure as well as on the hysteretic behavior of thin films.

The sharp interface theory treats phase boundaries as discontinuity surfaces of zero thickness. Across the interface certain quantities suffer discontinuity jumps that must obey specific conditions. These conditions can be taken by standard arguments and correspond to the famous Rankine-Hugoniot jump conditions. The problem of a moving interface in the context of sharp interface models remains ill-posed, thus additional constitutive information is needed. It has been proved that this drawback can be fixed by selecting a kinetic relation, namely a relation that determines the velocity of the phase boundary as a function of the exerted force. The selection of an appropriate kinetic relation depends on experimental observations and in fact it is not easy to guess the correct one. Our contribution was the use the level-set method to describe the kinetics of the phase boundary, i.e. the domain wall. The method is based on an implicit representation of the interface by considering a smooth scalar function, which changes sign across the interface. Thus the zero level set of the implicit function coincides with the interface. The motion of the interface is accomplished by using an evolution equation for the level set function, which is of Hamilton-Jacobi type. It is remarked that the introduction of such an internal variable results in a regularization of the sharp interface model in ferroelectrics. However, as in sharp interface models it is essential to provide a kinetic relation as well. We focused on the kinetics of domain walls and on the domain formation in ferroelectric materials. The material force method was proved to be very useful in order to compute the driving forces on the domain walls. Thus it was deduced that domain structures in ferroelectrics are due to inhomogeneity forces entering the material momentum equation. Our computational simulations concern the kinetics of domain walls under combined electromechanical loading and also the formation of typical microstructures of two dimensional ferroelectrics with tetragonal crystal symmetry. Apart from ferroelectrics, we used the level-set method to build a two-phase thermoelastic problem in a general theoretical framework. We proposed a simple one dimensional problem where we have been able to extract a kinetic relation rather that to take it by assumption. Our results indicate that the level-set method is

equivalently powerful to the phase-field models enhancing the state of the art modeling of crystalline materials undergoing phase transformations.

References

[1] Abeyaratne R., Bhattacharya K., Knowles J.K. Strain-energy functions with multiple local minima: modeling phase transformations using finite thermoelasticity. In: Y. Fu, R.W. Ogden (eds.), Nonlinear elasticity: Theory and Applications, Cambridge University Press, (2001) pp. 433-490. 55, 69, 71

[2] Abeyaratne R., Knowles J.K., Evolution of Phase Transitions: A Continuum Theory. Cambridge University Press, Cambridge, UK (2006). 55, 71

[3] Abeyaratne R., Knowles J.K., On the driving traction acting on a surface of strain discontinuity in a continuum, J. Mech. Phys. Solids 38 (1990) 345–360. 55, 60, 74

[4] Ahluwalja R., Cao W., Influence of dipolar defects on switching behavior in ferroelectrics, Phys. Rev. B 63, (2000). 94

[5] Arvanitakis A.I., Kalpakides V. K., Hadjigeorgiou E. P., Electric field gradients and spontaneous quadrupoles in elastic ferroelectrics, Acta Mechanica, in press (2010). 34

[6] Arvanitakis I. Antonios, Kalpakides K. Vassilios, The concept of material forces in phase transitions problems within the level-set framework, Archive of Applied Mechanics, accepted for publication (2010). 62, 66

[7] Balassas K.G, Kalpakides V.K., The equilibrium of material forces in a 1D phase transition problem, Comput. Methods Appl. Mech. Engrg. 196 (2007) 2161–2172. 55, 69, 80

[8] Balassas K.G., Kalpakides V.K., Hadjigeorgiou E.P., Simultaneous solution of 1D momentum and canonical momentum equations, Eur. J. Mech. A/Solids 26 (2007) 887–900. 69, 80

[9] Berezovski A., Maugin G.A. (2007) Moving singularities in thermoelastic solids. Int. J. Fract. Vol: 147, 191–198. 55, 56, 69, 71

[10] Berezovski A., Maugin G.A., On the velocity of a moving phase boundary in solids. Acta Mechanica Vol: 179 (2005) 187-196. 55, 56, 69, 71

[11] Berezovski A., Maugin G.A., Jump conditions and kinetic relations at moving discontinuities. ZAMM Z. Angew. Math. Mech. (2009) 1-7. 55, 56, 69, 71

[12] Berezovski A., Maugin G.A., On the thermodynamic conditions at moving phase–transition fronts in thermoelastic solids. J. Non-Equilib. Thermodyn. Vol: 28 (2003) 299–313. 55, 56

[13] Brennan, C., Model of ferroelectric fatigue due to defect domain interactions, Ferroelectrics 150 (1993) 199–208 . 93

[14] Brennan, C., Landau theory of thin ferroelectric films, Integrated Ferroelectrics 8 (1995) 335–346. 93

[15] Bechmann, R., Elastic, piezoelectric, and dielectric constants of polarized barium titanate ceramics and some applications of the piezoelectric equations. J. Acoust. Soc. Am. (1956) 28, 347-350. 40

[16] Burcsu E., Ravichandran G., Bhattacharya K., Large electrostrictive actuation of barium titanate single crystals. J. Mech. Phys. Solids (2004) 52, 843 46. 31, 41

[17] Cao W., Cross L.E., Theory of tetragonal twin structures in ferroelectric perovskites with a first-order phase transition. Phys. Rev. B 44 (1991) 5–12. 16, 35

[18] Chen L.Q., Hu H.L., Three-dimensional computer simulation of ferroelectric domain formation. J. Am. Ceram. Soc. 81 (1998) 492–500. 16, 17, 31

[19] Chen L.Q., Phase field models for microstructure evolution, Annu. Rev. Mater. Res. 32 (2002) 113 40. 16

[20] Chowdhury K.L., Glockner P.G., Constitutive equations for elastic dielectrics. Int. J. Nonlinear Mech. 11 (1976) 315–324. 16

[21] Chowdhury S., Li Y.L., C. Krill III, Chen L.Q., Effect of grain orientation and grain size on ferroelectric domain switching and evolution: Phase field simulations. Acta Materialia 55 (2007) 1415-1426 101, 102, 105

[22] Davi F., Mariano P.M., Evolution of domain walls in ferroelectric solids. J. Mech. Phys. Solids 49 (2001) 1701–1726. 16

[23] Dai, Z.R., Wang, Z.L., Duan, X.F. and Zhang J., Link-up of 90 domain boundaries with interface dislocations in $BaTiO_3/LaAlO_3$, Applied Physics Letters 68 (1996) 3093–3095. 93

[24] Damjanovic D., Hysteresis in Piezoelectric and Ferroelectric Materials. The Science of Hysteresis, Volume 3; I. Mayergoyz and G.Bertotti (Eds.); Elsevier, (2005). 94

[25] Devonshire A. F., (1949) Phil. Mag., 40, 1040; 1951, ibid., 42, 1065; 1954, Phil. Mag. Suppl., 3, 85. 6, 16

[26] Duan X.B., Ma Y. C., Zhang R., Shape-topology optimization of stokes flow via variational level set method. Appl. Math. Comput. 202 (2008) 200–209. 78

[27] Duan X.B., Ma Y. C., Zhang R., Shape-topology optimization for Navier-Stokes problem using variational level set method, J. Comput. Appl. Math. 222 (2008) 487–499. 78

[28] Eringen A. C., Maugin G.A., Electrodynamics of Continua I, Springer, (1990). 16, 21

[29] Esedoglu S., Smereka P., A variational formulation for a level set representation of multiphase flow and area preserving curvature flow, Commun. Math. Sci., 6, (2008), 125–148. 79

[30] Gurtin M.E., Configurational Forces as Basic Concepts of Continuum Physics, Applied Mathematical Sciences, 137, Springer, New York, (2000). 56, 79, 80

[31] Hadjigeorgiou E.P. ,Kalpakides V.K., Massalas C.V., A General Theory for elastic dielectrics-Part I. The vectorial approach. Int. J. Non-linear Mech. 34 (1999) 831–841. 16

[32] Hadjigeorgiou E.P. ,Kalpakides V.K., Massalas C.V., A General Theory for elastic dielectrics-Part II. The variational approach. Int. J. Non-linear Mech. 34 (1999) 967–980. 16, 21

[33] Hong L., Soh A.K., Song Y.C., Lim L.C., Interface and surface effects on ferroelectric nano-thin films. Acta Materialia, 56 (2008) 2966–2974. 48

[34] Hou T., Rosakis P., LeFloch P. G., A level-set approach to the computation of twinning and phase-transition dynamics, J. Comput. Phys. 150 (1999) 302–331. 67, 78, 79

[35] Kafadar C.B., Theory of multipoles in classical electromagnetism. Int. J. Eng. Sci. 9 (1971) 831–853. 16

[36] Kalpakides V.K., Arvanitakis A.I., Hadjigeorgiou E.P., The role of electric field gradient in modeling elastic ferroelectrics. Int. J. Frac., (2010) DOI 10.1007/s10704-010-9494-5. 26, 100

[37] Kalpakides V.K., Arvanitakis A.I., A level set approach to domain wall kinetics and domain patterning in elastic ferroelectrics. Comput. Methods Appl. Mech. Eng. (2010) DOI 10.1016/j.cma.2010.05.009. 62, 80, 81

[38] Kalpakides V.K., Arvanitakis A.I., Configurational Forces in Continuous Theories of Elastic Ferroelectrics, In: IUTAM Symposium, Progress in the Theory and Numerics of Configurational Mechanics, Vol. 17 (Dordrecht, 2009), pp. 229–238. 62, 80

[39] Kalpakidis V.K., Massalas C.V., Tiersten's theory of thermoelectroelasticity: An extension. Int. J. Engng. Sci. 31 (1993) 157–164. 16, 20

[40] Kalpakidis V.K., Hadjigeorgiou E.P., Massalas C.V., A variational principle for elastic dielectrics with quadrupole polarization. Int. J. Engng. Sci. 33 (1995) 793–801. 16, 21, 23

[41] Kalpakides V.K., Balassas K.G., Massalas C.V., Material forces and phase transitions in elasticity. Arch Appl Mech Vol: 77 (2007) 135-146. 55

[42] Kamlah M., Ferroelectric and ferroelastic piezoceramics - modeling of electromechanical hysteresis phenomena. Continuum. Mech. Thermodyn. 13 (2001) 219–268. 30

[43] Kontsos, A., Landis, C.M., Continuum modeling of domain wall interactions with dislocations in ferroelectric crystals. Int. J. Solids Struct. 46 (2009) 1491–1498. 93

[44] Kretschmer R., Binder K., Surface effects on phase transitions in ferroelectrics and dipolar magnets, Phys. Rev. B 20 (1979) 1065-1076 13, 14

[45] Li C., Xu C., Gui C., Fox M.D., Level set evolution without re-initialization: A new variational formulation, In: Proceedings of the 2005 IEEE Computer Society Conference on Computer Vision and Pattern Recognition (2005) (CVPR'05). 62, 76

[46] Lika K., Hallam T.G., Travelling wave solutions of a nonlinear reaction - advection equation. J. Math. Biol., 38 (1999) 346–358. 43

[47] Liu J.M., Wang K.F., Lau S.T., Chan H.L.W., Choy C.L., Dipole alignment and dielectric susceptibility of defective ferroelectric: Monte-Carlo simulation, Comput. Materials Sci., 33 (2005) 66–73. 94

[48] Loge R.E., Suo Z., Nonequilibrium thermodynamics of ferroelectric domain evolution, Acta Mater. 44 (1996) 3429–3438. 74, 79

[49] Maugin G.A., Material inhomogeneities in elasticity, Chapman and Hall, London, (1993). 56, 57, 59, 74, 80

[50] Maugin G.A., Nonlocal theories or gradient-type theories: a matter of convenience? Arch. Mech. 31 (1979) 15–26. 16

[51] Maugin G.A., Trimarco C., Driving Force on Phase-Transition Fronts in Thermoelectroelastic Crystals, Mathematics and Mechanics of Solids, 2, (1997) 199–214. 74

[52] Maugin G.A., Berezovski A., Introduction to the thermomechanics of configurational forces. Atti dellAccademia Peloritana dei Pericolanti Classe di Scienze Fisiche, Matematiche e Naturali. Vol: LXXXVI, (2008) C1S0801016 - Suppl. 1 57, 58, 66

[53] Mindlin R.D., Polarization gradient in elastic dielectrics. Int. J. Solids Struct. 4 (1968) 637–642. 16

[54] Mindlin R.D., Continuum and lattice theories of influence of electromechanical coupling on capacitance of thin dielectric films. Int. J. Solids Struct. 5 (1969) 1197–1208. 16

[55] Mueller R., Gross D., Lupascu D.C., Driving forces on domain walls in ferroelectric materials, Comput. Mater. Sci. 35 (2006) 42-52. 73, 74

[56] Muller R., Gross D., Schrade D., Xu B.X.,Phase field simulation of domain structures in ferroelectric materials within the context of inhomogeneity evolution. Int. J. Fract. 147 (2007) 173–180. 94

[57] Osher S., Fedkiw R., Level set methods and dynamic implicit surfaces, Springer, New York, (2002). 56, 62

[58] Osher S., Sethian J.A., Front propagating with curvature-dependent speed: Algorithms based on Hamilton Jacobi formulations, J Comput. Phys. 79 (1988) 22-49. 56, 62

[59] Rabe K.M., Ahn C.H., Triscone J.M., Physics of Ferroelectrics: A Modern Perspective. Springer. Berlin (2007) pp. 364–365. 10, 13, 40

[60] Schrade D., Mueller R., Xu B.X., Gross D., Domain evolution in ferroelectric materials: A continuum phase field model and finite element implementation, Comput. Methods Appl. Engrg. 196 (2007) 4365–4374. 30, 45

[61] Schrade D., Mueller R., Gross D., Utschig T., Shur V.Ya., Lupascu D.C., Interaction of domain walls with defects in ferroelectric materials, Mech. Mater. 39 (2007) 161–174. 73, 84

[62] Scott J.F., Dawber M., Oxygen-vacancy ordering as a fatigue mechanism in perovskite ferroelectrics, Applied Physics Letters 76 (2000) 3801–3803. 93

[63] Soh A.K., Song Y.C., Ni Y., Phase field simulations of hysteresis and butterfly loops in ferroelectrics subjected to electro-mechanical coupled loading. J. Am. Ceram. Soc. 89 (2006) 652–661. 16, 17

[64] Suhubi E.S., Elastic dielectrics with polarization gradient. Int. J. Engng. Sci. 7 (1969) 993–997. 16

[65] Su Y., Landis C.M., Continuum thermodynamics of ferroelectric domain evolution: Theory, finite element implementation, and application to domain wall pinning. J. Mech. Phys. Solids 55 (2007) 280–305. 16, 93, 94, 98, 99

[66] Tiersten H.F., On the nonlinear equations of thermo-electroelasticity. Int. J. Eng. Sci. 9 (1971) 587–604. 15, 20

[67] Tilley D.R., Zeks B., Landau theory of phase transitions in thick films, Solid State Commun. 49, 823 (1984) 13

[68] Toupin R.A., The elastic dielectric. J. Ration. Mech. Anal. 5 (1956) 849–915. 15, 16

[69] Trimarco C., How multipole electric moments enter into macroscopic Maxwell equations. Il Nuovo Cimento, Vol. 109 B, N.5 (1993). 20, 21

[70] Wang J., Shi S.Q., Chen L.Q., Li Y., Zhang T.Y., Phase field simulations of ferroelectric/ferroelastic polarization switching. Acta Materialia 52 (2004) 749–764. 17

[71] Wang J., Zhang T.Y., Size effects in epitaxial ferroelectric islands and thin films. Phys. R. B. 73 (2006) 144107. 48, 51, 52

[72] Webb J.F., On the physics of ferroelectrics. Sci. Progress 86 (2003) 203–234. 10

[73] Xiao Y., The influence of oxygen vacancies on domain patterns in ferroelectric perovskites. PhD Thesis, California Institute of Technology (2004) pp. 41–46. 35, 39, 41

[74] Xu B.X., Schrade D., Mueller R., Gross D., Micromechanical analysis of ferroelectric structures by a phase field method, Comput. Mater. Sci. 45 (2009) 832–836. 16

[75] Yang J.S., Zhou H.G., Li J.Y., Electric field gradient effects in an anti-plane circular inclusion in polarized ceramics. Proc. R. Soc. A 462 (2006) 3511–3522. 16, 26, 42

[76] Yang J.S., Elastic dielectrics with electric field gradient. In: Book of Abstracts, McNu'97, The 1997 Joint ASME, ASCE, SES Summer Meeting, June 29July 2, Northwestern University, (1997) p. 333 16

[77] Yang X.M., Hu Y.T., Yang J.S.,Electric field gradient effects in anti-plane problems of polarized ceramics. Int. J. Solids Struct. 41 (2004) 6801–6811. 16, 26

[78] Yang, T.J., Venkatraman, G.,Swart, P.J. and Mohideen, U., Direct observation of pinning and bowing of a single ferroelectric domain wall, Physical Review Letters 82 (20) (1999) 4106-4109. 93

[79] Yin-Zhong Wu, Dong-Lai Yao, Zhen-Ya Li, Monte-Carlo simulation of the switching behavior in ferroelectrics with dipolar defects, Solid State Communications, 122 (2002) 395–400. 94

[80] Yu S., Yu L., Effects of fatigue and damage on the hysteresis of ferroelectric ceramics. Microsyst. Technol., 15 (2009) 33–38. 94

[81] Zhang W., Bhattacharya K., A computational model of ferroelectric domains. Part I: model formulation and domain switching, Acta Materialia 53 (2005) 185–198. 16, 19, 40

[82] Zhang W., Bhattacharya K., A computational model of ferroelectric domains. Part II: grain boundaries and defect pinning, Acta Materialia 53 (2005) 199–209. 101, 102, 103, 104, 105

[83] Zhang X., Chen J-S., Osher S., A multiple level set method for modeling grain boundary evolution of polycrystalline materials, Tech. Rep., UCLA, (2006), CAM Report 06–69. 79, 104

[84] Zhang L., Ren Xb, Aging behavior in single - domain Mn - doped $BaTiO_3$ crystals: Implication for a unified microscopic explanation of ferroelectric aging. Phys. Rev. B 73 (2006) 094121. 94

[85] Zhao H.K., Chan T., Merriman B., Osher S., A variational level set approach to multiphase motion, J. Comput. Phys. 127 (1996) 179–195. 78, 81

[86] Zienkevich O.C., Taylor R.L., Zhu J.Z., The Finite Element Method: Its basis and fundamentals, sixth ed., Butterworth-Heinemann, Oxford (2005). 84

Declaration

I herewith declare that I have produced this paper without the prohibited assistance of third parties and without making use of aids other than those specified; notions taken over directly or indirectly from other sources have been identified as such. This paper has not previously been presented in identical or similar form to any other Greek or foreign examination board.

The thesis work was conducted from October 2006 to September 2010 under the supervision of Professor Vassilios K. Kalpakides at the Department of Materials Science and Engineering at University of Ioannina.

This research was supported financially from the *State Scholarships Foundation (I.K.Y.) of Greece.*

Ioannina, 2010

Antonios I. Arvanitakis